Carla Maria Sundermann

Production of Calcium Carbonate from Steelmaking Slag and Captured CO_2- Optimisation of the Carbonation Process and Product Quality

Master Thesis for the degree:

Nordic Master in Innovative Sustainable Energy Engineering, M.Sc. (Tech.)
Aalto University, Finland and Royal Institute of Technology, Sweden

Aalto University, Espoo, Date

Supervisor: Mika Järvinen, Associate Professor, D.Sc. (Tech.)
Advisor: Arshe Said, M.Sc. (Tech)

Aalto University
School of Engineering

Aalto University, P.O. BOX 11000, 00076 AALTO
www.aalto.f

Abstract of master's thesis

Author Carla Maria Sundermann

Title of thesis Production of Calcium Carbonate from Steelmaking Slag and Captured CO_2-Optimisation of Carbonation Process and Product Quality

Degree programme Degree Programme in Energy Engineering and HVAC

Major Innovative and Sustainable Energy Engineering **Code** IA3025

Thesis supervisor Mika Järvinen

Thesis advisor(s) Arshe Said

Date 25.11.2016 **Number of pages** 12+82 **Language** English

Abstract

The X2PCC pilot plant produces precipitated calcium carbonate (PCC) from calcium extracted from steel slag and CO_2 gas. This work investigates the carbonation process in order to optimise it to produce PCC of the desired morphology and size. A literature review is presented showing the potential effects of different parameters on the morphology, size and quality of the PCC produced. Experiments are conducted varying different parameters and the morphology and size of the PCC are analysed based on this. Supersaturation is seen as key to understanding and controlling the process, so a model is built to show the supersaturation of the system. This involves activity coefficient modelling using the Pitzer model and estimations of the CO_2 solubility and solubility product, K_{sp}. Pure rhombohedral calcite is produced and needle-like aragonite is produced up to a purity of 70%.

Keywords PCC, Precipitated Calcium Carbonate, Carbonation, Steel Slag, Crystallisation, Precipitation, Supersaturation, Pitzer Model, Bromley Model, CCS, Carbon Capture and Storage, Circular Economy.

Acknowledgements

Thank you Mika Järvinen for giving me the opportunity to do my thesis with the X2PCC project and for the support during this time. Thank you Arshe Said for being such a great advisor, teaching me everything and helping me through so many experiments and the modelling work. Thank you to the other X2PCC team members, especially Owais and Nico, for helping me with my work and giving good company during experiments. Thank you Vadim and everyone else working in the lab for support during experiments and everyone else in the department and K4 building for being friendly and nice to work with. Thank you Fiona, Helmut, Nils, Killian, Finn and Woodie for being excellent parents, siblings and dog. Danke Manfred und Gudrun für eure Unterstützung während meines Studiums und Danke Oma Margret für deine netten Anrufe und Briefe während dieser Zeit. Tack Valter för din hjälp genom mina studier.

Contents

List of Tables

List of Figures

Abbreviations

ACC	Amorphous calcium carbonate
CCS	Carbon capture and storage
CR	Carbonation reactor
DLS	Dynamic light scattering
ER	Extraction reactor
EU	European Union
GCC	Ground calcium carbonate
h	Hour
HX	Heat exchanger
IAP	Ion activity project
L	Litre
M	Molal/Molar
MJ	Mega Joules
Mt	Mega tonnes
PCC	Precipitated calcium carbonate
ppm	Parts per million
PSD	Particle size distribution
SEM	Scanning electron microscope
Slag2PCC	Refers to slag being used to produce precipitated calcium carbonate
SSA	Specific surface area
X2PCC	Refers to a raw material X being used to produce precipitated calcium carbonate
XRD	X-ray diffraction
XRF	X-ray fluorescence

Chemical compounds and minerals

Ca_2SiO_4	Larnite
$CaSiO_3$	Calcium silicate
$CaCl_2$	Calcium chloride
$CaCO_3$	Calcium carbonate
CaO	Calcium oxide (aka. lime, quicklime or unslaked lime)
$Ca(OH)_2$	Calcium hydroxide (aka. slaked lime, milk of lime or lime milk, hydrated lime)
CO_2	Calcium dioxide
CO_3	Carbonate
H_2O	Water
HCO_3	Bicarbonate
Na_2CO_3	Sodium carbonate (aka. soda ash)
NH_4Cl	Ammonium chloride
$(NH_4)_2CO_3$	Ammonium carbonate
NH_4OH	Ammonium hydroxide
OH	Hydroxide

Nomenclature

Parameter	Description
Δc	concentration driving force
ΔH	enthalpy of reaction
ΔG	free Gibbs energy change
A	Debye-Hückel constant
a	activity
c	molar concentration, concentration driving force
C	solubility, temperature dependency parameter
D	diffusivity coefficient, static dielectric constant
e	absolute electronic charge
f	fugacity coefficient
F	Faraday constant
Ha	Hatta number
I	ionic strength
J	rate of formation of nuclei
k	Boltzmann constant, kinetic constant
k_H	Henry's constant
k_L	mass transfer coefficient
K_{aq}	Gas-Liquid equilibrium constant
K_{eq}	Ionic/chemical equilibrium constant
K_{sp}	solubility product
p	partial pressure, pressure
m	molality
n	molar amount
N	unit ion or molecule
N_o	Avogadro's number
R	Universal gas constant
S	supersaturation ratio
T	temperature
v	number of ions per formula unit
V	volume
z	charge of ionic species
a, b, c, d	constants
A, B, C, D	molecule in question

Greek letters

α	Bunsen coefficient
β	agglomeration kernel
β_0	agglomeration constant
γ	activity coefficient
$\dot{\gamma}$	shear rate
ε_M	specific energy from mechanical agitation
ε_G	specific energy from gas bubbling

η_{Ca}	calcium extraction efficiency
λ	the molar limiting conductivity
μ	chemical potential
υ	kinematic viscosity
ρ_w	density of water
σ	percentage supersaturation, interfacial surface tension
Φ	reaction affinity
Ω	preexponential factor

Subscripts

aq	aqueous
g	gaseous
het	heterogeneous
i	of ion in question
l	liquid
s	solid
M, c, c'	denoting cations
X, a, a'	denoting anions

Superscripts

θ	at standard conditions
*	at equilibrium

1 Introduction

Global warming and the effects of climate change are some of the biggest challenges facing the world today. The greatest cause of climate change is human related carbon dioxide (CO_2) emissions. It estimated that in order to avoid disastrous consequences, the global temperature increase since pre-industrial times should be limited to 2 °C and carbon dioxide in the atmosphere limited to 350ppm [1] (current levels lie at 400ppm). Policies and targets are being put in place by governments and intergovernmental agencies to tackle this. One method of reducing CO_2 emissions is carbon capture and storage (CCS). Here, CO_2 from combustion processes is prevented from entering the atmosphere and e.g. stored underground or reacted to form stable minerals (mineral sequestration).

A further key issue facing the world is dealing with waste and the availability of natural resources. Landfills can adversely affect the environment and lead to greenhouse gas emissions. Additionally the production of new materials is energy intensive, resulting in CO_2 emissions and the depletion of natural resources. Policies and targets are likewise being made to reduce the waste going to landfills through reduction, reuse, recycling and energy production. Efforts are being made by the European Union (EU) to promote the concept of "the circular economy", where the generation of waste is minimised and the value of products, materials and resources are maintained in the economy for as long as possible [2].

The X2PCC project of Aalto University aims to produce precipitated calcium carbonate (PCC) out of calcium extracted from waste materials and carbon dioxide from flue gases. In this way, waste (e.g. steel slag or fly ash) that would otherwise be sent to landfill is reduced, CO_2 that would otherwise be emitted to the atmosphere is captured and a valuable material is produced in an environmentally and economically sustainable way. PCC is an inorganic mineral, widely used as a filler material and coating pigment in paper, plastic and paint industries, among others, with a worldwide annual consumption of about 13 Mt [3]. Conventional PCC is produced using limestone as a raw material in an energy intensive process. In Finland, 0,5Mt of PCC are produced each year [3]. Whilst the geological storage of CO_2 is not possible in Finland due to a lack of suitable locations, the mineral sequestration of CO_2 is of interest as a potential CCS method [4]. Finland also has industries producing suitable waste for the X2PCC process (e.g. steel slag) and consumers of PCC (e.g. paper industry).

The X2PCC project has been developed from the laboratory scale to pilot plant scale, with an industrial scale demonstration plant currently being planned. In order for the PCC produced by the process to be sold commercially, it needs to fit certain specifications regarding the size and morphology of the particles produced. This presents a challenge for the X2PCC process. The aim of this work is to study and optimise the process in order to produce particles of the desired quality.

1.1 Scope of Work

The aim of this work is to study and optimise the X2PCC carbonation process to produce PCC of the desired quality. This was to be achieved through both theoretical research and modelling of the process as well as through conducting experiments. Research was made into

crystallisation in order to better understand the kinetics involved in the carbonation process and relevant equations were gathered for use in modelling the X2PCC process. Potential modelling methods for the carbonation process were researched and presented and calculations related to this were made. Literature research was conducted to identify parameters influencing the carbonation process and the effects of these, as well as important characteristics for assessing the quality of PCC produced. Based on this literature research, key parameters were chosen and experiments conducted at the pilot plant level to see the effect on the PCC produced.

1.2 Structure

First an introduction to PCC is given in chapter 2, including: the conventional production methods, characteristics and quality requirements and end applications. Next, in chapter 3, the X2PCC process is described with focus on the carbonation process and the pilot plant is described. The following chapter goes in depth into the kinetics of the precipitation process. Chapter 5 presents and assesses the key parameters in the carbonation process. Chapter 6 presents modelling methods for the process and calculations undertaken relating to this. Chapter 7 describes the experiments conducted in this work. Finally, the results of this work are presented in chapter 8, conclusions made on this in chapter 9 and recommendations for future work given in chapter 10. The numbered references can be found at the end of the work.

2 Precipitated Calcium Carbonate

Calcium carbonate ($CaCO_3$) is a mineral which is common in the earth's crust in rocks such as limestone, chalk and marble. These are formed from the remains of shells and skeletons of ancient sea life deposits and the characteristics (e.g. colour, purity, density, crystal morphology) depend on the conditions of formation (e.g. temperature, pressure, tectonic activity) [5], [6]. The commercial extraction of calcium carbonate is only feasible when the rock is of sufficient purity, homogeneity, thickness and colour. Once extracted this calcium carbonate can be further processed (e.g. wet or dry ground) to produce ground calcium carbonate (GCC) [7]. Besides the production of calcium carbonate from naturally occurring rocks, calcium carbonate can be produced synthetically and is then known as precipitated calcium carbonate (PCC). Most PCC is produced using the carbonation process with limestone as the raw material. Motivations for producing PCC over GCC are that impurities present in the limestone can be removed and it is easier to control the properties of the end product, such as particle shape, particle size, surface area, surface chemistry and particle size distribution (PSD) [3], [8].

2.1 Conventional Production methods

There are three main processes where PCC is produced commercially: the carbonation process, the Solvay process and the lime soda process. Of these, only the carbonation process produces PCC as the main product. The Solvay process produces sodium carbonate and calcium chloride and the lime soda process produces sodium hydroxide, both with PCC as a by-product [9]. The carbonation process shall be briefly described here as it relates to the X2PCC process and is the system used in much of the literature investigated in this work for assessing the potential influence of different parameters during the carbonation step.

The carbonation process is the most widely used process to manufacture PCC and is considered the most cost efficient [10]. The reaction equations are shown below [9]:

$$CaCO_3(s) \overset{heat}{\longleftrightarrow} CaO(s) + CO_2(g)\ (\Delta H = 163 \frac{kJ}{mol} at\ 1000°C) \quad (1)$$

$$CaO(s) + H_2O(l) \leftrightarrow Ca(OH)_2(s)\ (\Delta H = -65 \frac{kJ}{mol} at\ 20°C) \quad (2)$$

$$Ca(OH)_2(s) + CO_2(g) \leftrightarrow CaCO_3(s) + H_2O(l)\ (\Delta H = -113 \frac{kJ}{mol} at\ 20°C) \quad (3)$$

First, crushed limestone is burned in a lime kiln at about 1000ºC as shown in eq. (1). Here, calcium carbonate from the limestone decomposes into calcium oxide (also known as lime, quicklime or unslaked lime) and carbon dioxide. This reaction is endothermic with a typical energy consumption of 3,5 MJ/kg_{CaO} and up to 8 MJ/kg_{CaO} [7]. The calcium oxide is then slaked with water to produce calcium hydroxide (often referred to as slaked lime or milk of lime [11]) as is shown in eq. (2). Impurities from the limestone are then removed and CO_2 is bubbled through the solution causing calcium carbon to precipitate as shown in eq. (3).

Usually with the CO_2 that was given off from the calcination process and has been purified is used [10]. The conditions of the process can be controlled to produce PCC of the required qualities (e.g. particle size distribution and morphology). This can then screened and dried or can be delivered in slurry form to the end user depending on the transport and distance. It is also possible to have the carbonation and calcination processes at different sites if necessary and appropriate regarding transportation [9]. Although the process uses CO_2 recovered from the calcination process, or from flue gases of power plants, recovery kilns or lime kilns, the carbon dioxide efficiency is at best 60% [12] resulting in emissions or high costs for recovering unused CO_2. The high energy requirement for burning lime also has a significant impact on CO_2 emissions and the production costs [7]. Thus it becomes clear that there is a potential for alternative methods to produce PCC with reduced energy consumption and CO_2 emissions.

2.2 Characteristics and Quality Requirements

There are many characteristics of PCC that are of importance for its end use. The importance of the various characteristics and the specific requirements differ depending on the end use of the product. Some examples of important characteristics are:

- Purity
- Morphology
- Habit
- Mean size
- Particle size distribution (PSD)
- Specific surface area (SSA)
- Brightness
- Surface charge
- Density
- Oil absorption

Two of the main challenges currently faced for the commercialisation of the X2PCC project are the ability to consistently produce PCC of the required morphology and size for commercial use. It has been decided for the scope of this work that these two quality parameters will be the main focus in assessing the PCC produced from the pilot plant. Thus they shall be discussed in more detail in the following section. PCC for commercial use should have a very high purity, generally above 99%, although some grades are above 97% [13]. This level of purity has already been successfully achieved by the X2PCC process. Further information on the characteristics and quality requirements of different commercial grade calcium carbonate products for various applications can be seen in Ciullo 1996 [5]. Zappa 2014 [13] conducted a review of commercially available PCC for products used in the paper industry, the results of this are presented in the Table 2.1 as a reference to the desired PCC qualities that are the aim of this work.

Table 2.1: Quality parameters of commercially available PCC products used in the pulp and paper industry [13].

PCC Product	Supplier	Application/Properties	Grade	Morphology	Purity (%$CaCO_3$)	Brightness (dry)	pH (slurry)	Median size d_{50} (µm)	Nominal SSA (m^2/g)
Albacar[1238]	SMI*	Filler: Increases paper whiteness, brightness, and opacity. HO grade best for optical properties, LO best for strength and calliper.	HO	Calcite, clustered scalenohedral	n/a	>94.5	7.5-9.5	1.3	12
			5970		98	98	n/a	1.9	7
			LO		n/a	>94.5	7.5-9.5	2.2	6
Albafil[1248]	SMI	Filler: Improved paper runnability, porosity control, enhanced scattering with minimal strength loss. S grade best for porosity control, XL for strength and sizing.	S	Calcite, prismatic	97	97	n/a	0.7	10
			M		97	97	n/a	0.9	8
			L		n/a	n/a	n/a	1.4	6
			XL		n/a	n/a	n/a	2.0	4
Megafil[1258]	SMI	Filler: Provides stiffness, strength, opacity and bulk. Grade 1000 is best for optical properties and porosity, 3000 best for strength and calliper.	1000	Calcite, prismatic	n/a	n/a	n/a	1.1	7
			2000		n/a	n/a	n/a	1.5	6
			3000		n/a	n/a	n/a	2.2	4
Albaglos[1268]	SMI	Coating: Paper and paperboard surface coating where high brightness and gloss (S) or matte is desired (XL)	S	Calcite, prismatic	n/a	n/a	n/a	0.6	9
			L		n/a	n/a	n/a	1.5	5
			XL		n/a	n/a	n/a	2.2	4
Opacarb[1278]	SMI	Coating: Gives high brightness and opacity increases not attainable with other PCC grades.A40 gives the highest gloss, A60 best fibre coverage.	A 40	Aragonite	n/a	n/a	n/a	0.4	12
			A 50		n/a	n/a	n/a	0.5	10
			A 60		n/a	n/a	n/a	0.6	9
Syncarb[9]	Omya	Filler: Pure white, anionically dispersed PCC for high brightness, opacity and bulk in papermaking	F0474-MJ 52%	Calcite, scalenohedral	99	95	9.3	1.8	5.5
Precarb[10]	Schaefer Kalk	No grade-specific uses given but Precarb is used in the pulp and paper, plastics, and pharmaceuticals industries	100	Calcite, scalenohedral	99	99 (DN 53163) 97 (R_{457})	n/a	1	9
			140	Calcite, scalenohedral	99	93 (R_{457})	n/a	1.3	9
			150	Calcite, scalenohedral	99	98 (DN 53163) 96 (R_{457})	n/a	3	5
			400	Calcite, scalenohedral + aragonite (35%)	99	99 (DN 53163) 97 (R_{457})	n/a	0.8	8
			724	Calcite, rhombohedral	99	98 (DN 53163) 96 (R_{457})	n/a	0.5	40
			800	Calcite, platelike	96	99 (DN 53163) 97 (R_{457})	n/a	1.1	17

n/a: not available

*Specialty Minerals Inc. (SMI) is a wholly owned subsidiary of Minerals Technologies Inc. (MTI)

2.2.1 Morphology

Calcium carbonate is polymorphic, meaning it can crystallise into different, but chemically identical crystalline forms. It can form calcite (triagonal-rhombohedral), aragonite (orthorhombic) and vaterite (hexagonal) [14]. Of the three calcium carbonate polymorphs, only calcite and aragonite are used commercially. Typical crystal shapes of calcite that are sought after are rhombohedral, prismatic and scalenohedral, whereas aragonite in a needle like form is usually desired [3]. These morphologies can be seen in Figure 2.1. The X2PCC pilot plant has succeeded in producing pure calcite in the rhombohedral form and aragonite/calcite mixtures. Vaterite has also been produced in small amounts. Scalenohedral calcite has only been produced on a laboratory scale. This work aims to assess the conditions required to consistently produce commercially useful PCC morphologies, with a special focus on finding the conditions to produce pure aragonite and scalenohedral, as these are of particular value in the industry.

The synthesis of nano PCC is also of increasing interest in recent years [15]. Nano PCC has particles with a size less than 100 nanometres or 0.1 micrometres in size [16]. Nano PCC is widely used as a filler in polymeric materials with the main goal of reducing costs, however it can also have beneficial impacts such as a higher impact resistance related to a higher elasticity modulus [17]. The emerging PCC market trends show a growing consumption of nano PCC [18]. Nano PCC is often reported as being of a spherical shape [19]–[21], although other shapes are also reported.

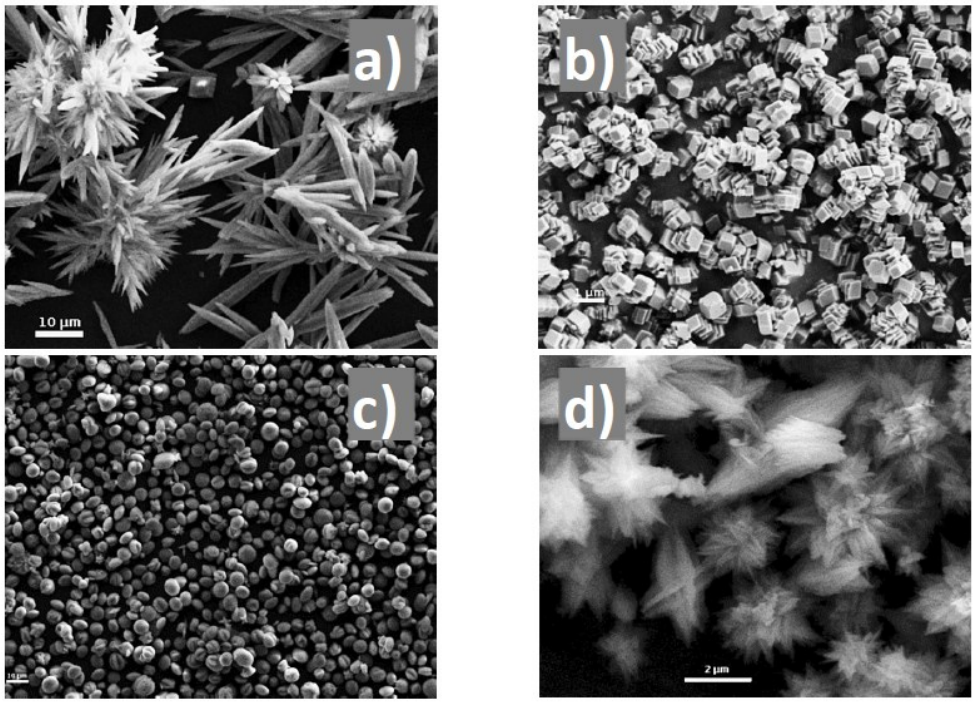

Figure 2.1: Scanning Electron Microscope (SEM) pictures of a) aragonite, b) rhombohedral calcite, c) vaterite and d) scalenohedral calcite produced with the X2PCC process. Scale bars 10µm in a) and c), 1µm in b) and 2µm in d). [22]

Of the three polymorphs, calcite is the most thermodynamically stable phase. Aragonite is metastable, as is vaterite which is the least stable of the three polymorphs. It is also possible for amorphous calcium carbonate (ACC) to form [21].

2.2.2 Size

There is variation in the size of individual particles produced from crystallisation processes. To account for this, a mean particle size is usually given, as well as a particle size distribution (PSD) to account for variations from this mean. Typical measurements of mean particle size are d_{50}, meaning 50% of particles are this size and smaller, or d_{90} meaning 90% of particles lie at this size or below. The PSD is very important in considering the size and uniformity of the particles produced. It is possible for two samples of PCC to have the same average particle size, yet one contains a mixture of very fine and very large particles and the other has a more uniform distribution of particles of a similar size.

Generally, a very small particle size and PSD are sought after for the commercial use of PCC. For example, for application as a pigment in the paper industry, particle sizes of between 0,3 and 2 μm are typically found, with a very narrow PSD, although significantly lower average sizes are found for special applications [7].

2.3 Applications

The global consumption of PCC in 2015 was 13,77Mt and it accounted for 17% of the calcium carbonate market (GCC making up the rest). The market for calcium carbonate has been rising in recent years [23]. The main application of PCC is in the paper industry can been in Figure 2.2 which show the applications of PCC in the EU (based on 2002 data [24]) and North America (based on 2011 data [25]). PCC is typically used as a filler and coating in the paper industry, as a pigment in paints and coatings, as a filler in adhesives, sealants and polymers, and in the pharmaceutical industry [5].

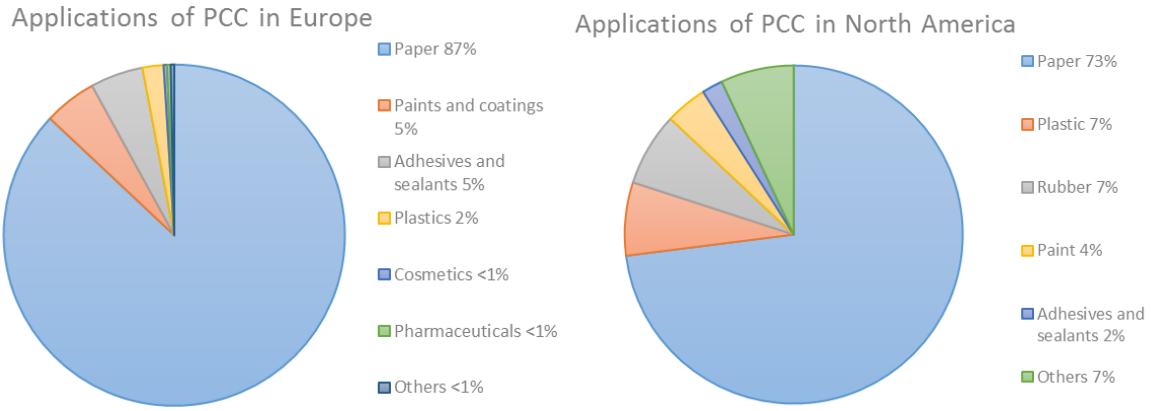

Figure 2.2: Applications of PCC in Europe and in North America

3 X2PCC process

The X2PCC process produces PCC by extracting calcium from calcium rich waste materials and using CO_2 gas captured from emission sources. The X2PCC project has been developed from the laboratory scale to a pilot plant (upon which the work of this thesis is based) and a demonstration plant in industry is currently being designed. Originally the project focused on the extraction of calcium from steel slag and was named Slag2PCC, however, it was renamed to encompass the potential for other calcium containing waste materials (represented by "X"). Currently tests are being made within the project on the production of PCC from fly ash. This work used only steel slag as a raw material.

The X2PCC process has two steps: an extraction step where the calcium is extracted from the raw material in question, and a carbonation step where calcium carbonate is precipitated from the calcium- rich solution by bubbling through CO_2 gas. Figure 3.1 gives an overview of the process with slag as the raw material. An aqueous solution of ammonium chloride, NH_4Cl, is used to extract the calcium from the steel slag in the extraction step. The steel slag is filtered from the solution which is now rich in calcium. This calcium rich solution is then carbonated with CO_2 in the carbonation step to produce PCC which is then filtered from the solution. The NH_4Cl solution can then be recycled and reused in the next extraction. This is very beneficial as it lessens the costs and materials needed.

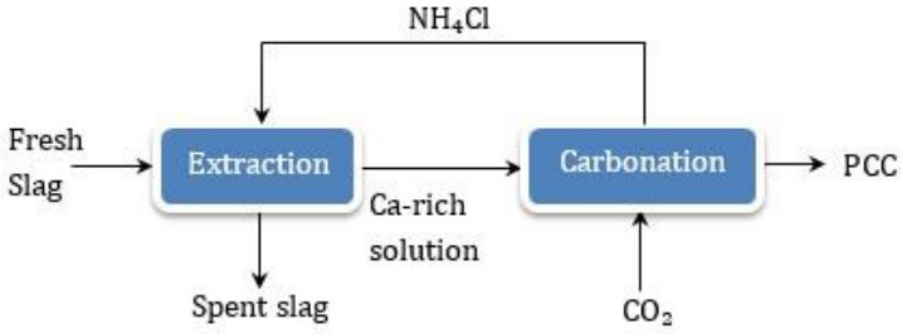

Figure 3.1: X2PCC process schematic [26]

The main chemical reactions involved in the X2PCC process, in the case where steel slag is the raw material, are as follows [22]:

$$CaO(s) + 2NH_4Cl(aq) + H_2O(l) \rightarrow CaCl_2(aq) + 2NH_4OH(aq) \quad (4)$$

$$Ca_2SiO_4(s) + 2NH_4Cl(aq) + H_2O(l) \rightarrow CaCl_2(aq) + CaSiO_3(s) + 2NH_4OH(aq) \quad (5)$$

$$2NH_4OH(aq) + CO_2(g) \leftrightarrow (NH_4)_2CO_3(aq) + H_2O(l) \quad (6)$$

$$(NH_4)_2CO_3(aq) + CaCl_2(aq) \leftrightarrow CaCO_3(s) + 2NH_4Cl(aq) \quad (7)$$

Of the calcium-containing compounds in the steel slag, only calcium oxide (CaO) and larnite (Ca_2SiO_4) react with the ammonium chloride solvent to a large extent, as can be seen in the

chemical reactions above. It can also be seen that after carbonation, ammonium chloride in its original form is left, which can easily be recycled back to the extraction step once the calcium carbonate has been filtered from it. This work focuses on the carbonation step. The extraction step shall be briefly described and the carbonation step investigated in detail, including the kinetics of the process and precipitation kinetics of calcium carbonate.

3.1 Extraction

The first step of the X2PCC process is the extraction of calcium from the raw material. There are many potential calcium containing waste materials that could be suitable for the production of PCC. Some examples of calcium containing solid industrial wastes that have been studied for the application of mineral carbonation are: steel slag, air pollution control residue, bottom ash from municipal solid waste or refuse derived fuel incineration, oil shale ash, waste concrete, waste marble dust, cement kiln dust and brines [9], [27]. This thesis and experimental work used LD steel slag from Mustajärvi supplied by Tapojärvi. Steel slag is produced when fluxing agents (e.g. limestone) are added to the furnace to remove impurities from the iron ore or steel. The mixture of these impurities and the fluxing agents, called slag, is lighter than the molten metal and floats on top and can be thus separated [3], [28]. Steel slag is often used as a raw material in cement and concrete production, however significant amounts are stockpiled or landfilled. Depending on the end application it is referred to as a by-product or waste material [29].

Fresh NH_4Cl solution is prepared by mixing NH_4Cl salt with tap water. A concentration of 1M is used as this has been found to give an optimum of calcium extraction efficiency whilst remaining selective towards calcium and avoiding the extraction of unwanted impurities and the need to wash the product. The extraction process is generally conducted over a period of 60 minutes at room temperature. This is beneficial as it avoids the need for heating and cooling which would increase the energy consumption and cost of the process. As a rule of thumb, for every kilogram of steel slag, about half a kilogram of PCC is produced.

3.2 Carbonation

In the carbonation process, CO_2 gas is fed into the calcium rich solution and solid calcium carbonate precipitates from the solution. The following reactions can occur during this process [28], [30]. Carbon dioxide reactions:

$$CO_2(g) \leftrightarrow CO_2(aq) \tag{8}$$

$$CO_2(aq) + H_2O(l) \leftrightarrow HCO_3^-(aq) + H^+(aq) \tag{9}$$

$$HCO_3^-(aq) \leftrightarrow CO_3^{2-}(aq) + H^+(aq) \tag{10}$$

$$CO_2(g) + OH^-(aq) \leftrightarrow HCO_3^-(aq) \tag{11}$$

Precipitation of calcium carbonate:

$$Ca^{2+}(aq) + CO_3^{2-}(aq) \rightarrow CaCO_3(s) \downarrow \quad (12)$$

$$Ca^{2+}(aq) + HCO_3^{-}(aq) \rightarrow CaCO_3(s) \downarrow + H^{+}(aq) \quad (13)$$

The reactions that describe the CO_2 are described as follows. CO_2 gas absorbs into the solution forming aqueous CO_2, eq.(8) and reacts with hydrogen dioxide to form bicarbonate and hydrogen ions, eq.(9). The bicarbonate then disassociates into carbonate and a further hydrogen ion, eq. (10). CO_2 can also react with hydroxide ions in the water to form bicarbonate, eq. (11). In the precipitation step, calcium ions react with carbonate ions to form the solid precipitated calcium carbonate, eq. (12). Likewise, bicarbonate ions can react with calcium ions to precipitate calcium carbonate, setting a hydrogen ion free in the process, eq. (13). Mattila 2012 did kinetic modelling to determine the equilibrium constants of these equations and found that the carbonation will mainly occur through the reaction of calcium and carbonate ions, with the bicarbonate ions just playing the role of providing more carbonate ions, as can be seen in eq. (10) [30].

The required CO_2 can be taken from cleaned flue gases of an industrial process thus reducing emissions and fixating it. In the pilot plant it comes from canisters, however, it can be mixed with nitrogen to better simulate flue gases which will not contain pure CO_2 but significant fractions of nitrogen and also other gases.

3.3 Pilot Plant Set up

The pilot plant (Figure 3.2) consists of three 200 litre reactors: an extraction reactor (ER) and two carbonation reactors (CR1 and CR2). The extraction reactor is equipped with a slag feeding system for the purpose of running continuous or semi-continuous experiments, however, the experiments conducted for this work were run only in batch mode. NH_4Cl solution is pumped into the extraction reactor and steel slag is added. The NH_4Cl solution can be freshly prepared solution from the fresh solvent tank, or recycled solution from a previous experiment stored in tank 2. After the extraction of calcium from the steel slag, the slurry is filtered by one of the extraction filters that can be seen in the diagram (1μm). In addition to this, the solution is then sent through a secondary filtration system which is not shown (two 1 μm filters and one 0,45 μm filter connected in series) before being sent to a storage tank 1 for the calcium-rich solution. These extra filters were added due to poor filtration performance during the commissioning of the system [13].

The calcium rich solution is then pumped to the carbonation reactor 1 (CR1), passing through a heat exchanger (HX1) along the way so it can be heated to the desired carbonation temperature. This is a plate heat exchanger heated or cooled by running tap water from the mains. The maximum temperature of the tap water is about 60 °C in summer and 80 °C in winter [13]. CO_2 is fed to the reactor through a gas sparger drilled with 1mm holes at the bottom of the reactor. The CO_2 is stored in gas bottles and can be mixed with N_2 in order to vary the concentration of CO_2 fed to the reactor as to better imitate the concentration of flue gases from a combustion process. The flow of the gas can be controlled using a rotameter. All of the reactors have agitators for mixing the solution. These consist of two blades at three levels in the reactors and can be operated at two speeds with a maximum speed of 202 rpm in

the extraction reactor and 170 rpm in the carbonation reactors. All reactors have temperature and pH readers connected to the computer system where the data is stored. Measurements are made at regular intervals (e.g. every 10 seconds) throughout the process and the temperature and pH profiles can be seen in real time on the computer.

After carbonation, the solution is filtered using filter bags in the PCC filter 1 or 2. The filtered solution goes to the solvent tank where it can be pumped to tank 2 for storage before being recycled again for the next extraction process. The purpose of the second carbonation reactor is that a small amount of calcium rich solution could be redirected there before carbonation and then later mixed with the filtered solution that has undergone carbonation in order to precipitate any leftover dissolved HCO_{3^-} so that it does not precipitate during the extraction phase if the solvent is recycled. In practice this was not a problem so this step is not used.

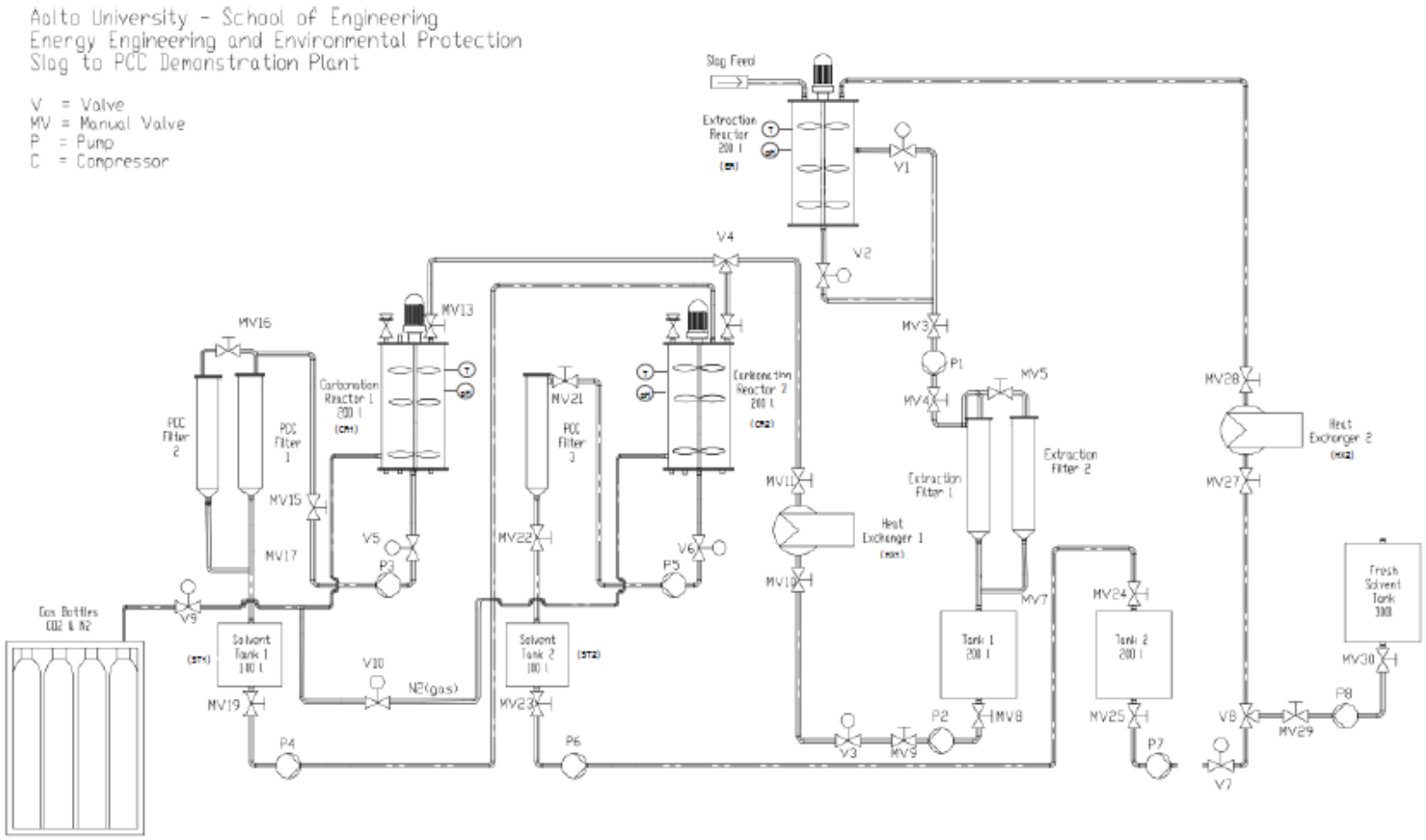

Figure 3.2: X2PCC pilot plant layout.

4 Precipitation kinetics

Crystallisation can be defined as a "phase change in which a crystalline product is obtained from a solution". Precipitation is a term generally used to describe "a relatively rapid formation of a sparingly soluble solid phase from a liquid solution phase" [31]. The distinguishing features of precipitation compared to other crystallisation processes include [14], [31], [32]:

- Precipitation processes are generally very fast crystallisation processes.
- Precipitates are usually produced as a result of chemical reactions and the products formed are often almost insoluble, implying an irreversible process (whereas crystallisation processes can often be reversed and the products redissolved at the original conditions).
- Precipitation is usually initiated at very high supersaturation levels, resulting in the creation of many small primary crystals. Agglomeration and ageing can have a big effect on the precipitates compared to crystallisation.

The X2PCC carbonation process involves a multiphase precipitation system (with reactants and products in solid, liquid and gaseous phases) with a number of physical-chemical processes taking place simultaneously making it quite complicated to model [33]. The presence of ammonium chloride in the calcium rich aqueous solution has a further effect on the process and cannot be neglected. The solution equilibria occurring in the carbonation process shall be described next and subsequently the precipitation process kinetics, which build from this, shall be described in detail.

4.1 Solution equilibria and equilibrium constants

A solution (gas, liquid or solid) is a mixture of two or more species forming a homogenous single phase. The term solvent commonly refers to the liquid components and solute which is solid at the conditions of interest [31]. In this work the solvent shall refer to the liquid solution (i.e. ammonium chloride, water, calcium ions, carbonate ions) and solute to the solid calcium carbonate. There are three kinds of equilibria occurring in a gas-liquid-solid system [34]:

- Gas-liquid equilibria between the gas and aqueous solution
- Ionic and/or chemical equilibria in the aqueous solution
- Solubility equilibria between crystals and the saturated aqueous solution

4.1.1 Activities and Ionic Strength

Activities are used to describe the deviation of a solution from ideal solution behaviour. They can be described as follows:

$$a_i = \gamma_i c_i \tag{14}$$

with the activity coefficient, γ, and the concentration, c, of the ion in question, i. In an ideal solution the activity coefficient can be assumed to be unity and the activity is equal to 1. It is

difficult to experimentally measure the activity of an ion in a solution. Generally only the mean activity coefficient of the solution can be measured as it is not possible to measure each of the individual ions. Various empirical and semi-empirical models exist to calculate the activity of an ion in a solution. These are limited in their range of applications, with the validity generally depending on the ionic strength of the solution. The ionic strength of a solution describes the concentration of ionic charge, as shown in eq. (15). It is used to reflect the effect of charges and interionic interactions when calculating electrolyte activities. [35], [36]

$$I = \frac{1}{2}\sum_{i} c_i z_i^2 \tag{15}$$

With c_i and z_i the concentration and charge of each ionic species i.

4.1.2 Gas-Liquid Equilibria

In the carbonation process, carbon dioxide gas is bubbled through the solution and is absorbed into the liquid. In order to know how much of this carbon dioxide is absorbed into the solution and involved in the precipitation process, it is necessary to know the solubility of carbon dioxide into the NH_4Cl-H_2O-Ca solution. The equilibrium constant for the gas-liquid solubility in a non-ideal solution can be described by:

$$K_{aq} = \frac{\gamma_l c_l}{f_g p_g} \tag{16}$$

With f, the fugacity of the gaseous species, p, the partial pressure of the gaseous species, γ and c, the activity coefficient and concentration, and the subscripts g, l and aq referring to gas, liquid and aqueous respectively. In practice, Henry's constant is often used in estimating the solubility of a gas in water. Henry's constant can be defined by:

$$k_H = \frac{c_{aq}}{p_g} \tag{17}$$

With c_{aq}, the concentration of the aqueous species and p_g, the partial pressure of that species in the gas phase. Tabulated values of Henry's constant for the solubility of CO_2 in water at standard conditions (25°C and atmospheric pressure) can be readily found. However, Henry's constant depends on the temperature and the ionic strength of the solution, so these cannot be directly used for the X2PCC carbonation process. Temperature dependent constants exist for adapting the solubility to different temperatures and the Sechenov constant can be used to describe the dependence of Henry's constants on the composition of a solution. However, Sechenov parameters are unknown for many species and do not always give accurate results in all systems [37], [38]. The temperature dependence of Henry's constant can be described with the following equation [35] [71].

$$k_H = k_H^{\theta}\, exp\left[C\left(\frac{1}{T} - \frac{1}{T^{\theta}}\right)\right] \tag{18}$$

with C, the temperature dependency parameter, T, the temperature, k_H, Henry's constant and the superscript, Θ, referring to standard conditions.

4.1.3 Ionic/Chemical equilibria

For an aqueous solution with the following reaction equilibrium [34]:

$$aA + bB = cC + dD \tag{19}$$

the ionic or chemical equilibrium can be shown to be [34]:

$$a\mu_A + b\mu_{\boldsymbol{B}} = c\mu_C + d\mu_D \tag{20}$$

with μ, the chemical potential. Using the activity coefficients, the equilibrium constant can be given by [34]:

$$K_{eq} = \frac{(\gamma_C c_C)^c (\gamma_D c_D)^d}{(\gamma_A c_A)^a (\gamma_B c_B)^b} \tag{21}$$

Mattila [30] calculated the equilibrium constants of the reactions occurring in the X2PCC process and Zappa [13] calculated the thermodynamic equilibrium constants and heat of reactions for the reactions occurring. It should be noted that both assumed activities to be one and made the calculations in terms of the concentrations. Both used the program HSC Chemistry 5 for making the calculations. In this work, however, the equilibria constant of interest is the solubility product explained in the following section.

4.1.4 Solubility equilibria between crystals and saturated solution

When we consider the solubility of calcium carbonate in our solution, represented by the equilibria of the following equation:

$$CaCO_3(s) = Ca^{2+}(aq) + CO_3^{2-}(aq) \tag{22}$$

the solubility product can be described by

$$K_{sp} = \frac{a^*_{Ca}\, a^*_{CO_3}}{a_{CaCO_3}} \tag{23}$$

where a, represents the respective activities, and * denotes at equilibrium conditions. If the $CaCO_3$ produced is a pure solid, then the activity is equal to one and the solubility product can be simplified to the following:

$$K_{sp} = a^*_{Ca}\, a^*_{CO_3} \tag{24}$$

Expressing this in terms of activity coefficients and concentrations:

$$K_{sp} = (\gamma^*_{Ca}\, c^*_{Ca})(\gamma^*_{CO_3} c^*_{CO_3}) \quad (25)$$

The activity based solubility product, K_{sp}, is different for each of the calcium carbonate polymorphs. It is also affected by many parameters such as temperature, pH, pressure and ionic strength of the system.

4.2 Supersaturation

In order for crystallisation to take place, the solution must be in a state of supersaturation [14]. In a solution, this occurs when the solute concentration in a solvent exceeds its solubility [40]. Supersaturation is the driving force for crystallisation. In a saturated solution the solid phase is in thermodynamic equilibrium. Solubility depends on the temperature of the solution as can be seen by the solubility curve in Figure 4.1. Generally solubility increases with temperature as is the case with this figure, however, it can also decrease in some cases. Below the solubility curve is a stable "undersaturated" region where crystallisation will not occur. Supersaturation is achieved when the concentration of solute in a solution at a given temperature exceeds the equilibrium concentration (i.e. the solubility line is crossed).

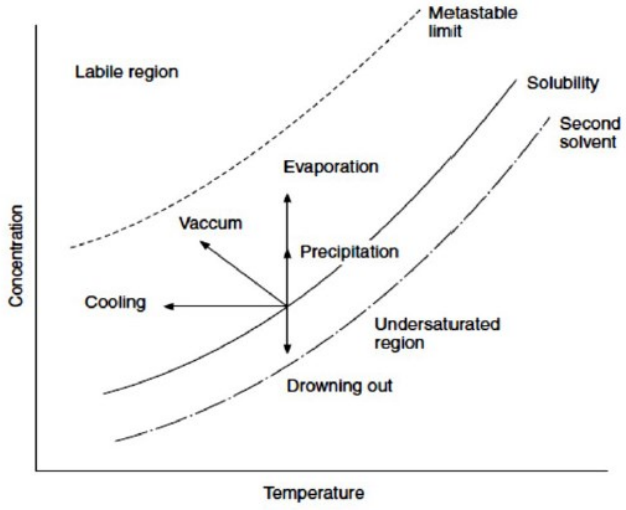

Figure 4.1: Solubility-supersolubility diagram [41]

Supersaturation can be achieved by [31], [40]:

- cooling the solution
- evaporating solvent from the solution
- putting the system under vacuum (causing the solution to cool and the solvent to evaporate)
- precipitation aka. chemical reaction (where two or more reactants react to produce a product of lower solubility)
- changing the solvent composition aka. drowning out (adding a third miscible component to change the solubility of the solute)

The effects of these five aforementioned different methods for achieving supersaturation (in other words crossing or moving the solubility line) are represented by arrows in the Figure 4.1. The X2PCC system is a precipitation system where supersaturation is achieved by bubbling carbon dioxide through a calcium rich solution to create an excess of carbonate and calcium ions that react together to form calcium carbonate.

Achieving supersaturation does not necessarily mean that crystallisation will start to spontaneously occur. The level of supersaturation and other factors (e.g. presence of other material in the solution) will dictate whether and when crystallisation will occur. This can be seen as an example in Table 4.1 which shows the length of time before the nucleation of water vapour based on the level of the supersaturation ratio. It can be seen that depending on the level of supersaturation, the induction time can vary from almost instantaneous to an almost infinite length of time. As is shown in Figure 4.1, after achieving supersaturation there is a metastable zone. In this area crystallisation is improbable, however, if a crystal seed were introduced growth would occur [14]. After passing the metastable limit, the unstable labile region is reached, where spontaneous crystallisation is probable (however not necessarily inevitable) [14].

Table 4.1 Induction time for nucleation of water vapour [31]

Supersaturation, S	Time
1.0	Infinity
2.0	10^{62} years
3.0	10^{3} years
4.0	0.1 seconds
5.0	10^{-13} seconds

Supersaturation can be expressed in a variety of ways, and is often described using the concentration driving force, Δc, the supersaturation ratio, S, the relative supersaturation, σ, or percentage supersaturation, 100σ. The relationship between these first three expressions is shown in the following equations, expressed in terms of concentration (note- this only applies to ideal solutions with an activity of 1).

$$\Delta c = c - c^* \tag{26}$$

$$S = \frac{c}{c^*} \tag{27}$$

$$\sigma = \frac{\Delta c}{c^*} = S - 1 \tag{28}$$

With c, the concentration of the solute, and c^*, the concentration at equilibrium conditions. In this work, chiefly the supersaturation ratio, S, is used. As can be seen in eq. (27), when S is equal to 1, there is a saturated solution and when $S > 1$ then supersaturation is achieved. When $S < 1$, the solution is undersaturated. The X2PCC system is not ideal, so activity coefficients must be taken into account and cannot be assumed to be 1. In the case of precipitation

systems, supersaturation is generated as a result of a chemical reaction between two or more reactants, resulting in the supersaturation ratio of a sparingly soluble electrolyte $A_{v+}B_{v-}$ to be described by [14], [31]:

$$S = \left(\frac{a_A^{v^+} a_B^{v^-}}{K_{sp}}\right)^{\frac{1}{v}} \qquad v = v^+ + v^- \tag{29}$$

Where a refers to the activity of the ionic species in the solution, v is the number of ions in a formula unit of salt, and K_{sp} refers to the activity-based solubility product (e.g. of the calcium carbonate polymorph in question). In some sources the ionic activity product $a_A^{v^+} a_B^{v^-}$ given in this formula is referred to as IAP [13], [14] or as π [31]. And in the case of our system, this can be rewritten as [42], [43]:

$$S = \sqrt{\left(\frac{\gamma_{Ca}\, c_{Ca} \cdot \gamma_{CO_3} c_{CO_3}}{K_{sp}}\right)} = \sqrt{\left(\frac{\gamma_{Ca}\, c_{Ca} \cdot \gamma_{CO_3} c_{CO_3}}{\gamma^*_{Ca} c^*_{Ca} \cdot \gamma^*_{CO_3} c^*_{CO_3}}\right)} \tag{30}$$

With γ, the activity coefficient and c, the concentration of the respective ion and * denoting equilibrium. Thus, in order to calculate the supersaturation ratio, the activities coefficients, concentrations and the solubility product should be known. The calculation of these shall be described in the "Modelling" chapter.

4.3 Nucleation

Supersaturated solutions are not in a state of equilibrium. In order to move to an equilibrium state, crystallisation occurs; the supersaturation is relieved by a combination of nucleation and crystal growth [31]. Nucleation refers to the "birth" of crystals. The nucleation process ultimately determines the number and size of crystals formed in a precipitation process [44]. Nucleation can be divided into primary and secondary nucleation as are shown in Figure 4.2. In the case of a precipitation system, secondary nucleation generally does not occur. The rapidly occurring precipitation in these systems is not affected by the presence of solute crystalline material. Due to the high supersaturation levels experienced in precipitation systems, nucleation plays a major role [31].

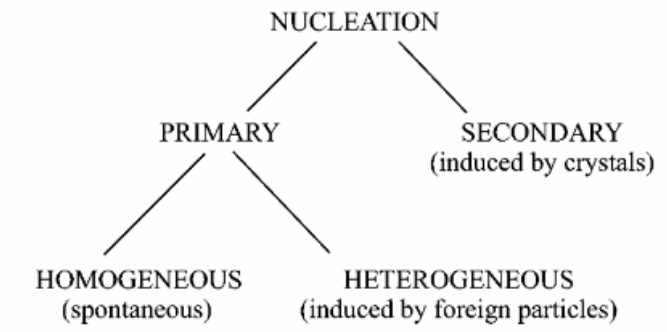

Figure 4.2: Description of nucleation mechanisms

4.3.1 Homogenous nucleation

In classical nucleation theory, homogenous nucleation is assumed to occur following an addition mechanism, where clusters are formed through the addition of atoms or molecules, *N*, until a critical size is reached [14], [31], [40]:

$$N + N \leftrightarrow N_2 \tag{31}$$

$$N_2 + N \leftrightarrow N_3 \tag{32}$$

...

$$N_{c-m} + N \leftrightarrow N_c \ (critical\ cluster) \tag{33}$$

Further additions to this critical cluster result in the nucleation and subsequent growth of the nucleus [14]. The formation of such clusters is due to local concentration fluctuations or areas of high supersaturation, which give rise to ordered microregions or clusters [31]. It should be noted that there are many different notations used by different sources when describing the kinetics of nucleation. In the following equations, the expressions by Myerson [31] and Randolph and Larson [40] were both referenced, however as both have differing notation, that of Myerson shall be used to avoid confusion. The free Gibbs energy change, ΔG, that occurs for a crystal to homogenously nucleate from a supersaturated solution can be described by [31]:

$$\Delta G = -N\Phi + A\sigma \tag{34}$$

With *N*, equal to the number of molecules or ions in the crystal, Φ, the reaction affinity, *A*, the area of the crystal ($A \sim N^{2/3}$) and σ, the surface tension. The reaction affinity can be described by:

$$\Phi = kT \ln\left(\frac{a}{a^*}\right) \quad \text{or} \quad kT \ln S \tag{35}$$

With *k* the Bolzmann constant, *T* the temperature, *a* the total activity of the solution, a^* the total activity of the solution at equilibrium and *S* the supersaturation ratio.

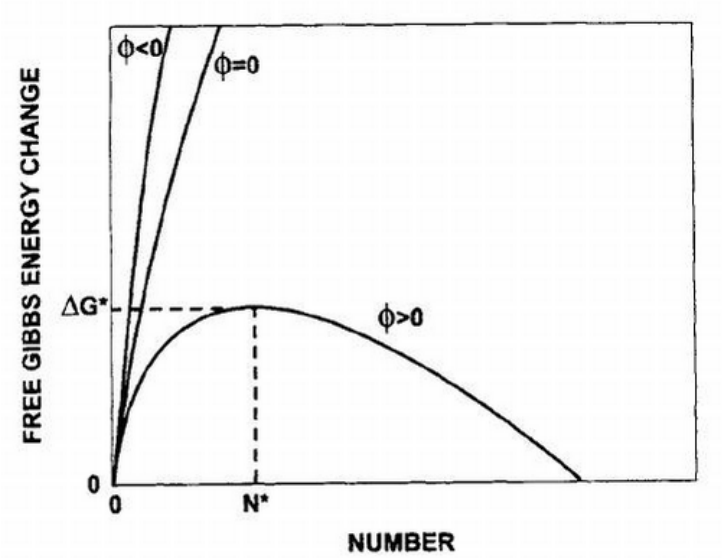

Figure 4.3: The free Gibbs energy change, *ΔG*, as a function of the number of ions or molecules forming a crystal. [31]

When we look at the term describing the change in free Gibbs energy *ΔG*, we can see that an increase in the number of molecules/ions *N* will lead to an increase in both the first term (always negative) and the second term (positive). When we look at this in the diagram above, we can see that the free Gibbs energy change increases initially as the *N* grows (i.e. the embryo-nucleus grows) until the point *ΔG*, N** (the point at which the critical size has been reached and a nucleus is formed) where it reaches a maximum, decreasing thereafter. The rate of the formation of these nuclei, *J*, can be described by an Arrhenius-type expression (similar to those representing the rate of a chemical reaction):

$$J = \Omega exp\left(-\frac{\Delta G^*}{kT}\right) \tag{36}$$

With *Ω* a preexponential factor reported to have values 10^{25} to 10^{30} for sparingly soluble salts [40] or 10^{25} to 10^{56} $s^{-1}m^{-3}$ according to [31]. To express the nucleation rate in terms of the supersaturation ratio and assuming a spherical critical embryo-nucleus, the expression is formed:

$$J = \Omega\, exp\left[\frac{-16\pi\sigma^3 v^2}{3k^3T^3(lnS)^2}\right] \tag{37}$$

With *v* representing the number of moles of ions formed from one mole of electrolyte (for a non-electrolyte *v*=1). According to Randolph and Larson, this equation only predicts nucleation at very high supersaturations, however, this is the case in some reaction precipitation systems. With this equation it becomes clear that the nucleation rate increases with increasing supersaturation and temperature and decreases with increasing surface energy [31]. Increasing supersaturation generally leads to smaller mean crystal size due to increased nucleation being favoured over growth [45].

4.3.2 Heterogeneous nucleation

Heterogeneous nucleation refers to nucleation in the presence of foreign substances. These can act as a catalyst to nucleation by reducing the surface tension, σ, as seen in the free Gibbs energy equation. Even with very "clean" systems, the presence of foreign substances can be significant, according to Myerson [31], even a liquid that has had physical impurities removed can contain 10^{13} to 10^{23} contaminants per m^3. An expression for heterogeneous nucleation based on the expression for homogenous nucleation has been proposed, however it should be noted that it has been criticised for its reliance on surface energy (interfacial tension), σ, which is probably of little physical significance at such small molecular assemblies [31].

$$J_{het} = \Omega_{het} \exp\left(-\frac{\Delta G^*_{het}}{kT}\right) \tag{38}$$

With $\Omega_{het} < \Omega$ and $\Delta G^*_{het} < \Delta G^*$.

Precipitation processes occur very quickly and are typically not affected by the presence of solute crystalline material (seeding) so secondary nucleation does not play a role [31] and shall not be discussed further here.

4.3.3 Ostwald's rule of stages

According to Ostwald's Law of Stages, for the crystallisation of a polymorphic material, the least stable polymorphs will form first (or even amorphous forms) and will transform into the more stable forms over time [32]. It should be noted that there are exceptions to this rule. A visualisation of this can be seen in Figure 4.4. The result of this is that if a sample is taken during the crystallisation process, it could be of a different crystalline phase than the end product.

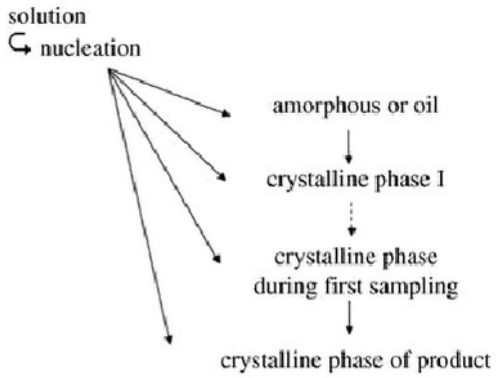

Figure 4.4: Ostwald's rule of stages-Nucleation of crystalline phases [32]

4.4 Growth

Once a nucleus of critical size has been formed it will start to grow into a crystal. The growth of crystals is very complex and there are many different theories for describing the mechanisms and growth rate of crystals, Markov 2008 can be referred to for an in depth

treatment of crystal growth [46]. Generally there are two sequentially occurring processes involved in the growth of crystals: a diffusion step and a surface integration step [14], [31]. The diffusion step involves the transport of growth units from the solution bulk to the surface of the crystal. Coming to the crystal surface, the solute must desolvate and the solvent must counterdiffuse away from the surface [14]. Close to the surface, surface integration mechanisms predominate over diffusion mechanisms and the growth units are incorporated into the crystal lattice [14], [31]. Depending on the rate of these two processes, the growth is controlled by either the diffusion step or the surface integration step [31].

4.5 Agglomeration and ageing

There are multiple terms often used interchangeably to describe the tendency of particles in a liquid suspension to cluster together including: "agglomeration", "aggregation", "coagulation", "loose agglomerates" and "flocculation" [14] [40] [47]. Here the definitions given by Randolph and Larson 1988 shall be used, where agglomerates refer to a "collection of two or more particles held together by strong interparticle forces" (e.g. crystal bonds) and aggregates or flocculates both refer to "a collection of two or more particles held together with weak cohesive forces" (e.g. Van der Waals forces). Agglomerates cannot be broken up unless forces are high enough to cause a fracture in the crystal whereas aggregates or flocculants can be broken up by shear forces and/or solvents [40].

Agglomeration is often high in precipitation systems due to the high particle density and supersaturation which increases the collision frequency and binding of particles [32]. Agglomeration can be distinguished as perikinetic (resulting from static fluid and particles in Brownian motion) and orthokinetic (resulting from agitated dispersions). In a stirred reactor, orthokinetic agglomeration is naturally predominant [14]. In the case of the X2PCC system, the reactor is stirred mechanically and also agitated by the bubbling of carbon dioxide. A small particle PCC size is desired, so agglomeration should be avoided as it leads to an increase in the average particle size and PSD. Schnebelen et al. 2015 [47], describe the mechanism through which agglomeration happens by the following three steps:

- "approach of the particles due to the Brownian movement or the reactor hydrodynamics";
- "collision of the particles thanks to electrostatic forces";
- "building of a crystalline bridge induced by crystal growth".

The agglomeration kernel β can be used to describe the agglomeration rate of a substance and can be determined by measuring the particle size distribution (PSD) by experimentation and solving a population balance. The agglomeration constant β_0 which is contained in the agglomeration kernel expression, "describes the tendency of a substance to agglomerate and takes into account the characteristics of the substance and the environment in which it evolves" [47]. Hostomsky and Jones 1991 found that the agglomeration of individual previously formed crystals was the dominant mechanism in increasing particle size at higher reagent concentrations as opposed to primary crystal growth.

Ageing refers to changes that happen to the precipitated crystals when left in the mother liquid over time. Ostwald ripening refers to the fact that when solid particles are dispersed in a saturated solution, there is a tendency for smaller particles to dissolve and be deposited on to larger particles, leading over time to a reduction in the number of crystals and a growth in the size of crystals and PSD. According to Mullin, this generally only occurs when the primary crystals are smaller than 1 μm. Another ageing process that can occur is phase transformation, resulting from Ostwald's rule of stages, where less stable polymorphs transform into more stable ones [14].

5 Carbonation Parameters

The following list shows an example of many parameters that could have an effect on the carbonation process and the PCC produced from it. The control of such a process is quite complicated due to the amount of parameters influencing it and also the fact that many parameters are interrelated with others.

- Temperature
- pH
- Agitation
- CO_2 (concentration, flow rate, dispersion method)
- Calcium concentration
- Shear rate (agitation, CO_2 bubble energy)
- Additives (presence or absence)
- Residence time
- Conductivity
- NH_4Cl concentration
- Ionic strength
- Pressure
- Seeding
- Calcium to carbonate ratio $[Ca_2^+]/[CO_3^{2-}]$
- Reactor type
- Post crystallization processing
- Supersaturation
- Batch, continuous, semi-batch
- Other (e.g. magnetic fields and microwave irradiation)

When considering the X2PCC process and pilot plant, key parameters were identified to be investigated for the basis of experiments and the analysis of results. The parameters were divided into primary, secondary and fixed parameters. Primary parameters can be directly controlled and changed in experiments. Secondary parameters are controlled indirectly by changing the primary parameters and can be measured or calculated accordingly. Fixed parameters are those which are key to the results and calculations, however do not change in any of the experiments.

Primary parameters:
- Temperature
- CO_2 concentration
- CO_2 flow rate
- Calcium concentration
- Residence time/end pH

Secondary parameters:
- Supersaturation
- Calcium to Carbonate Ratio $[Ca^{2+}]/[CO_3^{2-}]$

Fixed parameters:
- Agitation
- NH_4Cl concentration
- Pressure

The main interest of this thesis is to consistently produce PCC of a desired morphology (especially aragonite and scalenohedral calcite) with a small enough size. The following

section presents how carbonation parameters affect the morphology and size of PCC based on a literature review.

5.1 Aragonite production

Assessing the conditions required to produce pure aragonite was seen as key in this work. Interest in aragonite has increased substantially from the viewpoint of technical application (Lei et al. 2014) and it has many valuable applications e.g. as a biomedical material and as a filler due to some desirable qualities over calcite. It has also been successfully produced at a high concentration in a number of previous experiments at the X2PCC pilot plant, but the precise parameters causing this were unsure and pure aragonite has yet to be achieved. Thus an extensive review of literature was made to assess key parameters for the production of aragonite. The results of this are shown in the following table, with key observations marked in bold.

Table 5.1:Aragonite key parameters, effects and ranges from literature review

Parameter	Effect
Temp-erature	**Generally, it is agreed that high temperatures are favourable for the production of aragonite.** Han et al. 2006 [48] produced aragonite at 60°C (CO_2/N_2 gas in $CaCl_2$ solution) as did Hu and Deng 2003 [49] (sparingly soluble calcium sulphate as reactants), Altay et al. 2007 [50] isolated high fractions of aragonite above ca. 50°C (reacting calcium nitrate (calcium chloride) and sodium carbonate) and Matsumoto et al. 2010 [51] claimed aragonite is formed above temperatures of 50°C, according to Gupta 2004 [52], aragonite is formed predominantly at 70°C (from highly saturated aqueous solutions) and Carmona et al. 2004 [53] say the formation of aragonite is favourable at temperatures over 40°C. Li et al. 2014 [54] on the other hand produced it at room temperature (25°C) and found increasing the temperature reduced the aragonite concentration (40 % CO_2 in $CaCl_2$–NH_4Cl solution for 2 h, and then ageing for more than 12 h.). Experiments at the X2PCC pilot plant have previously produced high fractions of aragonite at a temperature of 45°C.
pH	**Generally, it is agreed that a high pH is favourable for the production of aragonite.** According to Hu et al. 2003 [49], a high pH has been found to favour the formation of aragonite. Liu et al. 2008 [55] prepared it at a pH of 9 and 60°C. Altay et al. 2007 [50] find pH to be the most important factor with the pH range of 10-12 giving rise to aragonite. At high temperatures (58 °C) almost pure aragonite was also produced at a pH lower than 10. Matsumoto et al. 2010 [51] claim high pHs are favourable for producing aragonite and observed aragonite crystallization at a solution pH of 9.3 and aragonite as the major product from the pH range 9.7 to 10.5. Kitamura et al. 2002 [56] produced aragonite from a highly alkaline solution of pH 13,5.
Residence time and ageing time	**Generally, shorter carbonation times are thought to favour aragonite,** as it is metastable in structure and transforms into steady state calcite. However, Li et al. 2014 [54] found in their experiments that longer ageing times (greater than 2h) favoured aragonite and shorter times favoured calcite and vaterite. This was performed at room temperature and they theorise that a possible reason may be the influence of NH_4 ion impurities in the solution or the longer ageing time. Franke and Mersmann 1995 [42] also found that long residence times favoured aragonite formation. Ageing time is also a critical factor in the morphosynthesis of $CaCO_3$. According to Altay et al. 2007 [50], long ageing is known to enhance the recrystallization of initially formed aragonite into calcite, leading as well to an increase in average particle size as a consequence of Ostwald ripening. They found that shorter ageing times were observed to favour aragonite formation.
Super-saturation	**Generally, it is agreed that lower supersaturation favours the formation of aragonite.** This also agrees with the fact that higher temperatures favour aragonite-higher temperatures result in lower supersaturation (see results of supersaturation modelling). Franke and Mersmann 1995 [42], found that low reactant concentrations (which would result in lower supersaturation) favour aragonite formation. They measured supersaturations in the range of 2.2-6. Hu and Deng 2003 [49] formed needle like aragonite in a low supersaturation region, Altay et al. 2007 [50] likewise concluded that the formation at higher temperatures is attributed to a decrease in supersaturation conditions. Kitamura et al. 2002 [56] also state that aragonite is formed at low supersaturation.

Additives	**Additives can be used to promote aragonite, most notably magnesium**. According to Hu and Deng 2003 [49], among inorganic additives, much attention has been paid to magnesium-containing compounds. Also many chelating agents have been studied to improve the formation of aragonite. Altay et al. 2007 [50] tested with PDDA, CTAB, and EDTA and found they all suppressed aragonite formation. Matsumoto et al. 2010 [51] claims that impurities such as Mg2+ tend to favour the generation of aragonite and investigations have found with the presence of Mg2+, Ni2+, Co2+, Fe3+, Zn2+, and Cu2+ as trace impurities the metastable aragonite tended to crystallize. Lei et al. 2006 [57] produced aragonite in mixed solutions of different organic solvents and water in the presence of CTAB at 80°C and found that pure aragonite was obtained in the presence of 20% glycol, glycerine, glycol-methyl ether solution with CTAB at 80 °C, respectively. They deduce that "at high temperature (e.g. 80 °C), the amphiphilic property of organic solvent is a crucial factor in influencing the crystal forms and morphologies of $CaCO_3$ particles and is in favour of forming aragonite." Kobe et al. 2002 [58] found the presence of impurity ions such as Cu and Si are preferential for the formation of aragonite and vaterite. Kitamura 2001 [59] reports the effect of the magnesium ion on accelerating the crystallisation of aragonite. However, he also found calcite and vaterite to precipitate in the presence of the magnesium ion. Kawano et al. 2009 [60] describes that the addition of ions such as Mg2+ which can form a solid solution with calcite inhibit calcite formation and promote aragonite formation whereas ions such as Ba2+ form a solid solution with aragonite, resulting in the opposite. Isopescu et al. 2010 [61] claim that the use of nonionogen additives increased the concentration of aragonite.
Other	**Microwave irradiation and magnetic fields could promote aragonite formation**. Rizutti and Leonelli 2008 [62] use microwave irradiation for producing aragonite from a calcium bicarbonate solution. According to Knez and Pohar 2005 [63], magnetic treatment favours the precipitation of aragonite. Kobe et al. 2002 [58] produce aragonite applying magnetic fields (between 0,4 and 1,5 mT) to a bicarbonate solution. Cefalas et al. 2008 [64] claim that the "transfer of energy from the magnetic field to the flow drives the system to a state of higher energy during the initial stage of crystallization, favouring crystallization of $CaCO_3$ in the form of aragonite". Alimi et al. 2007 [65] quotes that the precipitation in the presence of a magnetic field is marked by a slower nucleation rate and a faster crystalline growth, favouring aragonite over vaterite and calcite. Kitamura et al. 2002 [56] also found an increase in solution volume and stirring rate effective for the increase of discrete needle-like aragonite and the decrease of agglomerated fine calcite.
CO_2	Li et al. 2014 [54] extracted calcium from dolomite using a $CaCl_2$–NH_4Cl solution and produced aragonite at room temperature with a concentration of 40% CO_2. Matsumoto et al. 2010 [51] produced it mixing CO_2 with NH_3 and found at a low ratio and small bubble size aragonite was maximised. It could be that lowering the CO_2 concentration and/or flow rate could favour aragonite by leading to a lower carbonate concentration in the carbonation solution and hence lower the supersaturation.

5.2 Scalenohedral calcite production

According to Ukrainczyck et al. 2007 [33], a higher [Ca]/[CO_3] ratio favours scalenohedral crystals over rhombehedral. Higher supersaturation favours the formation of calcite according to Hu and Deng 2003 [49], and according to Matsumoto et al. 2010 [66]. Carmona et al. 2003 [67] likewise found that an increase of [Ca]/[CO_3] ratio and an increase of supersaturation favours scalenohedral over rhombohedral. They succeeded in producing scalenohedral PCC at 30, 45 and 60°C. Cizer et al. 2012 [68] found that an excess of calcium ions and a high pH lead to the formation of scalenohedral. They found that longer exposure times to CO_2 and higher CO_2 pressures favoured rhombehadral over scalenohedral morphology. Sun et al. 2011 [69] produced scalenohedral PCC at room temperature found that an increase of the carbonation temperature (20-80°C) led to a gradual change from scalenohedral to rhombohedral calcite. Within the X2PCC project, Mattila 2014 [22] produced scalenohedral at laboratory scale with 0,01M ammonium chloride solution at 45°C. Martinez Miras 2016 [26] tried to recreate these conditions at the pilot scale but was not successful in producing pure scalenohedral. It was found in labatoratory scale experiments that the tests with the lowest CO_2 flow rates had the most promising results for scalenohedral. Zappa 2014 [13] also tried to reproduce these experiments of Mattila, as well as those from US patents by Fairchild and Kroc 1997 [70] and Bleakey and Jones 1993 [71] to produce scalenohedral but was also unsuccessful.

	Extraction				Carbonation					
Test	Solvent (L)	SLR (g/L)	Slag (kg)	[NH_4Cl] (M)	Solution (L)	Starting T (°C)	Agitation (rpm)	CO_2 Flow (L/min)	CO_2CR (min^{-1}) Est.	Act.
HPM Test	150	100	15	1.0	126	20	55	3[a]	-	0.0032
Scal-Test	150	50	7.5	1.0	120	50	170	14[b]	0.028	0.024
Arag-Test	150	50	7.5[d]	1.0	114	58	170	13[c]	0.028	0.023

a) CO_2 flow scaled up from laboratory flow using GLR= 0.018 L CO_2/L.min
b) CO_2 flow set based on estimated [Ca^{2+}] of 0.18M and setting CO_2CR in the typical range employed in Kroc and Fairchild [142] (0.028 min^{-1})
c) CO_2 flow set based on estimated [Ca^{2+}] of 0.18M and setting CO_2CR in the typical range employed in Kroc and Fairchild [142] (0.028 min^{-1})
d) Slag added stage-wise in three 2.5 kg increments, waiting 5 minutes after each addition

Table 5.2: Test conditions to produce scalenohedral in Zappa's work [13]. HPM Test refers to the reproduction of Mattila's laboratory scale experiments [22] and the Scal-test is based on the US patents by Fairchild and Kroc 1997 [70] and Bleakey and Jones 1993 [71].

According to Zappa's research the production of scalenohedral PCC by carbonation of Ca(OH)2 typically rely on the use of additives such as monosaccharides (e.g. fructose, glucose), disaccharides (e.g. sucrose), polysaccharides (e.g. starch) at a level of 0.1-0.5 wt%, or amines such as triethanolamine, mannitol, N-ethyl diethanolamine added during the slaking of quicklime or prior to carbonation [13].

5.3 Particle size and nano PCC

The PCC particles currently produced by the X2PCC process are too large by two orders of magnitude compared to commercially available grades. A literature review was made on how the carbonation parameters affect the size of PCC. Additionally, nanosized PCC (less than 100nm) is sought after in industry and literature was investigated for conditions favourable to

producing this. It was found that high levels of supersaturation lead to smaller mean crystal size due to increased nucleation being favoured over growth [13], [45], [72]. Conversely to this Ukrainczyk et al. 2007 [43] found higher supersaturation (measured by following conductivity) leads to a larger SSA and mean diameter. It was also found that higher levels of supersaturation can lead to higher agglomeration [43], [73] which ideally should be avoided. According to Ukrainczyk et al. 2007 [43], increased temperature leads to smaller particle size and SSA. This conflicts with the supersaturation, as higher temperatures result in lower supersaturation. According to Ukrainczyk et al. 2007 [43], low temperature (25°C) and high supersaturation favours nano PCC.

According to Xiang et al. 2004 [19], it is expected that a faster carbonation rate is necessary for synthesising nano PCC and one method to accelerate the carbonation process is by enhancing the absorption of CO_2 bubbles. They found that reducing the nozzle size (2mm, 1mm and 0,7mm were used) of the CO^2 feeding led to the formation of smaller particles. They hypothesise that this could be due to the fact that finer bubbles produced by the smaller nozzles were favourable for the dispersion and mass transfer of CO^2 bubbles. The morphology of the calcite produced was unaffected by nozzle size [15]. Xiang et al. 2004 also investigated the effect of stirring speed on the morphology and size of PCC from carbonation process. They found that an increase in stirring speed lead to a decrease in particle size and that lower stirring speeds favoured spindly particles mixed with spherical particles whereas higher speeds produced spherical particles. They explain this by the improvement of mass transfer of CO_2 bubbles in the $Ca(OH)_2$ slurry due to higher stirring speeds, which is favourable for the formation of spherical particles.

Schnebelen et al. 2015 [47] claim that the shear rate can be an important factor in the agglomeration of PCC particles. The shear rate depends on the kinematic viscosity of the suspension, the specific energy from mechanical agitation and the specific energy from gas bubbling. They studied the effect of shear rate on the agglomeration constant, β_0, during the carbonation of PCC and found that it initially increases with shear rate, reaches a maximum and then reduces. They explain this tendency because increasing the shear rate increases the relative speed of the particles and the probability of a collision increases, leading to the initial increase, however, the mechanical constraints on the crystalline bridges leads to a separation of the agglomerated particles, thus we see a maximum.

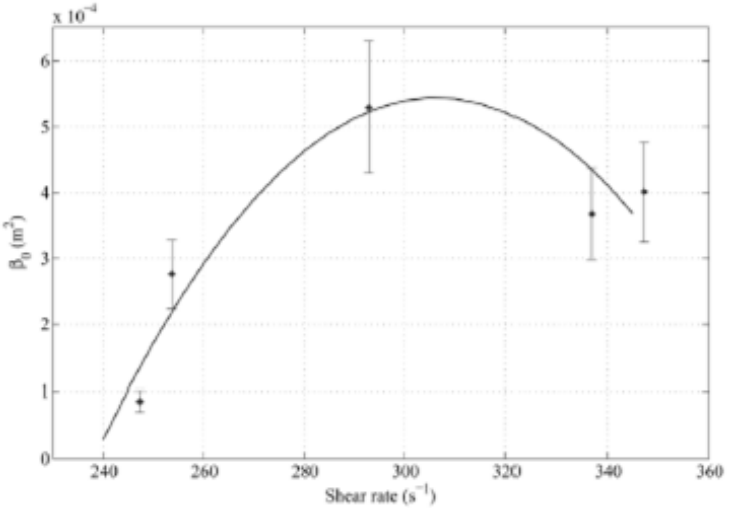

Figure 5.1: Agglomeration kernel as a function of the shear rate [47].

They use the following formulae for calculating the shear rate:

$$\dot{\gamma} = \sqrt{\frac{\varepsilon_M + \varepsilon_G}{\upsilon}} \tag{39}$$

With υ the kinematic viscosity of the suspension, ε_M the specific energy from mechanical agitation and ε_G the specific energy from gas bubbling. Finally, Sonawane et al. 2008 [74] found it was possible to reduce particle size when synthesising PCC with the assistance of ultrasonication over conventional methods of preparation. The particles were also reduced with an increase in the concentrations of $Ca(OH)_2$ and increasing CO_2 flow rate with both methods.

6 X2PCC precipitation kinetics and modelling

There are two main theories relating to the carbonation of PCC, the "film model" and the "clear film model". Ponzo 2015 [41] conducted a review of different studies that have been made on the carbonation of calcium carbonate and modelled the process based on these, describing them as the following. The clear film model assumes that the kinetics of reactions and crystallisation in the diffusion layer of the gas-liquid interface are very slow and can be neglected. Thus the nucleation and growth occur mainly in the bulk fluid. The film model assumes that there is an area (film) of very high supersaturation surrounding the carbon dioxide bubble, and nucleation occurs mainly in the film before being diffused into the bulk fluid. Schnebelen et al. 2015 found the film model held for their system, the batch carbonation of a lime solution. They found that nucleation predominantly occurs in the liquid film between the liquid bulk and gas phase. This is due to the high Hatta number (2,9) of the gas-liquid reaction. In this liquid film, the supersaturation and hence nucleation rate are extremely high. The PCC produced in the film then diffuses into the bulk liquid. Any non-precipitated calcium carbonate in the bulk is highly diluted, due to the fact that the film volume is much smaller than the suspension volume (a ratio of about 10^{-5}). As a result of this, the bulk has a very low supersaturation and hence an insignificant nucleation rate. The crystals in the bulk grow very slowly, however this growth consumes reactants from the bulk solution, further decreasing supersaturation and slowing the growth rate, resulting in a small PCC crystal size [75]. The Hatta number (Ha) is a dimensionless parameter that compares the rate of reaction in a liquid film to the rate of diffusion through the film, and is described with the following equation by Schnebelen et al. 2015 [75]:

$$Ha^2 = \frac{(2kC_{\mathrm{Ca(OH)_2}}D_{CO_2})}{k_L^2} \tag{40}$$

with k, the kinetic constant of the chemical reaction between the hydroxyl ions and carbon dioxide, $C_{\mathrm{Ca(OH)_2}}$, the solubility of calcium hydroxide, D_{CO_2}, the diffusivity of carbon dioxide, and k_L the mass transfer coefficient. Thus it could be hypothesised that the precipitation kinetics of the X2PCC process follows one of these aforementioned models, or a combination of both.

6.1 Modelling

Since the level of supersaturation is seen as integral in the carbonation process and controlling the products coming from this, it was important to find a way to measure and calculate this. As was seen in eq. (41), the supersaturation of the carbonation process depends on the activity coefficients, γ_{Ca} and γ_{C0_3}, the concentrations, c_{Ca} and c_{C0_3}, and the activity based solubility product, K_{sp}. Of these parameters, only the concentration of calcium can be measured directly from the experiments. Thus the activity coefficients, carbonate concentration and solubility product needed to be determined. The methods for this are presented in the following subsections and the resulting supersaturation models can be seen in the results chapter. In addition, research was made into different modelling methods that could be useful in

understanding the X2PCC carbonation process further. These are presented at the end of this chapter.

$$S = \sqrt{\left(\frac{\gamma_{Ca}\, c_{Ca} \cdot \gamma_{CO_3} c_{CO_3}}{K_{sp}}\right)} = \sqrt{\left(\frac{\gamma_{Ca}\, c_{Ca} \cdot \gamma_{CO_3} c_{CO_3}}{\gamma^*_{Ca} c^*_{Ca} \cdot \gamma^*_{CO_3} c^*_{CO_3}}\right)} \tag{41}$$

6.2 Concentration of Carbonate

As the concentration of carbonate ions in the solution could not be measured, the following assumption was made that the concentration of carbonate equals that of the carbon dioxide absorbed into the solution.

$$CO_3 \approx CO_2(aq) \tag{42}$$

Data on the solubility of CO_2 in NH_4Cl aqueous solutions at different concentrations and temperatures was found [76]. However, only the experimental data of Gerecke 1969 [77] encompassed the temperatures and NH_4Cl concentrations used in the carbonation process. Figure 6.1 shows the solubility of CO_2 based on Gerecke's data for 1M NH_4Cl, compared to the solubility of CO_2 in pure water.

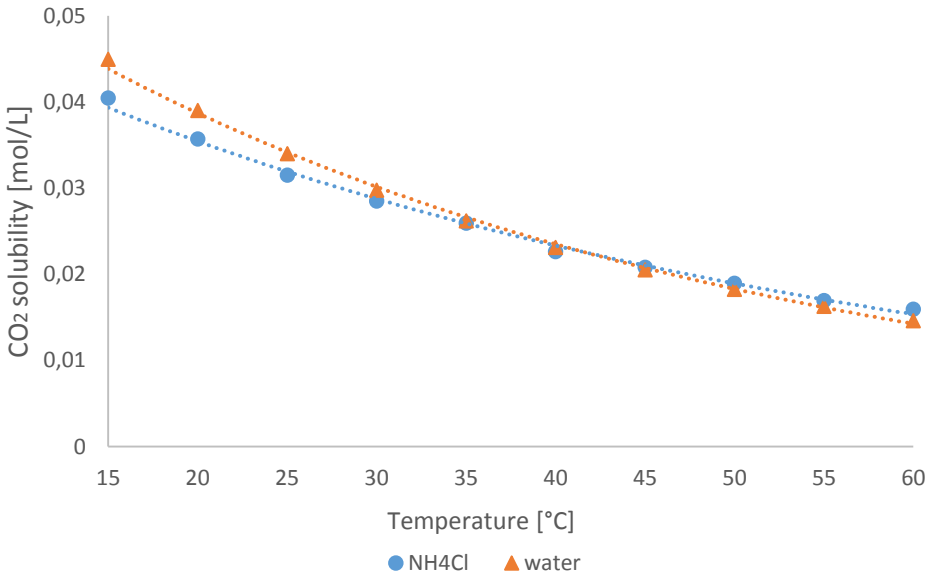

Figure 6.1: CO_2 solubility in water (based on Henry's constant) and in a 1M NH_4Cl solution (based on data from Gerecke 1969) with increasing temperatures [77].

Comparing these results, it can be seen that the difference in solubility of CO_2 in pure water compared to 1M NH_4Cl solution is very small. It should be noted though, that these values do not account for the presence of calcium ions in the solution. Due to a lack of data on CO_2-Ca-NH_4Cl-H_2O solutions, the presence of calcium was neglected. The calculation of the solubility of CO_2 in water in the above graph was based on Henry's constant, defined as:

$$k_H = \frac{c_{aq}}{p_g} \tag{43}$$

With c_{aq}, the concentration of the aqueous species and p_g, the partial pressure of that species in the gas phase. Tabulated values of Henry's constant at standard pressure can be found in literature. The values of CO_2 in water at different temperatures was calculated with the following temperature dependence equation [35] [71]:

$$k_H = k_H^{\Theta}\, exp\left[C\left(\frac{1}{T} - \frac{1}{T^{\Theta}}\right)\right] \tag{44}$$

with C, the temperature dependency parameter, T, the temperature, and the superscript, Θ, referring to standard conditions. The values k_H^{Θ} of 0,0034 mol/Latm and C of 2400K were used [37].

The solubility data given by Gerecke had to be converted as it was in terms of the Bunsen coefficient, α. The Bunsen coefficient is defined as the volume of gas reduced to 273,15K and 1 atmosphere pressure which is absorbed per unit volume of solvent (at the temperature of measurement) under a partial pressure of 1 atmosphere [78]:

$$\frac{V(g)}{V(l)} = \frac{\alpha T}{273{,}15} \tag{45}$$

With $V(g)$ the volume of gas absorbed, $V(l)$ the original volume of the solvent, and T, the actual temperature. The CO_2 solubility was converted from this volume basis to a molar concentration basis using the ideal gas law ($V = \frac{nRT}{p}$) as follows:

$$CO_{2(aq)}\left(\frac{mol}{L}\right) = \alpha \frac{p}{RT}\frac{T}{273{,}15} = \frac{\alpha p}{273{,}15R} \tag{46}$$

With p, the pressure, R, the universal gas constant.

6.3 Activity Coefficient Modelling

For the calculation of the activity coefficients, the Pitzer method was used. In order to judge the accuracy of the results, the activity coefficients were additionally computed with the Bromley model and the results of both compared. A simplification was made for the calculations that only the main ions of the system, namely Ca^{2+}, CO_3^{2-}, Cl^- and NH_4^+, were considered and other ions that may exist in the solution or the water were neglected. This was due to the complexity of the equations and the difficulty in finding the relevant parameters needed in the models for all the individual ions.

The original theory on calculating activity coefficients is the Debye-Hückel theory which was introduced in 1923. This is also the foundation for the work done on developing subsequent

models for calculating activity coefficients [34]. The original model assumes ions to be point charges in a continuous dielectric system and only takes long-range interactions into account, making it only valid for systems with very low ionic strengths [79]. Extensions to the original Debye-Hückel model were made in order to make it applicable at higher ionic strengths. An overview of the equations of the original Debye-Hückel and various extensions of this, as well as their validity ranges are shown in Table 6.1 [34]:

Table 6.1: Debye-Hückel models and validity ranges

Model	Equation	Validity
Debye-Hückel	$log\gamma_{\pm} = -A\lvert z_+ z_- \rvert\sqrt{I}$	I<0,001
Extended Debye-Hückel	$log\gamma_{\pm} = -\frac{A\lvert z_+ z_- \rvert\sqrt{I}}{1+\beta a\sqrt{I}}$	I<0,1
Güntelberg	$log\gamma_{\pm} = -\frac{A\lvert z_+ z_- \rvert\sqrt{I}}{1+\sqrt{I}}$	I<0,1
Guggenheim	$log\gamma_{\pm} = -\frac{A\lvert z_+ z_- \rvert\sqrt{I}}{1+\sqrt{I}} + Bm$	
Davies	$log\gamma_{\pm} = -A\lvert z_+ z_- \rvert\left(\frac{\sqrt{I}}{1+\sqrt{I}} - 0{,}3I\right)$	I<0,5

With I, the ionic strength, z, the ion charge and A, the Debye-Hückel constant [80]:

$$A = \frac{1}{2{,}303}\left(\frac{e}{\sqrt{DkT}}\right)^3\sqrt{\frac{2\pi N_0\rho_w}{1000}} \qquad (47)$$

Here e is the absolute electronic charge, D, the static dielectric constant of pure water, T, the temperature in Kelvins, N_o, Avogadro's number, ρ_w, the density of water and k, the Boltzmann constant. Due to the high ionic strength ($I > 1$) of our system, these simpler equations are not applicable. However, they are still shown here as the subsequent models used build up from this theory. Debye-Hückel theory has been used by different literature sources in calculating the activity coefficients for $CaCO_3$ precipitation. The Davies equation was used by Rigopolous and Jones 2003 in the gas-liquid precipitation of $CaCO_3$ in a bubble column reactor [81], by Collier and Hounslow 2004 in calcite precipitation from seeded batch experiments [82] and by Beck et al. 2013 [83]. Pitzer theory has also widely been used for $CaCO_3$ precipitation systems [83]–[86]. The Bromley method has likewise been used for $CaCO_3$ and other similar precipitation processes [42], [87], [88].

Pitzer

The Pitzer model is widely used by chemical engineers and geochemists to calculate the activity coefficients in electrolyte solutions with high ionic strengths [89], [90]. The model uses semi-empiric equation systems to describe the non-ideal behaviour [91]. The Pitzer equations are quite complex and there are variations in the way they are expressed, and the notations used, depending on the source material. The calculations used in this work were

based on those given by Plummer et al. 1988 [92], the respective page numbers are given beside this reference for the following equations. The natural logarithm of the activity coefficient of the cation in question, $ln\gamma_M$, and the anion in question, $ln\gamma_X$, are defined as follows [92, p.2]:

$$ln\gamma_M = z_M^2 F + \sum_a m_a(2B_{Ma} + ZC_{Ma}) + \sum_c m_c(2\Phi_{Mc} + \sum_a m_a\psi_{Mca}) + \sum_{a<}\sum_{a'} m_a m_{a'}\psi_{aa'M} + |z_M|\sum_c\sum_a m_c m_a C_{ca} \quad (48)$$

$$ln\gamma_X = z_X^2 F + \sum_c m_c(2B_{cX} + ZC_{cX}) + \sum_a m_a(2\Phi_{Xa} + \sum_c m_c\psi_{Xac}) + \sum_{c<}\sum_{c'} m_c m_{c'}\psi_{cc'X} + |z_X|\sum_c\sum_a m_c m_a C_{ca} \quad (49)$$

With *z*, the charge, and *m*, the molality and of the ion in question. The subscripts *M*, *c* and *c'* denote cations and *X, a* and *a'* denote anions. The double summations *c* < *c'* and *a* < *a'* refer to pairs of dissimilar cations and ions. The parameters Φ and ψ are for aqueous mixtures of two salts, with Φ accounting for cation-cation and anion-anion interactions and ψ accounting for cation-cation-anion and anion-anion-cation interactions. These two parameters were neglected from calculations as the relevant parameters for the ions in our system could not be found. Thus the above equations are simplified somewhat, with all terms containing Φ and ψ now equal to zero.

$$ln\gamma_M = z_M^2 F + \sum_a m_a(2B_{Ma} + ZC_{Ma}) + |z_M|\sum_c\sum_a m_c m_a C_{ca} \quad (50)$$

$$ln\gamma_X = z_X^2 F + \sum_c m_c(2B_{cX} + ZC_{cX}) + |z_X|\sum_c\sum_a m_c m_a C_{ca} \quad (51)$$

The remaining parameters *F*, *B*, *Z* and *C* are shown as follows [92, p.3]:

$$F = -A^\phi\left[\frac{\sqrt{I}}{1+b\sqrt{I}} + \frac{2}{b}\ln\left(1+b\sqrt{I}\right)\right] + \sum_c\sum_a m_c m_a B'_{ca} + \sum_{c<}\sum_{c'} m_c m_{c'}\Phi'_{cc'} + \sum_{a<}\sum_{a'} m_a m_{a'}\Phi'_{aa'} \quad (52)$$

With *I*, the ionic strength, eq. (15), and *b* equal to 1,2. As discussed above, the last two terms containing Φ are neglected, resulting in the following simplified equation:

$$F = -A^\phi\left[\frac{\sqrt{I}}{1+b\sqrt{I}} + \frac{2}{b}\ln\left(1+b\sqrt{I}\right)\right] + \sum_c\sum_a m_c m_a B'_{ca} \quad (53)$$

A^ϕ is defined by Pitzer to be equal to the Debye-Hückel constant in eq. (47), but with the first term $\left(\frac{1}{2{,}303}\right)$ replaced by $\left(\frac{1}{3}\right)$ [92, p.2]:

$$A^{\phi} = \frac{1}{3}\left(\frac{e}{\sqrt{DkT}}\right)^3 \sqrt{\frac{2\pi N_0 \rho_w}{1000}} \tag{54}$$

Bradley and Pitzer 1979 [93] listed temperature dependent values for A^{ϕ} which were used in the calculations. It should be noted that in some literature, archaic units are used for the Debye-Hückel constant, which can result in confusion when calculating using modern SI units. *B* and *B'* for any salt containing a monovalent ion are defined as [92, p.3]:

$$B_{MX} = \beta_{MX}^{(0)} + \beta_{MX}^{(1)} g\left(\alpha\sqrt{I}\right) \tag{55}$$

$$B'_{MX} = \frac{\beta_{MX}^{(1)} g'\left(\alpha\sqrt{I}\right)}{I} \tag{56}$$

And for 2-2 electrolytes and higher valence types as [92, p.4]:

$$B_{MX} = \beta_{MX}^{(0)} + \beta_{MX}^{(1)} g\left(\alpha_1\sqrt{I}\right) + \beta_{MX}^{(2)} g\left(\alpha_2\sqrt{I}\right) \tag{57}$$

$$B'_{MX} = \frac{\beta_{MX}^{(1)} g'\left(\alpha_1\sqrt{I}\right)}{I} + \frac{\beta_{MX}^{(2)} g'\left(\alpha_2\sqrt{I}\right)}{I} \tag{58}$$

For interactions involving monovalent ions, α_1=2 and the last term in both equations falls away. For interactions involving 2-2 electrolytes (i.e. in the case of Ca^{2+} and CO_3^{2-}), α_1=1,4 and α_2=12. The functions *g(x)* and *g'(x)* are defined as follows, with *x* substituted with the relevant parameters shown in the previous equation [92, p.4]:

$$g(x) = \frac{2[1 - (1 + x)e^{-x}]}{x^2} \tag{59}$$

$$g'(x) = \frac{-2\left[1 - \left(1 + x + \frac{1}{2}x^2\right)e^{-x}\right]}{x^2} \tag{60}$$

The coefficient *Z* is given by [92, p.4]:

$$Z = \sum_i m_i |z_i| \tag{61}$$

And the coefficient C_{MX} is given by [92, p.4]:

$$C_{MX} = \frac{C_{MX}^{\phi}}{2\sqrt{|z_M z_X|}} \tag{62}$$

Thus, in order to calculate all of the above equations, the Pitzer interaction parameters (β_0, β_1, β_2, C_ϕ) need to be found for all ions in the system. A literature review was conducted to find these and the results are presented in Table 6.2. The majority came from Plummer et al. 1988

[92] who conducted an extensive literature review when compiling data for a computer program to calculate geochemical reactions in brines. The source reference from his publication is shown in circle brackets in the reference column.

Table 6.2: Pitzer interaction parameters collected from literature

Ion pair	Parameters from literature				Reference
at 25°C	β_0	β_1	C_ϕ	β_2	
NH_4^+ / Cl^-	**0,05192**	**0,19346**	**-0,00298**		[86], [90]
	0,05191	0,17937	-0,00301		[94]
	0,522	0,1918	-0,00301		[92, p.165] (89)
	0,3603	0,29619			[92, p.165] (5)
	0,04568	0,20431	-0,01731		[92, p.165] (10)
Ca^{2+} / Cl^-	**0,3159**	**1,614**	**-0,00034**		[92, p.166] (48)
	0,3159	1,614	-0,00034		[92, p.166] (49)
	0,3159	1,614	-0,000339411		[92, p.166] (89)
	0,30534	1,7083	0,002153		[92, p.166] (82)
	0,3053	1,708	0,000761		[92, p.166] (85)
	0,31231	1,64585			[92, p.166] (5)
	0,41328	0,53043	-0,01425		[92, p.166] (10)
Ca^{2+} / CO_3^{2-}	**0,16**	**2,1**		**-69**	[92, p.169] (107)
	-11,9				[92, p.169] (75)
NH_4^+ / CO_3^{2-}	**0,1288**	**1,433**	**0,0005**		[92, p.169] (114)

The parameters chosen are shown in bold. These parameters were chosen based on the fact that they were used in literature, the values from multiple sources agreed and/or that they were the only ones available [86], [90], [92], [94]. These parameters are defined for a temperature of 25°C. The temperature dependence for some of these parameters were given by Plummer et al. [92] and is shown in Table 6.3, once again with the values used marked bold.

Table 6.3: Temperature dependence of Pitzer parameters

Ion pair	$d\beta_0/dT$	$d\beta_1/dT$	dC_ϕ/dT	$d\beta_2/dT$	Reference
NH_4^+ / Cl^-	**7,79E-05**	**1,26E-03**	**2,10E-05**		[92, p.182] (121)
	5,79E-04	1,071E-03	-5,00E-05		[92, p.182] (114)
Ca^{2+} / Cl^-	**-1,73E-04**	**3,90E-03**			[92, p.182] (121)
	1,04E-04	3,54E-03	-1,57E-01		[92, p.182] (82)
Ca^{2+} / CO_3^{2-}					
NH_4^+ / CO_3^{2-}	**1,10E-03**	**4,36E-03**			[92, p.182] (114)

Using these, the values of β_0, β_1, β_2 and C_ϕ at different temperatures were calculated, with the following equation (here β_0 is used as an example, however the same applies to β_1, β_2 and C_ϕ):

$$\beta_0(T) = \beta_0 + (T - 25)\frac{d\beta_0}{dT} \tag{63}$$

with T representing the temperature in question in degrees Celsius, β_0 the reference parameter at 25°C from Table 6.2 and $d\beta_0/dT$ the temperature dependence of the Pitzer parameter in question from Table 6.3. Thus a Pitzer model was made, that took the calcium concentration as an input and gave the activity coefficients for the temperature range 15-60 °C (at 5°C intervals) as the output.

Bromley

The Bromley method is said to give accurate results for calculating the mean activity coefficients in strong electrolytes up to an ionic strength of 6 M [34], [42], [79], [87]. It can allow for an easier yet still accurate compromise over the Pitzer method in determining the activity coefficients of complex and concentrated solutions [79]. The following formula for a multicomponent system, as given by Lalleman et al. 2012 [79], was used:

$$log\gamma_{\pm,m,M_1X_1} = -A_m|z_+z_-|\frac{\sqrt{I_m}}{1+\sqrt{I_m}} + \frac{|z_+z_-|}{|z_+|+|z_-|}\cdot\left[\frac{F_1}{z_+}+\frac{F_2}{z_-}\right] \qquad (64)$$

With the subscript, *m*, representing on a molar basis, the subscript *1* refers to the component in question (in a multicomponent system), *M* and *X* refer to the anion and cation, z_+ and z_- refer to the charge of the anion and cation, *A* refers to the Debye-Hückel constant, *I*, the ionic strength and F_1 and F_2 are factors defined as:

$$F_1 = \sum_j \dot{B}_{M_1X_j}\bar{Z}^2_{M_1X_j}\,m_j \qquad (65)$$

$$F_2 = \sum_i \dot{B}_{M_iX_1}\bar{Z}^2_{M_i1}\,m_i \qquad (66)$$

With *m*, the molality of the ions *i* and *j*. $\dot{B}_{M_iX_j}$ and $\bar{Z}_{M_1X_j}$ are defined as:

$$\dot{B}_{M_iX_j} = \frac{(0{,}06+0{,}6B_{M_iX_j})|z_+z_-|}{(1+\frac{1{,}5}{|z_+z_-|}I_m)^2} + B_{M_iX_j} \qquad (67)$$

$$\bar{Z}_{ij} = \frac{|z_+|+|z_-|}{2} \qquad (68)$$

$$B_{M_iX_j} = B_+ + B_- + \delta_+\delta_- \qquad (69)$$

Thus for the calculation of the Bromley model, the factors, B_+, B_-, δ_+ and δ_- need to be known for each of the individual ions. These were taken from Bromley 1973 [95] and are shown in Table 6.4.

Table 6.4: Bromley factors for ions in the system

Cation	B_+	δ_+
Ca^{2+}	0,0374	0,119
NH_4^+	-0,042	-0,02
Anion	B_-	δ_-
CO_3^{2-}	0,028	-0,67
Cl^-	0,0643	-0,067

The Bromley method only computes the mean activity coefficient at 25°C. In order to compare the results of the Pitzer model, the mean activity coefficient was calculated from the individual activity coefficients [92]:

$$\gamma_\pm = (\gamma_+^{\nu_+}\,\gamma_-^{\nu_-})^{\frac{1}{\nu_+ + \nu_-}} = \sqrt{\gamma_{Ca^{2+}}\gamma_{CO_3^{2-}}} \tag{70}$$

Figure 6.2 compares the activity coefficients at 25°C of calcium and carbonate using the Bromley and the Pitzer methods, dependent on the calcium concentration of the solution. Both models give a reasonably similar mean activity coefficient, however the Bromley result shows less variation with increasing calcium concentration. At lower calcium concentrations, the difference in the activity coefficient calculated from the Bromley and Pitzer models is greater than at higher calcium concentrations. Additionally the same calculations were made for NH_4^+ and Cl^- to compare if the Pitzer and Bromley models also agreed for this case. In Figure 6.3 it can be seen that although they initially give similar results at a low calcium concentration, these grow widely apart as the calcium concentration increases. The Pitzer method shows a slightly increasing mean activity coefficient with increasing calcium concentration, whereas the Bromley method shows a decrease. It should be noted that, when comparing activity coefficients calculated using different models, very differing results can occur, especially at high ionic strengths [96].

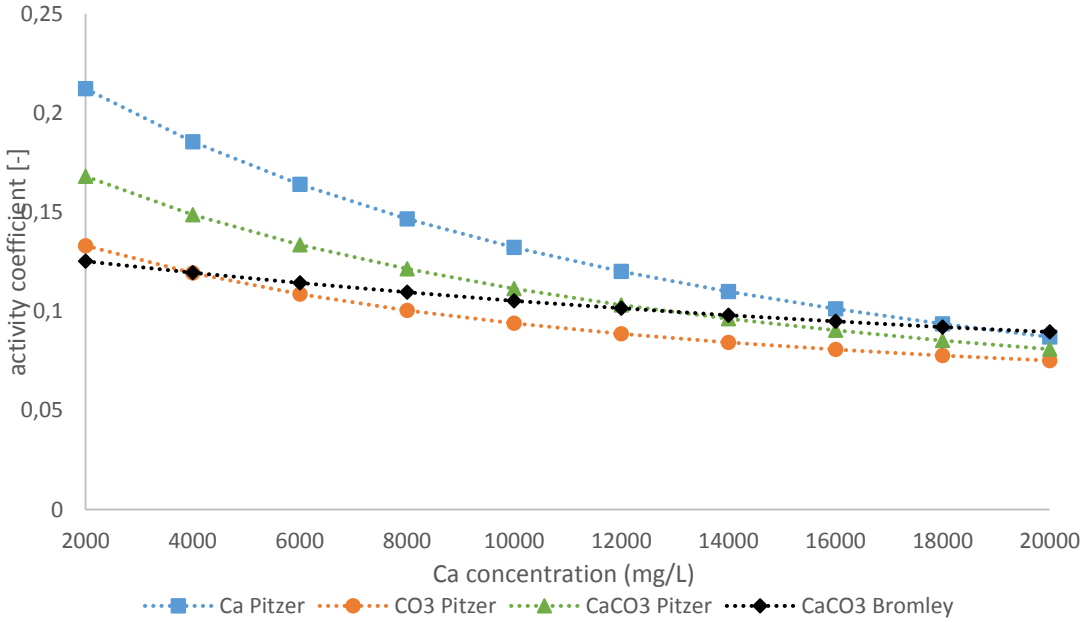

Figure 6.2: Comparison of the mean calcium carbonate activity coefficient based on Pitzer and Bromley models at 25°C with increasing calcium concentrations. Additionally, the individual activity coefficients of calcium and carbonate ions using the Pitzer method at 25°C are displayed.

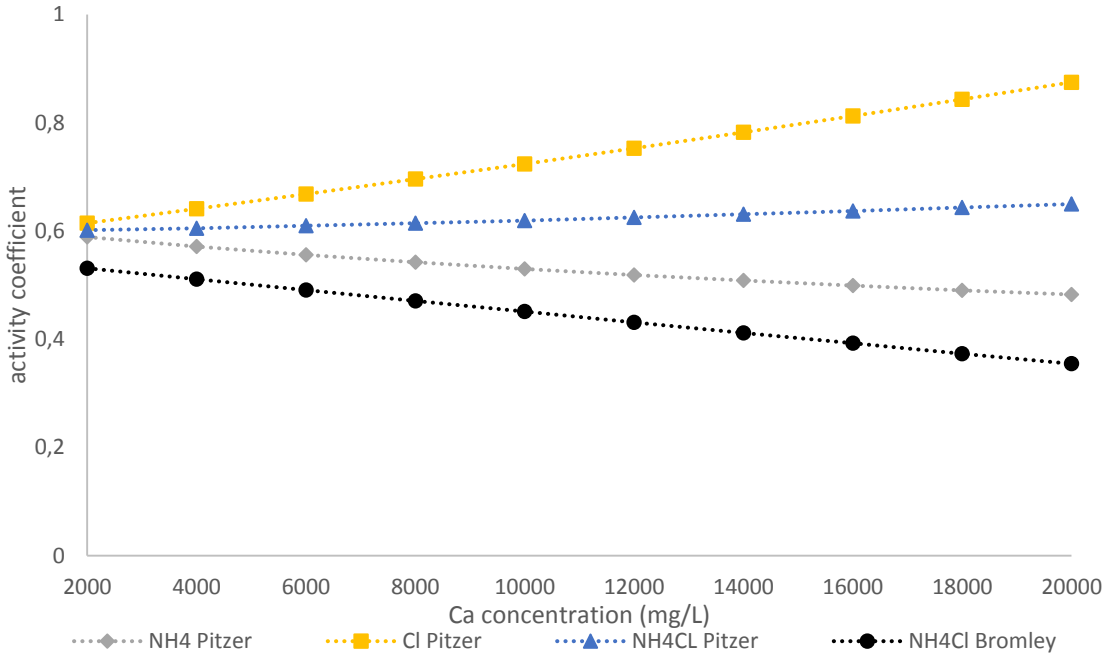

Figure 6.3: Mean and individual ammonium and chloride activity coefficient based on Pitzer and Bromley models at 25°C

The temperature dependence of the activity coefficients is shown in Figure 6.4. For comparison the mean activity coefficient at three different calcium concentrations (2000, 10000 and 18000 mg/L) is shown. It can be seen that there is a small decrease of the activity coefficient with increasing temperature for all three concentrations.

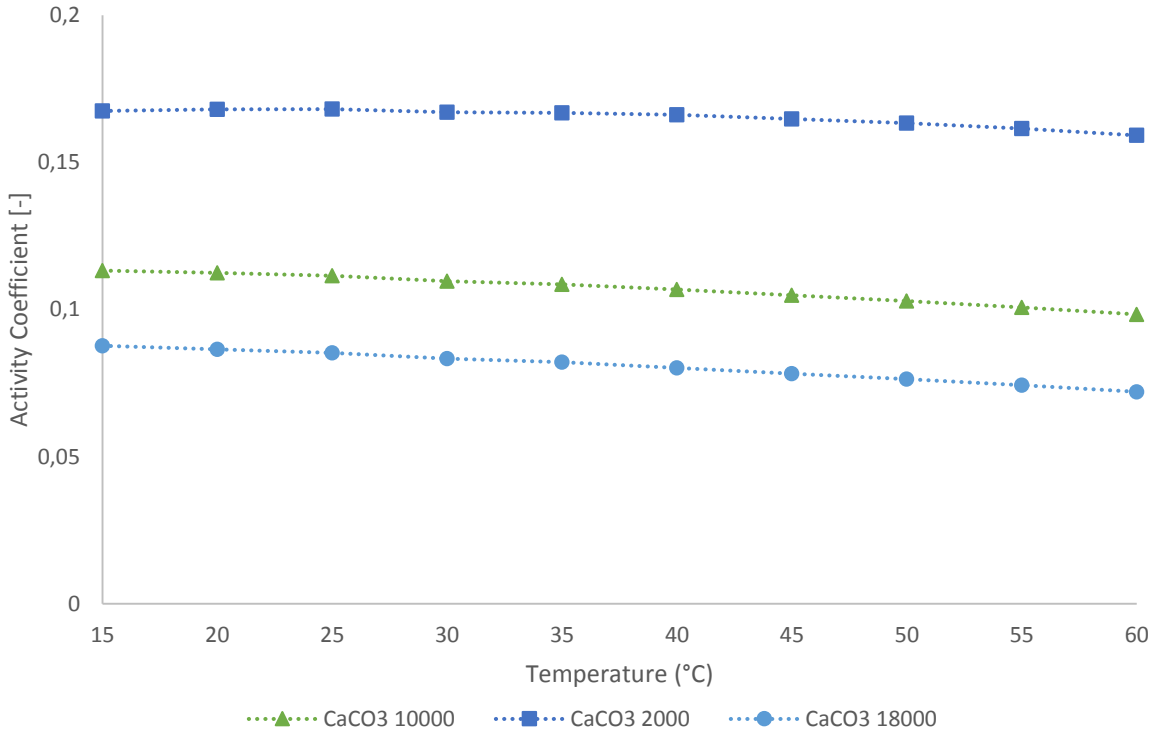

Figure 6.4: Temperature dependence of the mean calcium and carbonate activity coefficients at a calcium concentration of 2000, 10000 and 18000 mg/L

6.4 Solubility Product

The presence of NH_4Cl affects the solubility of calcium carbonate polymorphs. In Figure 6.5, the solubility of calcite and aragonite in a 1M NH_4Cl aqueous solution based on the experimental results of Zhao [97] and Seidell [98] and in water based on Coto et al. 2012 [99] is shown. The solubility in pure water decreases with increasing temperature, whereas the solubility in the NH_4Cl is roughly ten times higher and increases with temperature.

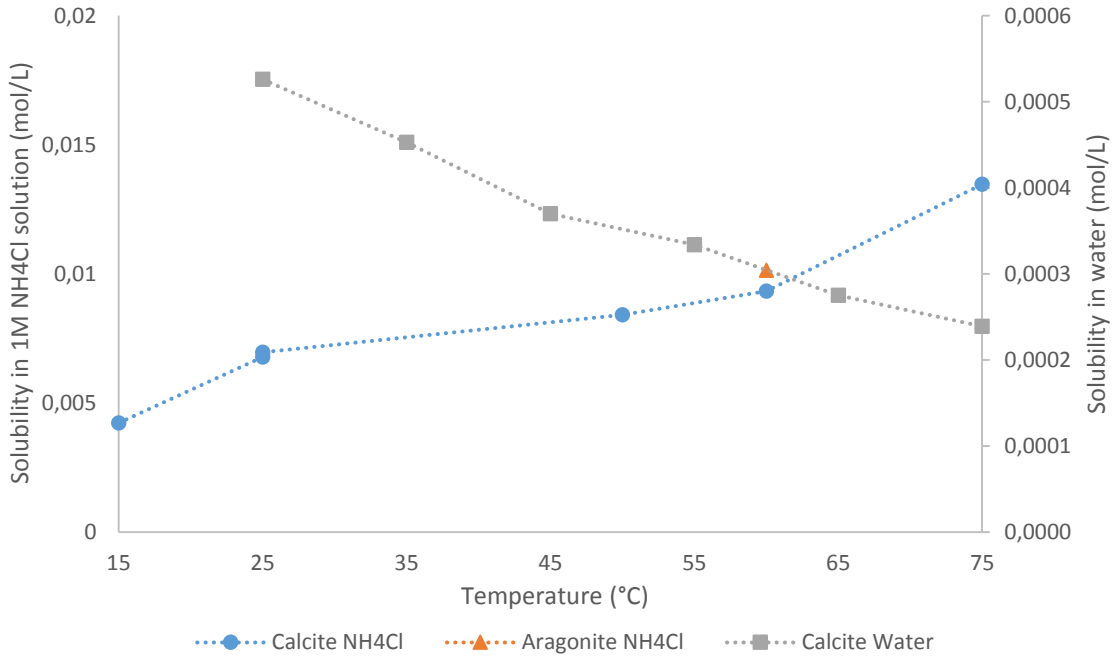

Figure 6.5: Solubility of calcite and aragonite in a 1M NH4Cl solution shown on the left axis and the solubility of calcite in pure water shown on the right axis for comparison.

The activity based solubility product, K_{sp}, is different for each of the calcium carbonate polymorphs. It is also affected by many parameters such as temperature, pH, pressure and ionic strength of the system. The following equations describe the solubility product of the different polymorphs dependent on temperature given by Plummer and Busenberg 1981 for a H_2O-CO_2-Ca system [100], [101]:

$$logK_{sp,Calcite} = -171{,}9065 - 0{,}077993 \cdot T + \frac{2839{,}319}{T} + 71{,}595 \cdot logT \quad (71)$$

$$logK_{sp,Aragonite} = -171{,}9773 - 0{,}077993 \cdot T + \frac{2903{,}293}{T} + 71{,}595 \cdot logT \quad (72)$$

$$logK_{sp,Vaterite} = -171{,}1295 - 0{,}077993 \cdot T + \frac{3074{,}688}{T} + 71{,}595 \cdot logT \quad (73)$$

However, this does not account for the presence of NH_4Cl, which as was seen in Figure 6.5, can have a strong effect on the solubility. Thus, it was decided to calculate K_{sp} using the concentrations taken from the solubility data given by Zhao [97] and Seidell [98] using:

$$K_{sp} = \gamma^*_{Ca} c^*_{Ca} \cdot \gamma^*_{CO_3} c^*_{CO_3} \quad (74)$$

The concentrations of calcium and carbonate ions in the solution at equilibrium, c^*_{Ca} and $c^*_{CO_3}$, were assumed to equal the molar solubility of $CaCO_3$ and the activity coefficients, γ^*_{Ca} and

$\gamma^*_{CO_3}$, were calculated by inputting the calcium and carbonate concentrations into the Pitzer model. Figure 6.6 shows the results of this. As Zhao [97] and Seidell [98] only have the solubility of calcite at four temperatures and the solubility of aragonite at one temperature (when considering a 1M NH4CL solution), it was assumed that the K_{sp} values for calcite and aragonite are linear, and the difference between the K_{sp} of aragonite and calcite is constant. For comparison, the solubility products of calcite and aragonite were additionally calculated using the equations given above from Plummer and Busenberg 1981 and are graphed Figure 6.6 (denoted by P and using the secondary y-axis).

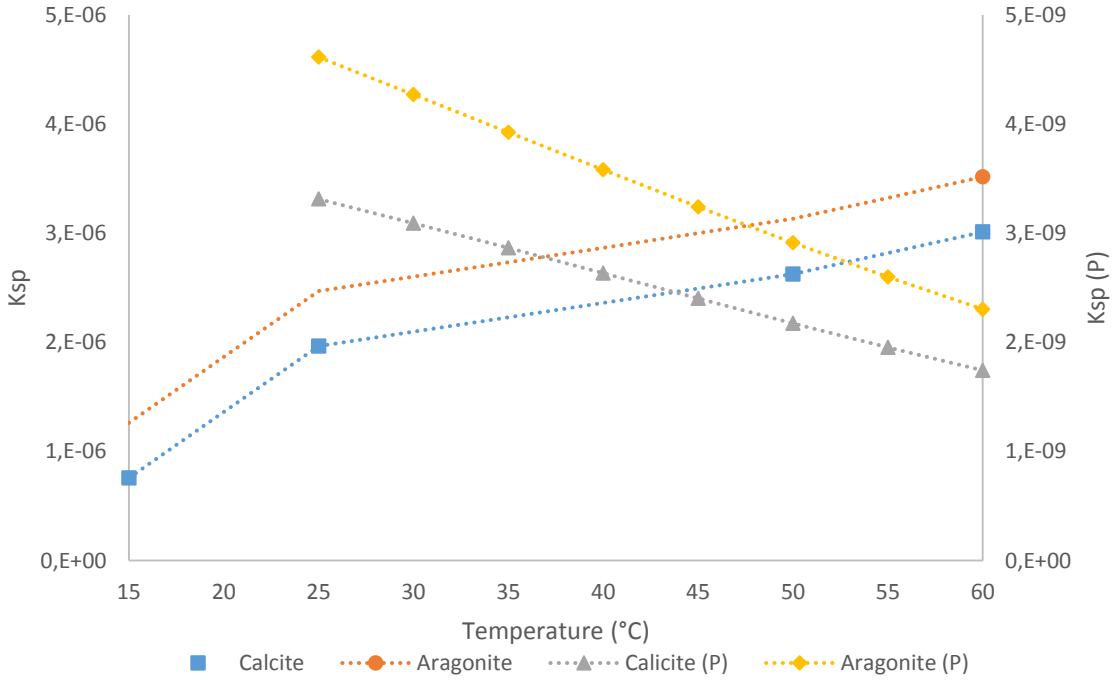

Figure 6.6: Calculated K_{sp} for calcite and aragonite in 1M NH_4Cl solution using eq. 74. shown on the left axis. For comparison the calculated K_{sp} for calcite and aragonite in water based based on Plummer and Busenberg's eqs. 71 and 72 are shown on the right axis and denoted by (P).

We can see that the calculated K_{sp} for the NH_4Cl solution is several magnitudes greater than that of the CO_2-H_2O-$CaCO_3$ system used by Plummer and Busenberg. This can be explained by the increased solubilities of $CaCO_3$ in the NH_4Cl solution which lead to an even greater increase of K_{sp}, as the solubility is effectively squared in the above equation, and the non-ideal behaviour of our system due to the high ionic strength.

6.5 Other modelling methods

Previously, the design of crystallisers was mainly an empirical art, involving factorial design and trial and error to investigate the effects of process parameters on the product characteristics (e.g. yield, size, morphology) [102]. Modern developments in modelling methods, including population balances, kinetic models, computational fluid dynamics (CFD)

and mixing theory, have greatly improved the understanding of individual crystallisation processes, as well as the possibility to develop innovative product and system designs with quicker development times until commercialisation [103]. In this work focus was laid on consistently producing PCC of the desired morphologies, so it was seen as key to model the supersaturation in order to better understand this. During the literature review, other modelling methods were investigated that could be employed to better understand the X2PCC process, however due to time constraints these were not conducted in the scope of this thesis. The general overview is presented below for future use.

6.5.1 Population balance

Conservation equations (e.g. heat, mass and momentum balances) are widely used in analysing and designing chemical engineering systems. In the case of crystallisation systems, a further conservation equation, the population balance, is required to account for the particle numbers. The population balance can be used in sizing and predicting the performance of crystallisers, by coupling the balance with the rate processes for particle formation (e.g. nucleation, growth and agglomeration) to estimate the mass yield and particle size distribution (PSD). The population balance equations are generally solved using numerical solutions for the partial integro-differential equations, and due to their complex nature, simplifications are often employed [103]. The X2PCC pilot plant works as a batch system although experiments are underway to make continuous tests. In continuous systems the assumption of steady state operation can be made, however for batch systems the calculated PSD is both time and size dependent [40]. Figure 6.7 shows the information flow of a population balance for a batch system. It should be noted that the equations shown here are not all directly applicable to the X2PCC system. For example, it can be seen that the supersaturation involves only concentrations and not activities, assuming an ideal solution.

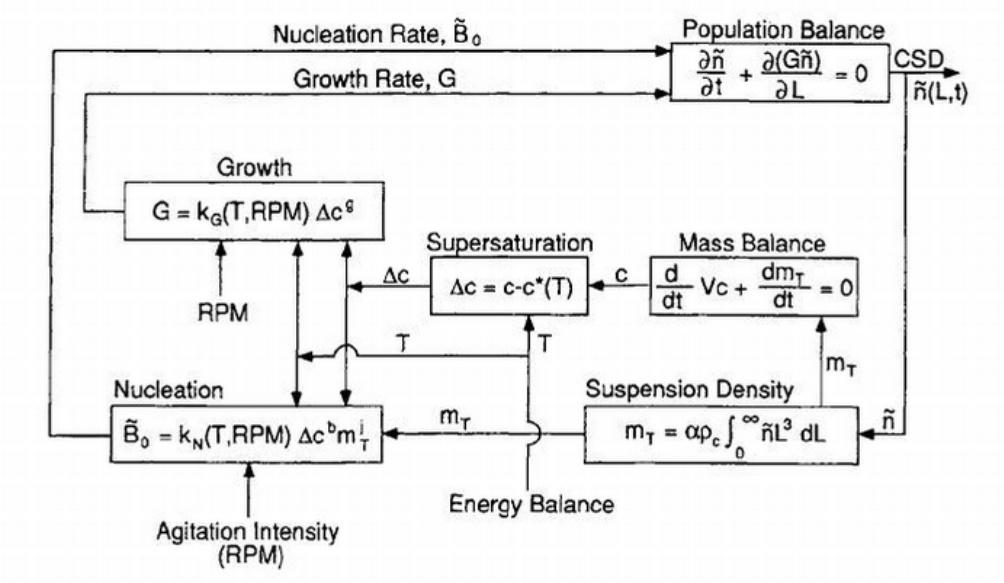

Figure 6.7: Information flow diagram showing interrelationships of batch conservation equations, nucleation and growth kinetic equations, and the resulting crystal size distribution (CSD) in batch suspension crystallisers [31]

Randolph and Larson 1988 [40] is one of the pioneering works on population balances for crystallisation systems and Myerson 2002 [31] also gives a good insight. Ramkrishna 2000 [104] gives an in depth treatment of population balance theory, and although it was not investigated for this work, it is widely cited. Other works have applied population balance theory to the precipitation of PCC and similar systems [47], [73], [75], [81], [87], [105]–[108]. Perhaps most noteworthy of these for comparison with the X2PCC system is the work of Schnebelen et al. 2015 [47], [75] who synthesised nano PCC from the batch carbonation of a suspension of lime. They present a method for determining the nucleation and crystal growth rates of calcium carbonate and other characteristics (e.g. agglomeration) by following two macroscopic parameters against time:

- Mass production rate by precipitation
- Specific surface area (SSA)

6.5.2 Precipitation Diagrams

Precipitation diagrams can be used to show the regions where solid phases of uniform composition, morphology and habit exist based on the concentration, pH or other properties [31]. Kawano et al. 2009 produced a precipitation diagram of calcium carbonate polymorphs from $CaCl_2$ and Na_2CO_3 [60]. Chen et al. 1997 [109] also construct a precipitation diagram for calcium carbonate from a gas-liquid-solid system. Figure 6.8 shows the construction of a precipitation diagram for PCC, with the y-axis showing the natural logarithm of the activity product of calcium and carbonate ions, and the x-axis showing the temperature. The equilibrium curves for the different polymorphs are shown on the diagram. It should be noted that due to the amount of interacting parameters in the precipitation system, the formation of

such diagrams can be challenging. According to Andreasson et al. 2012 [110], "the fact that aragonite is detected even at the lowest temperatures studied, although in small amounts, tells us that generalized rules and polymorph diagram as a function of temperature is virtually impossible to construct due to the simultaneous large effect of the initial supersaturation"

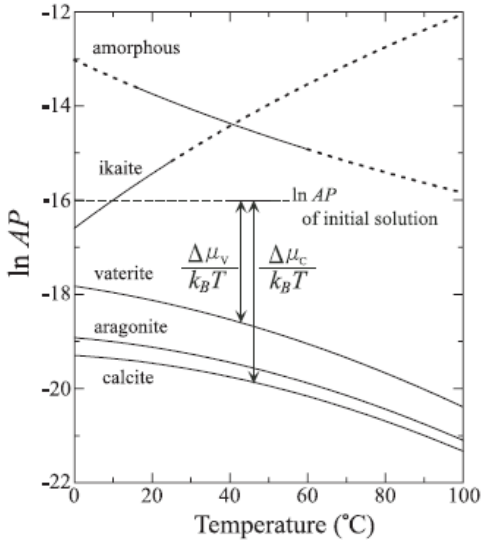

Figure 6.8: Example of a precipitation diagram construction for calcium carbonate [60]. AP refers to the activity product, $AP \equiv a_{Ca^{2+}} \cdot a_{CO3^{2-}}$.

6.5.3 CFD

CFD modelling can be used to give valuable insights into the optimal operating conditions and equipment parameters and help with the scaling up of crystallisers [111]. Wei and Garside 1997, discuss the application of CFD modelling on precipitation systems [72], as do Jones et al. 2005 [103] and briefly Yu et al. 2007 [111]. Al-Rashad and Jones 1999, made a 2D model of a batch gas-liquid precipitation of calcium carbonate [106]. Other authors have modelled barium sulphate precipitation using CFD [87], [112].

7 Experiments

7.1 Measuring solution characteristics

Measurements of the dynamic viscosity, density, diffusion coefficient, specific heat capacity and the thermal conductivity of the calcium rich NH_4Cl solution were made in order to better understand the characteristics of the solution used for carbonation, as well as to determine certain parameters useful for modelling the process. As a reference, measurements were also made on a pure 1M NH_4Cl solution at 25°C, to understand the characteristics of the solution used for the extraction process and for understanding the effect that calcium ions have on the solution.

The density was measured by placing hydrometers in the solution within a glass cylinder and reading of the values. A reference measurement was made of the 1M NH_4Cl solution at room temperature (25 °C) and following this, measurements were made on the calcium rich solution at 25, 45 and 60 °C. The sample was heated by placing it in a glass beaker in a water bath upon a plate heater. The solution was mixed to ensure a homogenous temperature distribution and the temperature was measured with a thermometer directly in the solution until the desired temperature was reached. The dynamic viscosity of the calcium rich solution was measured using a rotational rheometer at 20, 45 and 60°C. Additionally the dynamic viscosity of the reference NH_4Cl solution was measured at 20°C, as was that of deionised water for calibrating the machine, and that of deionised water and 1M NH_4Cl to see if the use of tap water has an effect on the result. The device was equipped with its own heating system for increasing the temperature of the fluid samples. Two measurements were made for each sample at each temperature and an average was taken. The specific heat capacity was measured for the reference NH_4Cl solution and the calcium rich solution using differential scanning calorimetry (DSC). The temperature range used was 20-60°C and a mean of two heating and cooling curves was taken when calculating the specific heat capacity in each case.

The thermal conductivity measurement was attempted using the C-therm TCi thermal conductivity analyser; however this was not successful, most likely due to technical problems with the measurement device. As this measurement was not possible with the available device, it was neglected. An attempt was also made to measure the diffusivity coefficient using dynamic light scattering (DLS), however this was also not successful. Only some large particles (most likely dust) showed up; probably the ions in the solution were too small to measure. Thus, instead of using experimental measurements, the diffusion coefficient was calculated with the Nernst-Einstein equation:

$$D = \frac{RT\lambda}{F^2 z^2} \left(\frac{10^{-5} cm^2}{s} \right) \tag{75}$$

With z, the charge number of the ion in question, F, Faradays constant of 96485 C/mol, R, the gas constant of 8,314 J/kmol, T, the temperature and λ, the molar limiting conductivity.

7.2 Extraction

All tests were run for 60 minutes. Samples were taken before and after the extraction to analyse the calcium concentration. Tests 1-8 were conducted at room temperature with varying slag mass, liquid volumes and slag to liquid ratios (SLR) in order to see how these parameters effect the calcium extraction and to produce solutions of varying calcium concentrations for the carbonation process. During these experiments samples were additionally taken at 10minute intervals to analyse the calcium extraction throughout the extraction process. Test 9 was conducted at a high temperature of 40 °C to assess the effect of a higher temperature on the calcium extraction. Tests 10-15 were conducted at room temperature with 170L of solution, 17kg of slag and an SLR of 0,1 as is seen as the standard and most effective extraction conditions based on previous work at the pilot plant.

Table 7.1: Extraction experiments

Test no.	Slag [kg]	Liquid [L]	SLR [kg/L]	T [°C]	Time [mins]
1	19	190	0,10	25	60
2	19	150	0,13	25	60
3	19	120	0,16	25	60
4	19	150	0,13	25	60
5	19	120	0,16	25	60
6	20	100	0,20	25	60
7	3	150	0,02	25	60
8	9	150	0,06	25	60
9	17	173	0,10	40	60
10	17	170	0,10	25	60
11	17	170	0,10	25	60
12	17	170	0,10	25	60
13	17	170	0,10	25	60
14	17	170	0,10	25	60
15	17	170	0,10	25	60

7.3 Carbonation

Tests 1-9 were run with the aim of assessing the influence of increased/decreased calcium concentration (resulting from the varying extraction conditions previously mentioned) on the produced PCC. They were run at temperatures of 35 or 45 °C in the hope of producing scalenohedral calcite or aragonite. It is hypothesised that an excess of calcium is a requirement for scalenohedral PCC and it has previously been produced at a lower temperature at the laboratory scale [113]. Aragonite had been previously produced in the pilot plant at 45 °C. Tests 10 and 11 were conducted as a reproduction of 2 previous tests that produced high quantities of aragonite in order to ascertain the main operational parameters affecting the production of aragonite. Tests 12-15 were conducted with varying end pH's at 45 °C in the hope of finding the conditions to produce pure aragonite. The solutions were carbonised all with pure CO_2 and a flow rate of 10 L/min based on positive results with these levels in previous experiments. It should be noted that the Test 1B had a problem with the CO_2 feeding during the experiment which led to the extended time duration.

Table 7.2: Carbonation experiments

Test	Liquid [L]	start pH	End pH	CO_2 [L/min]	T [°C]	Time [h:min]
1	174	9,98	8,46	10	35,0	1:40
2	120	9,94	8,53	10	45,0	1:17
3	120	10,12	8,03	10	45,0	1:20
4	120	10,20	8,05	10	35,0	2:08
5	114	10,37	8,08	10	35,0	1:28
6	80	10,96	8,14	10	35,0	1:05
7	143	9,20	8,00	10	45,0	0:45
8	137	9,52	8,09	10	35,0	1:05
9	167	10,21	8,65	10	45,0	1:03
10	140	9,89	8,60	10	45,0	0:58
11	137	9,98	8,60	10	45,0	1:05
12	157	9,88	9,05	10	45,0	0:43
13	137	10,08	8,80	10	45,0	0:58
14	120	9,59	8,61	10	51,0	0:49
15	153	9,55	8,60	10	54,5	0:35

Samples of the solution after carbonation were taken to be sent for calcium analysis in order to assess the calcium conversion efficiency. After the filtration of PCC, a sample of the PCC slurry was taken and washed with water and set in an oven overnight at 100 °C to dry. These samples were then sent for XRD and SEM image analysis in order to assess the morphology. In some cases samples were also sent for PSD analysis in order to assess the mean particle size and distribution. It was hypothesised that smaller particles may get lost during the filtration and lead to a higher PSD when the sample is taken after filtration, thus samples were also taken directly from the reactor to test this.

8 Results and Discussion

8.1 Supersaturation Modelling Results

The following two graphs show the calculated supersaturation ratios for calcite and aragonite. Figure 8.1 shows the supersaturation as a function of calcium concentration at constant temperatures. For comparison the highest and lowest temperatures considered in the model are shown as well as a mid-temperature. The second graph shows the dependence on temperature at constant calcium concentrations. For comparison the highest and lowest calcium concentrations considered in the model are shown as well as a mid-value.

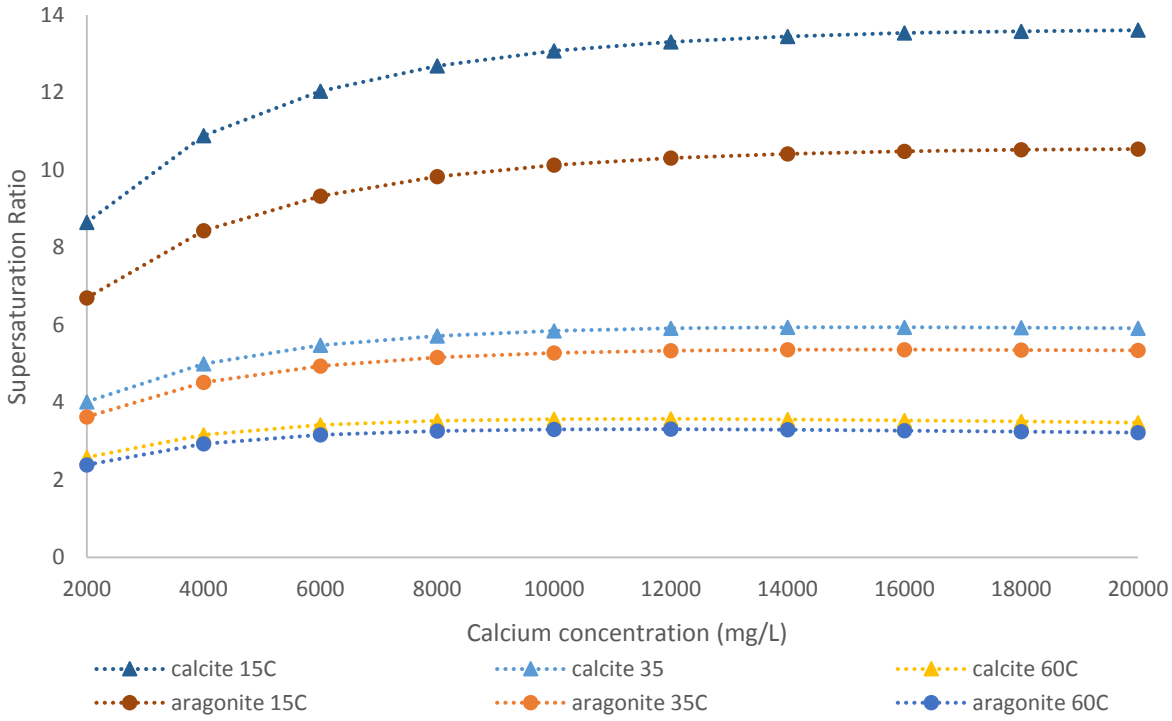

Figure 8.1: Supersaturation ratio of aragonite and calcite as a function of calcium concentration.

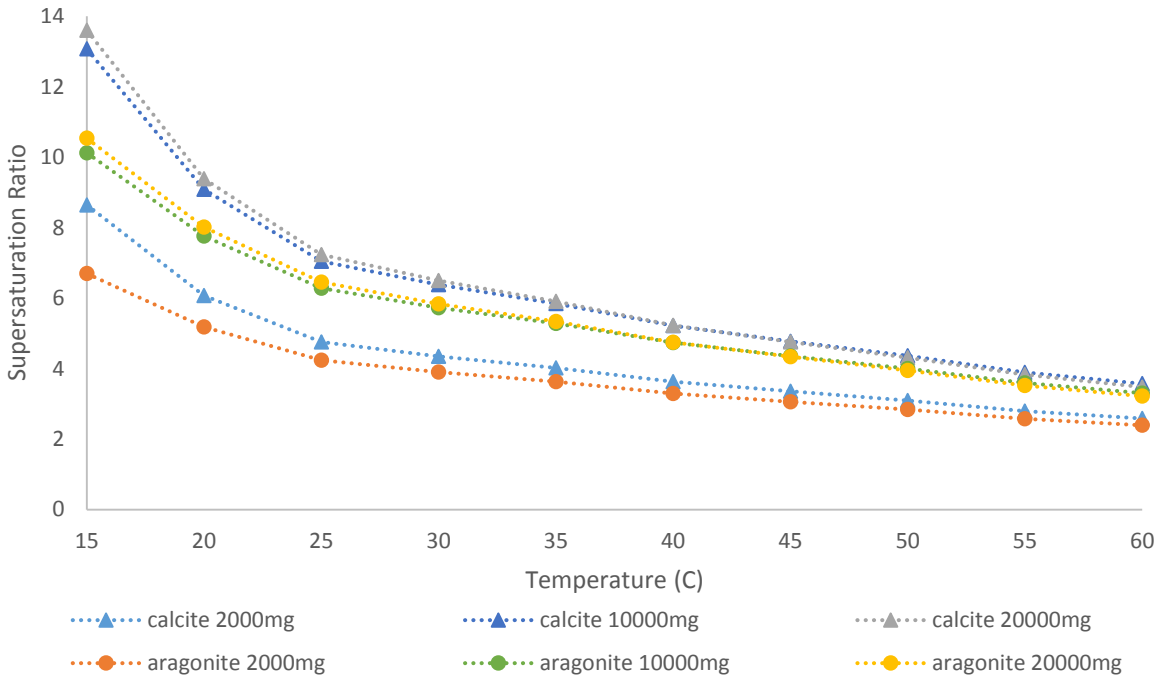

Figure 8.2: Supersaturation ratio of calcite and aragonite as a function of temperature.

It can be seen that all supersaturation ratios are above 1, confirming that the solution is in a state of supersaturation. In all cases, the supersaturation for aragonite is lower than that for calcite. Figure 8.1 shows that the supersaturation increases with increasing calcium concentration. However, this increase becomes much lower (almost reaching a constant value) as the calcium concentration becomes higher. This is influenced by the fact that the activity coefficients decrease as the calcium concentration increases. It can also be seen that the difference between calcite and aragonite is much more marked at lower temperatures. Figure 8.2, shows that the supersaturation ratio decreases with increasing temperature. The decrease is much more marked at the lowest temperatures considered and reaches a more constant rate after this.

Figure 8.3 shows the actual supersaturation ratio of experiments based on the actual experimental conditions (temperature, initial and end calcium concentration). The following assumptions were made to calculate this:

- the calcium concentration decreases at a constant rate during the experiment (i.e. it is consumed at a constant rate by the nucleation and growth of crystals).
- the temperature remains constant (in reality there it increases slightly).
- The carbonate concentration remains constant as fresh CO_2 is constantly bubbled through the solution providing carbonate ions to replace those consumed in the precipitation process.

Tests 1 and 7 are not shown here as no samples were taken after the carbonation process so it was not possible to calculate the end supersaturation. When considering the procession of the

supersaturation ratio over time, the longer experiments show a bigger drop at the end of the experimental time. When considering the morphology results (see Table 8.6), it seems that the tests with significant fractions of aragonite (tests 9-15 have approx. 20-70% aragonite) present a more constant supersaturation over the experimental time. Those with mainly fractions of calcite (tests 1-8 have over 90% calcite) show a longer experimental time and a bigger drop in the supersaturation ratio.

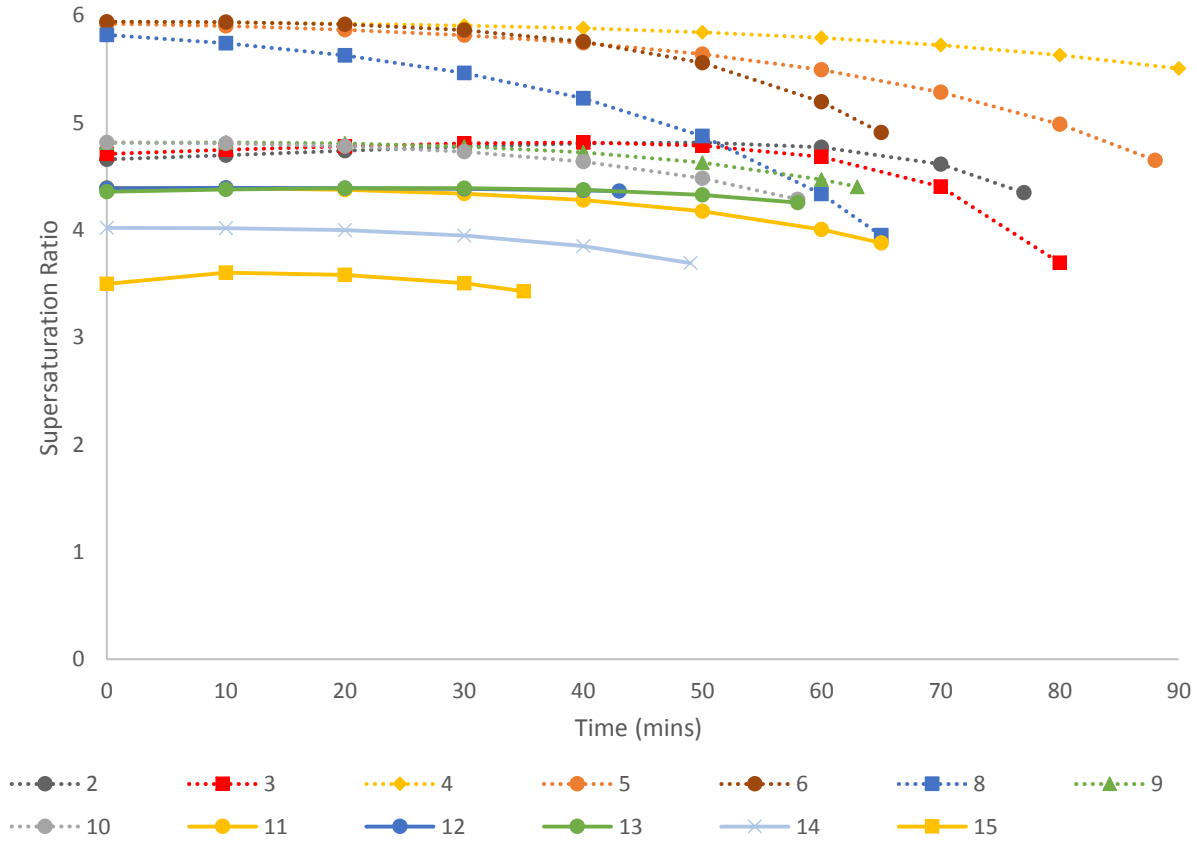

Figure 8.3: Supersaturation progression over the experimental time for all experiments with adequate data. Dotted lines represent that calcite was the main product, solid lines represent that aragonite was the main product.

As to whether the values are reasonable, the supersaturation ratio is strongly affected by the individual system; the components, temperature and other process parameters. A review of literature was made of different stated supersaturations for comparison. Chen et al. 1997 show relative supersaturations of 2,1 to 22 for the carbonation of a CaCl solution (as mentioned before, relative supersaturation is equal to the supersaturation ratio minus 1). Rizutti et al. 2008 [62], working with calcium bicarbonate solutions prepared with carbonated water, reported supersaturation ratios ranging between 4 and 23. Vucak et a.l 2003 [114] reports supersaturations of between 1 and 50 during the carbonation process (32.2% CO_2 in air) of a calcium nitrate and MEA solution. When comparing with these values, those calculated here seem to be on the lower end of these, this can be due to e.g. the effect of the different system properties or assumptions made in the calculations.

8.2 Solution Characteristics Experimental Results

In Table 8.1, the density of the reference NH_4Cl solution and the calcium rich solution can be seen at different temperatures. Additionally in Figure 8.4 these results are graphed and compared to the density of water. It can be seen that the presence of NH_4Cl in the water increases the density slightly and the presence of calcium ions increases the density further. The density of the calcium rich solution decreases with the temperature in a similar way as water.

Table 8.1: Density results of the NH_4Cl solution and the calcium rich solution at different temperatures

T [°C]	NH_4Cl [kg/m^3]	Ca rich [kg/m^3]
25	1,02	1,03
45		1,021
60		1,015

In Table 8.2, the dynamic viscosity of deionised water, a 1M NH_4Cl solution prepared with deionised water, a 1M NH_4Cl solution prepared with tap water (usual method of preparation) and of the calcium rich solution at various temperatures can be seen. Additionally in Figure 8.4: Density of the calcium rich solution and of water at increasing temperatures.
Figure 8.5 these same values compared with water can be seen in a graphical form. It becomes clear that the dynamic viscosity is increased by the presence of NH_4Cl in the water and further increased by the presence of calcium ions. The dynamic viscosity of the calcium rich solution decreases with increasing temperature in much the same way as with water.

Table 8.2: Dynamic viscosity of deionised water, the NH_4Cl solution in deionised water and in tap water (usual method) and of the calcium rich solution

T [°C]	Deionsed water [cP]	NH_4CL deionised [cP]	NH_4Cl [cP]	Ca rich [cP]
20	1	0,975	1,04	1,11
45				0,645
60				0,485

In Table 8.3, the specific heat capacity of the NH_4Cl reference solution and the calcium rich solution at various temperatures can be seen. The values for both solutions are very close, with those of the calcium rich solution lying slightly below those of the NH_4Cl reference solution. Additionally these results can be seen in graphical form and compared to pure water in Figure 8.6. It can be seen that the presence of NH_4^+, Cl^- and Ca^{2+} ions leads to a reduction in specific heat capacity and the heat capacity increases with increasing temperature. The effect of temperature appears stronger than in the case of water.

Table 8.3: Specific heat capacity measurement results

T [°C]	NH4CL [kJ/kgK]	Ca Rich [kJ/kgK]
20	3,861	3,855
25	3,889	3,865
30	3,878	3,879
35	3,883	3,879
40	3,893	3,880
45	3,902	3,893
50	3,901	3,896
55	3,911	3,929
60		3,946

In Table 8.4, the results of the calculated diffusivity coefficients of the calcium rich solution are shown. Additionally these results are shown in a graphical form in Figure 8.7. It can be seen that the diffusivity coefficient increases linearly with increasing temperature. As mentioned in the Chapter 7, these were calculated with the Nernst-Einstein equation:

$$D = \frac{RT\lambda}{F^2 z^2} \left(\frac{10^{-5} cm^2}{s} \right) \tag{76}$$

Table 8.4: Calculated diffusivity coefficient of the calcium rich solution at different temperatures.

T [°C]	Ca^{2+} [10^{-5} cm^2/s]	Cl^- [10^{-5} cm^2/s]	$NH4^+$ [10^{-5} cm^2/s]	$CO3^{2-}$ [10^{-5} cm^2/s]
20	0,7789	1,9989	1,9256	0,9072
25	0,7922	2,0330	1,9584	0,9226
45	0,8453	2,1694	2,0898	0,9845
60	0,8852	2,2716	2,1883	1,0309

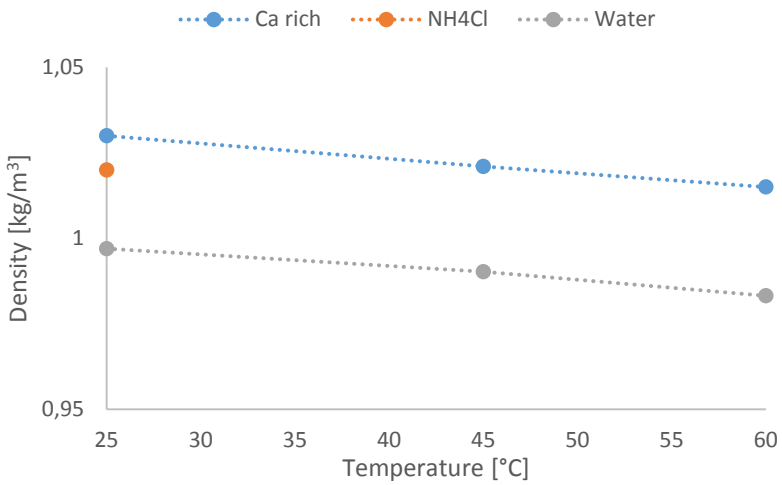

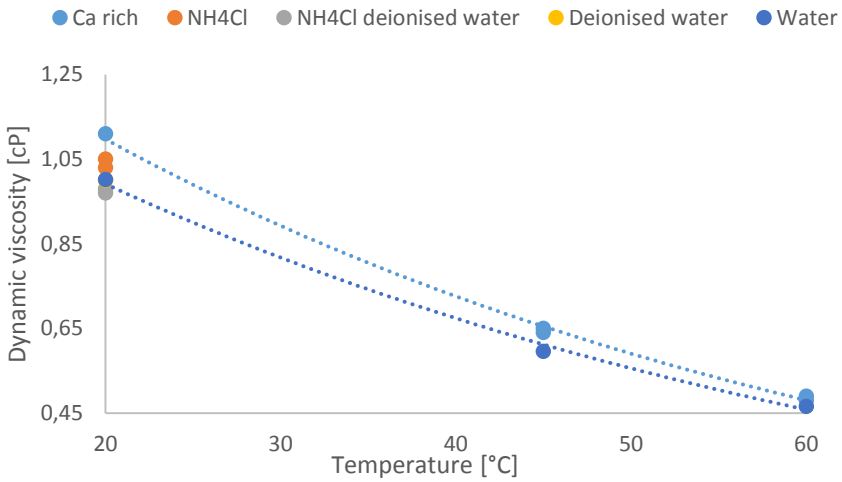

Figure 8.4: Density of the calcium rich solution and of water at increasing temperatures.
Figure 8.5: Dynamic viscosity of the calcium rich solution and water with increasing temperatures.

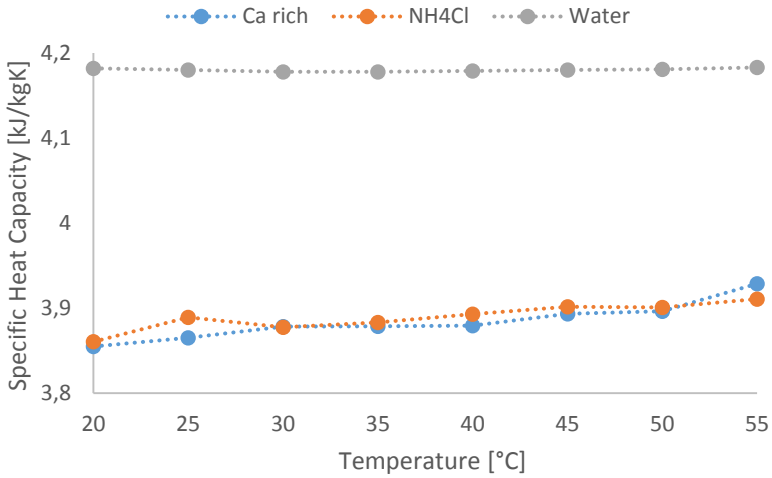

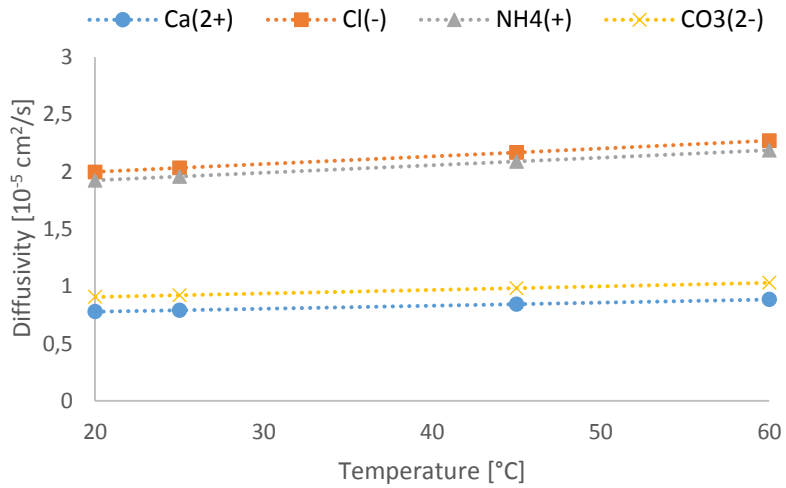

Figure 8.6: Specific heat capacity of the reference NH_4Cl solution, calcium rich solution and water at increasing temperatures.
Figure 8.7: Calculated diffusivity coefficient of the calcium rich solution with increasing temperatures.

8.3 Calcium Extraction Experimental Results

The calcium concentration of the solution was seen as a key parameter in the carbonation process, thus the first nine extraction experiments aimed to see how to increase/decrease the calcium concentration of the solution. The parameters that changed were the solution volume, the slag mass and one experiment was conducted at a high temperature. The results of the calcium extraction experiments can be seen in Table 8.5. It should be noted that for test 1, the sample was stored for a long time period before the calcium analysis was made, which may explain the abnormally low calcium concentration. It is possible that some calcium in the solution reacted with residual carbonate ions to form PCC, as the sample appeared to have some particles in it after the long time period. Tests 2 and 3 gave surprisingly high results in the calcium analysis. To verify this, the tests were repeated with the same conditions (tests 4 and 5) and much lower calcium concentrations resulted, which were more in line with the other results.

Table 8.5: Results of the extraction experiments, b/e refers to before extraction, a/e refers to after extraction, η_{Ca1} refers to the calcium extraction efficiency and η_{Ca2} refers to the adjusted calcium extraction efficiency.

Test	Slag [kg]	Solution [L]	SLR [kg/L]	Temp [°C]	Ca in slag [g]	max Ca [g/L]	Ca [g/L]	Ca b/e [g/L]	Ca a/c [g/L]	η_{Ca1} [%]	η_{Ca2} [%]
1	19	190	0,10	25	4826	25,40	4706			18,53%	
2	19	150	0,13	25	4826	32,17	27041		4907	84,05%	
3	19	120	0,16	25	4826	40,22	23317	4907	2587	57,98%	45,78%
4	19	150	0,13	25	4826	32,17	14496	2587	2700	45,06%	37,02%
5	19	120	0,16	25	4826	40,22	12621	2700	3093	31,38%	24,67%
6	20	100	0,20	25	5080	50,80	15960	3093	3732	31,42%	25,33%
7	3	150	0,02	25	762	5,08	6126	3732		120,59%	47,13%
8	9	150	0,06	25	2286	15,24	9408		1908	61,73%	
9	17	173	0,10	40	4318	24,96	14382	4482	5229	57,62%	39,66%
10	17	170	0,10	25	4318	25,40	13044	2556	4590	51,35%	41,29%
11	17	170	0,10	25	4318	25,40	13656	3510	4446	53,76%	39,94%
12	17	170	0,10	25	4318	25,40	14679	4446	10197	57,79%	40,29%
13	17	170	0,10	25	4318	25,40	18315	10197	7582	72,11%	31,96%
14	17	170	0,10	25	4318	25,40	13365	7582	5135	52,62%	22,77%
15	17	170	0,10	25	4318	25,40	13968	5135	6098	54,99%	34,78%

In Figure 8.8 the calcium concentration as a function of the SLR is shown. The three outlying results mentioned previously are marked as red squares and omitted from the analysis. It can be seen that the calcium concentration increases initially as the SLR increases, however after an SLR of 0,1 there is no significant increase. It has previously been found that an SLR of 0,1 gives an optimum result for calcium extraction and efficiency. However, it was hoped that a higher calcium concentration might be achieved by varying the SLR at a cost of efficiency, as a high calcium concentration is seen as key to producing scalenohedral calcite. From the results it seems that increasing the SLR above or below a ratio of 0,1 does not dramatically

increase the calcium. Likewise from the experiment performed at a 40°C, does not show an increase in the calcium concentration compared to experiments performed at room temperature with the same conditions.

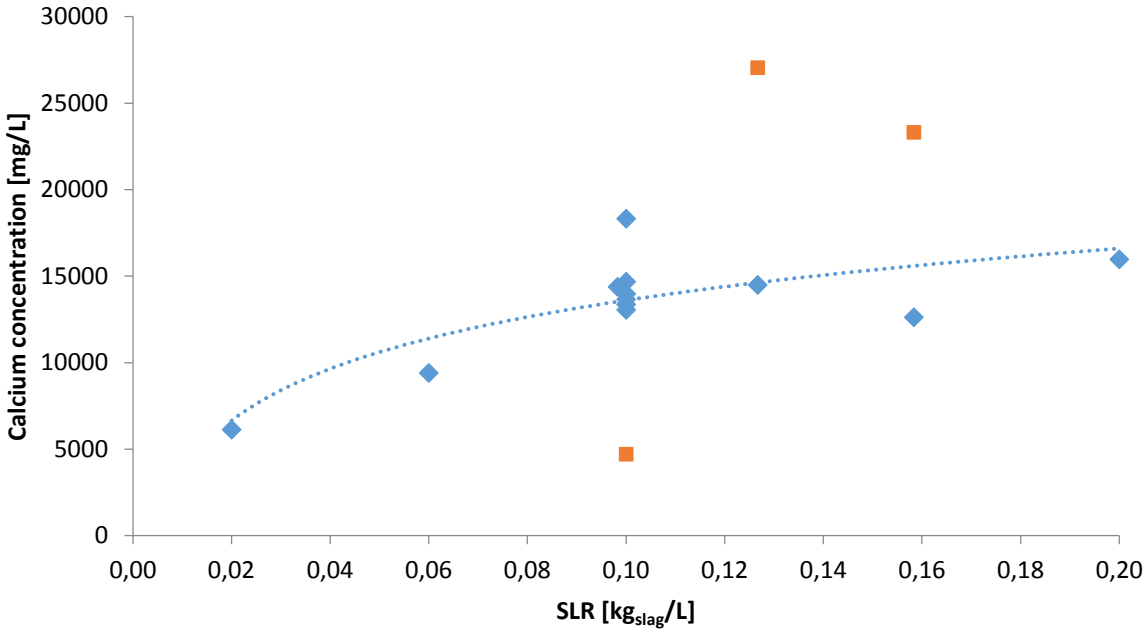

Figure 8.8: Calcium concentration as a function of SLR based on experimental results. Red markers represent anomalies that were not included in the trend line.

The limit to increasing the calcium content in the extraction experiments can be explained by Figure 8.9. At a NH_4Cl concentration of 1 M, it can be seen that above a ratio of about 0,12 there is not enough solvent for all the reactive calcium and slow kinetics. It should be noted that the maximum calcium concentrations achieved by these experiments are lower than the theoretical maximum, so perhaps improving the experimental conditions (e.g. mixing) could lead to slightly higher values. But clearly the current extraction process with 1M NH_4Cl is limited in its ability to produce high calcium concentrations which may be necessary to produce certain morphologies, to increase the supersaturation and also the yield in the carbonation process. In order to achieve higher calcium concentrations, alternative ideas could be investigated, e.g. running the extraction process twice with fresh slag to ensure all the reactive NH_4Cl has been used up, higher NH_4Cl concentrations at the price of needing to wash the products, or the use of additives.

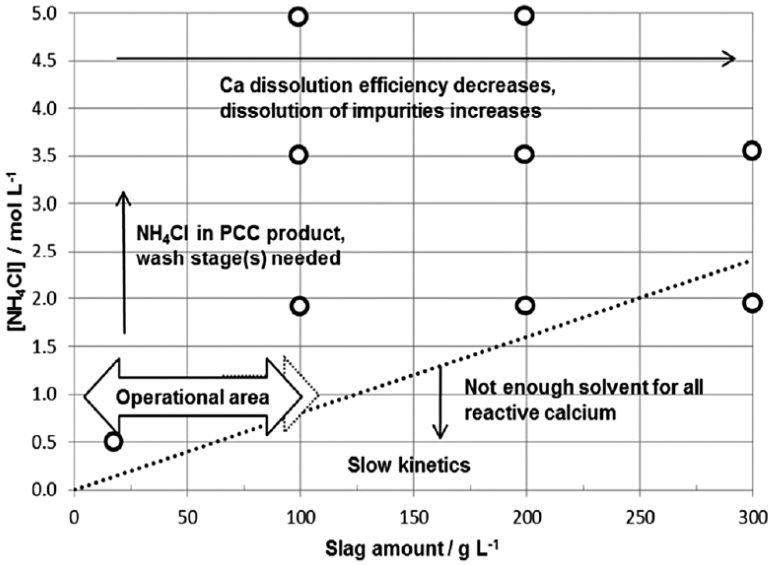

Figure 8.9: Optimum operational area of SLR and NH4Cl concentration in the X2PCC extraction process [115]

The calcium extraction efficiency was investigated using the following equation:

$$\eta_{Ca} = \frac{Ca}{Ca_{max}} \tag{77}$$

Where Ca_{max} refers to the maximum theoretically available calcium in the slag and Ca refers to the actual calcium content after the extraction experiment. When investigating the efficiencies, it was found that in test 7, the calcium extraction efficiency was over 100%. After considering this, it was concluded that the residual calcium in the recycled NH_4Cl solution from the previous carbonation experiment was leading to the higher efficiencies. Before this, the calcium content before the extraction experiments had not been measured, so in the following experiments, samples were taken before and after the extraction. In the case of some experiments, samples had been taken from the solution after the previous carbonation experiment, so these were assumed to be the starting calcium efficiency. Based on this, a new calcium efficiency was calculated with the following equation:

$$\eta_{Ca} = \frac{Ca - Ca_{residual}}{Ca_{max}} \tag{78}$$

Where $Ca_{residual}$ refers to left over calcium in the solution from the previous experiment. When this is considered the calcium extraction efficiency is much lower, as is shown in Figure 8.1. The calcium extraction efficiency is higher at a low SLR and decreases as the SLR increases. However, although the calcium extraction efficiency is higher at a low SLR, the net calcium extracted may be lower due to the fact that there is less calcium available in the slag. It can also be seen that when there is already a residual high calcium concentration before the extraction, higher calcium concentrations are achieved after the extraction, as is seen in

experiment 13 which achieved the highest calcium concentration, and had a very high initial concentration. This might indicate that repeating extraction experiments twice could be used to maximise the calcium concentration, although at the price of extraction efficiency.

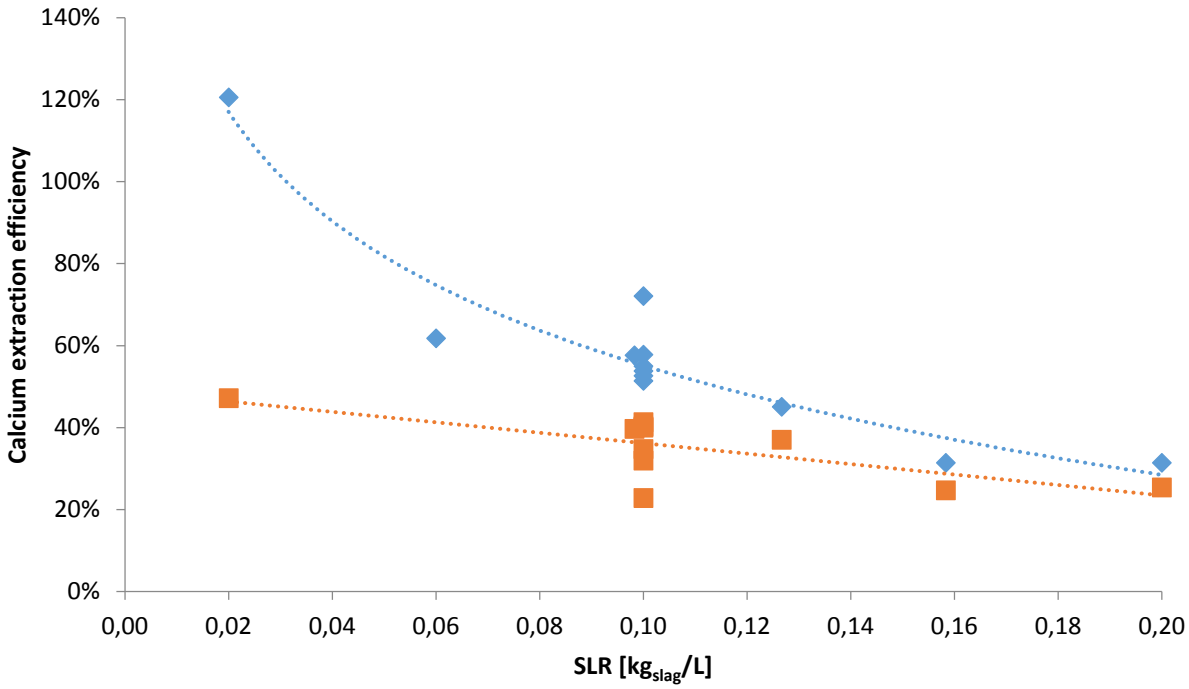

Figure 8.10: Calcium extraction efficiency as a function of SLR based on original calculation method (blue diamonds) and on the adjusted method (red squares)

For some of the tests 2-9, samples were taken at 10 minute intervals during the extraction process and the results of this are shown in Figure 8.11. Besides the results from tests 2 and 3 (which seem to be anomalies), it can be seen that the calcium concentrations appear to remain reasonably constant throughout the experiment. This would indicate that the experiments need not be conducted over such a long period. A one hour extraction had been found based on previous work at the pilot plant to give an optimum of calcium extraction when considering time. It should be noted that the samples were taken directly from the reactor during the process and the solution in the reactor may not be homogenous. The samples taken after the extraction are taken after the filtering of the solution when significant mixing has occurred.

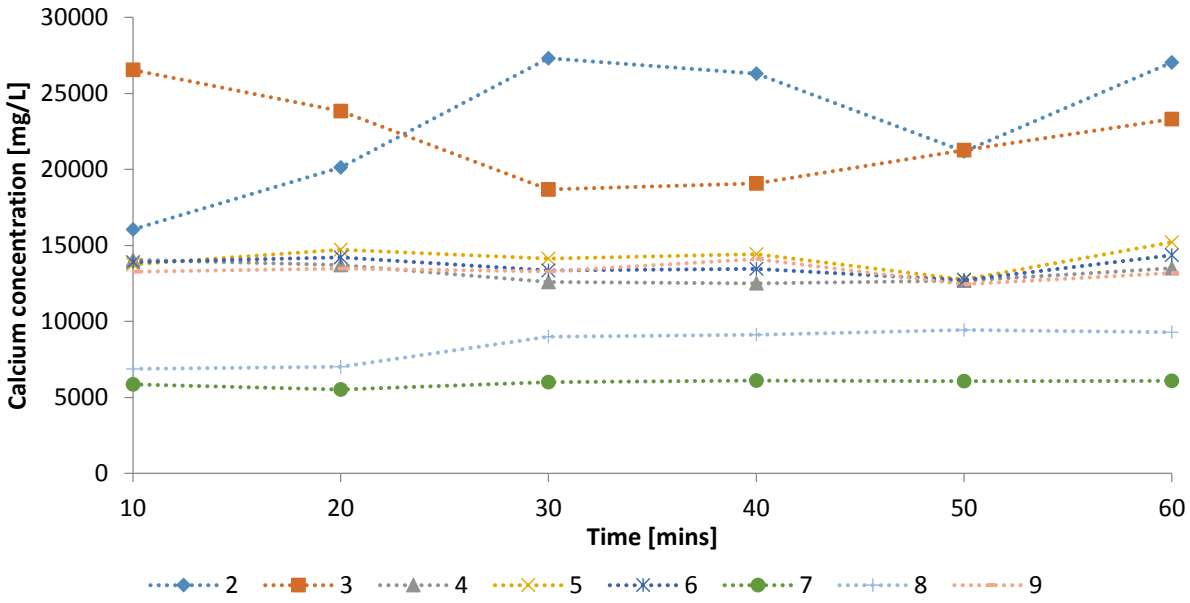

Figure 8.11: Calcium concentration as a function of time for tests 2-9

8.4 Morphology Experimental Results

In Table 8.6, the results for morphology from the XRD analysis can be seen as well as the start and end pH, test time, initial calcium concentration and the calculated initial and final supersaturation. In four of the fifteen tests, other compounds were found present besides calcium carbonate, constituting between 0,5 and 15,7% of the product. These compounds were magnesite (test 1), ilmenite (test 7), calcium manganese phosphate fluoride and sodium hydroxide (test 11) and salammoniac (test 15). It is possible that these could be due to errors in the analysis or an inhomogeneous sample, for example test 9 originally showed very high amounts of other compounds but when a second analysis was made it returned pure calcium carbonate. In order for the PCC to be used commercially it should have a very high purity close to 100% and this was met in the majority of these tests.

Table 8.6: Morphology results and key parameters of the carbonation process. C refers to calcite, A to aragonite, V to vaterite, O to other, T to temperature and S to supersaturation.

Test	C [%]	A [%]	V [%]	O [%]	T [°C]	Ca [g/L]	start pH	end pH	Time [h:min]	Initial S	Final S
1	93,5			6,5	35	4,71	9,98	8,46	01:40	5,20	
2	97,6	2,4			45	27,04	9,94	8,54	01:17	4,66	4,35
3	97,6	2,4			45	23,32	10,12	8,03	01:20	4,71	3,66
4	93,7	3,1	3,3		35	14,45	10,19	8,05	02:08	5,94	4,46
5	95,4	2,7	1,9		35	12,59	10,37	8,08	01:28	5,92	4,65
6	96,3		3,7		35	15,98	11,00	8,14	01:05	5,94	4,91
7	96,4	3,1		0,5	45	6,13	9,30	8,00	00:45	4,53	
8	100,0				35	9,41	9,52	8,09	01:05	5,82	3,95
9	79,1	20,9			45	14,38	10,21	8,60	01:03	4,82	4,40
10	58,8	42,2			45	13,04	9,89	8,60	00:58	4,82	4,29
11	29,3	70,7			45	13,66	9,98	8,60	01:05	4,39	3,88
12	25,5	58,8		15,7	45	14,68	9,87	9,05	00:43	4,39	4,36
13	44,3	55,7			45	18,32	10,09	8,80	00:58	4,36	4,26
14	39,5	60,5			51	13,365	9,59	8,61	00:49	4,02	3,69
15	30,2	59,8		9,9	54,5	13,968	9,55	8,60	00:35	3,50	3,43

In order to investigate the effect of the experiment time, initial calcium concentration, start pH and end pH on the PCC morphology, these have been graphed in Figure 8.13. At longer experiment times the PCC formed was almost exclusively calcite. At shorter experiment times (≤ 1 hour) significant fractions of aragonite occurred. At low (≤12 g/L) and high (≥23 g/L) initial calcium concentrations, calcite was formed, whereas in the mid-range, significant amounts of aragonite were formed. When the start pH was between 9,5 and 10,3 significant fractions of aragonite were formed whereas at the higher and lower start pHs calcite was formed. At an end pH below 8,5 predominantly calcite was formed, whereas at a pH above 8,6 the predominant polymorph was aragonite. Vaterite only occurred at the lowest end pHs.

When considering the temperature, at 35 °C the morphology was mainly calcite with only very small traces of aragonite (< 3,2 %) occurring. Vaterite was only present in small amounts at 35 °C and not at the higher temperatures. Above 45 °C large amounts of aragonite were formed. No strong difference can be noted in the morphology between the tests performed and 51 and 54,5 °C compared to those at 45 °C. The highest temperature that could be produced was 54,5 °C as the solution is heated by tap water through heat exchangers and in the summer time the maximum hot water temperature lies at 60 °C.

When considering these results, it seems that the temperature, end pH and the test time are the most important parameters for the morphology produced and have a clear effect (i.e. longer experiment times and lower end pHs favour calcite, shorter experiment times, higher temperatures and higher end pHs favour aragonite). These results agree with the literature review (see Table 5.1). It should be noted that many parameters were changed in these experiments and that the majority are interrelated. Thus for more accurate results and in order

to draw more definite conclusions, a greater range of experimental data would be required. Considering the initial calcium concentration and start pH graphs in Figure 8.13, it is hard to see a definite trend, and these may not be causal.

During the initial experiments (tests 1-8) only small fractions of aragonite were formed, despite the knowledge that aragonite had previously been produced in high amounts at 45°C at the X2PCC pilot plant. Tests 10 and 11 were reproductions of two previous tests that had produced high fractions of aragonite; these were reproduced with the aim of ascertaining which parameters are critical for aragonite production. They were successful and it became clear that the end pH (or time as these are both related) was the critical parameter and that the initial tests had been ending at too low an end pH or too long a time. This may be explained by the Oswald's rule of stages (see chapter 4.3.3) which posits that the least stable polymorph will form first and will transform into more stable forms over time. Thus aragonite may have originally been formed and transformed into calcite due to the experimental time being too long. The end pH is generally used as the indicator for when the precipitation process is ending, when it reached a pH close to that of the original 1M NH_4Cl solution. It drops over time during the precipitation process, thus the experimental time and end pH are closely related. The time it takes to reach a certain end pH depends on the start pH which is affected by the initial calcium concentration of the solution and other factors (e.g. CO_2 feeding). Thus it is hard to draw conclusions on the optimal experimental time for producing aragonite as it may be different in each case. Generally a temperature of 45°C and an end pH of 8,5 or above lead to aragonite with the exception of test 2. Perhaps in this case the experiment ran for too long or the very high initial calcium concentration prevented the product from being aragonite.

When investigating the morphology as a function of the initial supersaturation, Figure 8.12, some interesting trends occur. Vaterite is only found in very small amounts at the highest supersaturations. Calcite is the main polymorph at higher initial supersaturations (above 4,5), whereas at lower supersaturations aragonite is the main polymorph. This agrees with the results of the literature review, that low supersaturations favour aragonite (see Table 5.1) and higher supersaturations favour calcite. No noticeable trends were found when considering the final supersaturation.

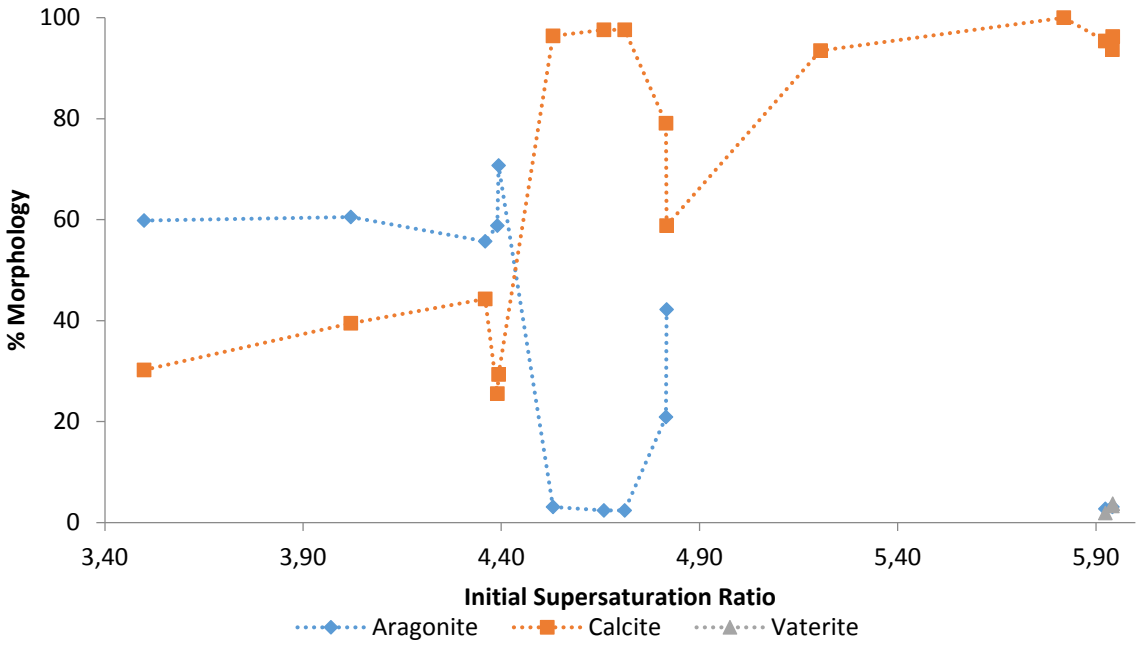

Figure 8.12: Morphology as a function of the initial supersaturation ratio

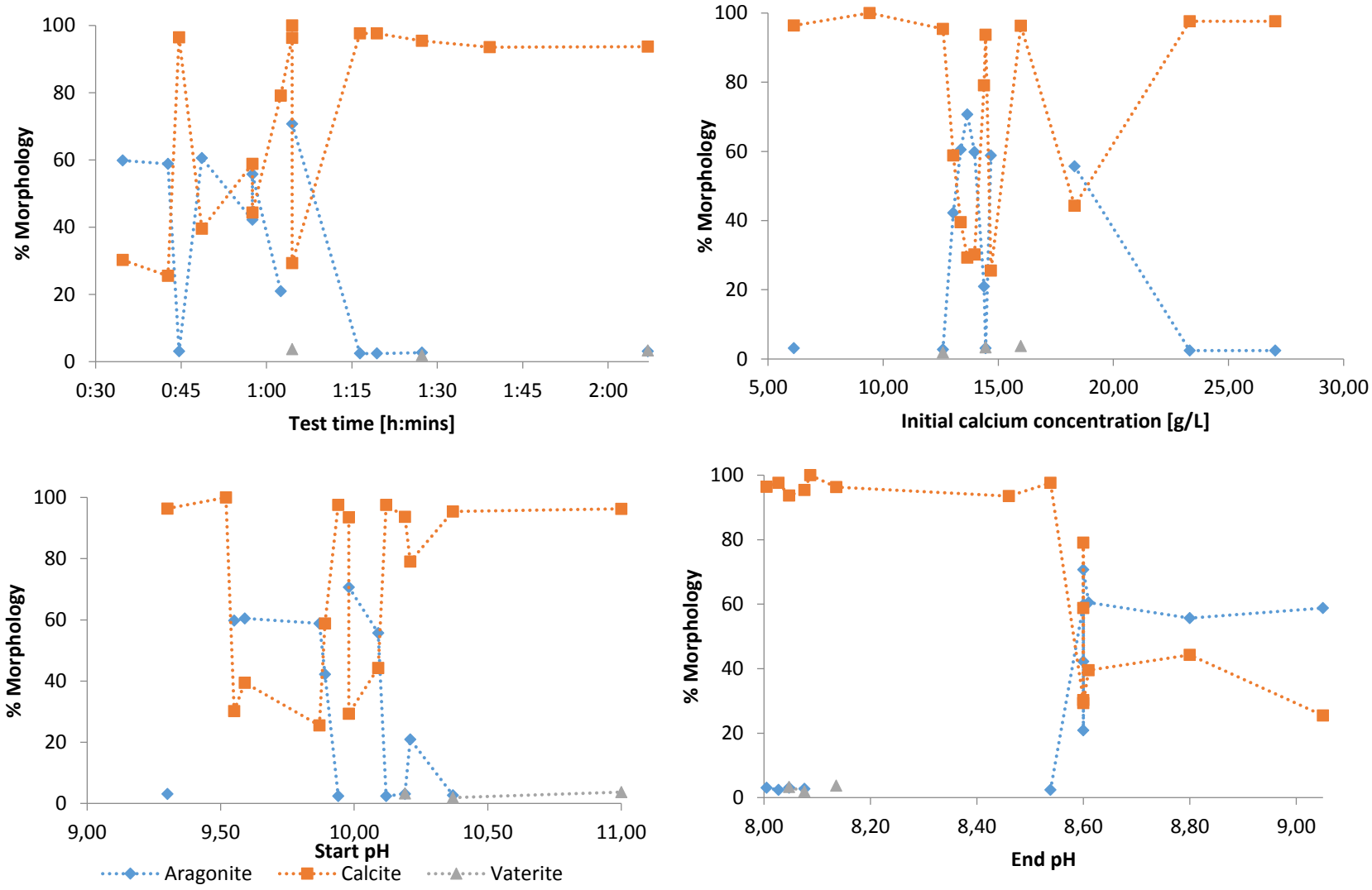

Figure 8.13: Effects of different parameters on the morphology of the PCC produced.

SEM images were taken to analyse the morphology of the produced PCC. The calcite produced was mainly in the rhombohedral form (Figure 8.14) and no traces of scalenohedral calcite were found. Aragonite occurred in a needle like form (Figure 8.15). Mixtures of calcite and aragonite were found at different degrees (Figure 8.16) Agglomeration was present in many of the samples (Figure 8.17).

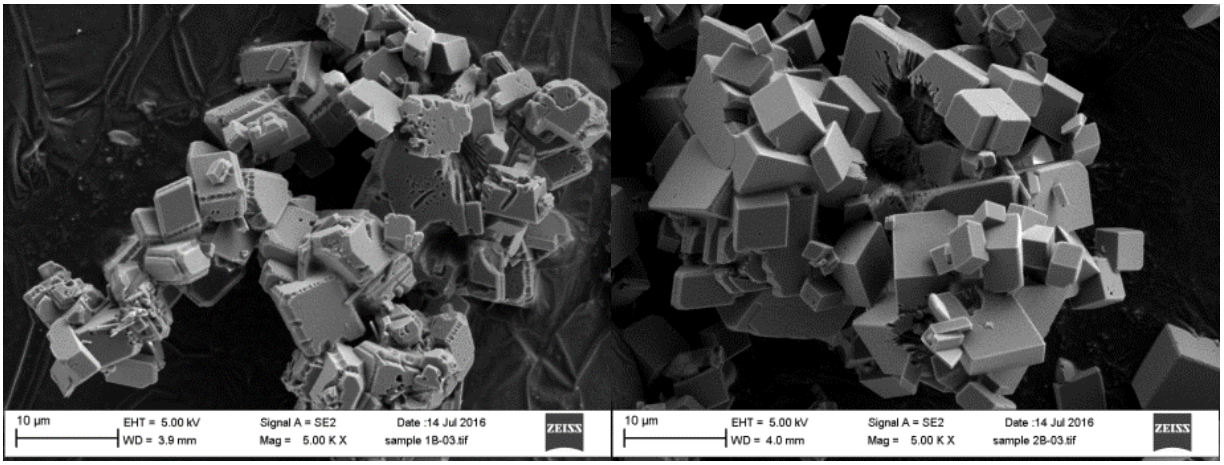

Figure 8.14: Rhombohedral calcite samples from tests 4 and 5

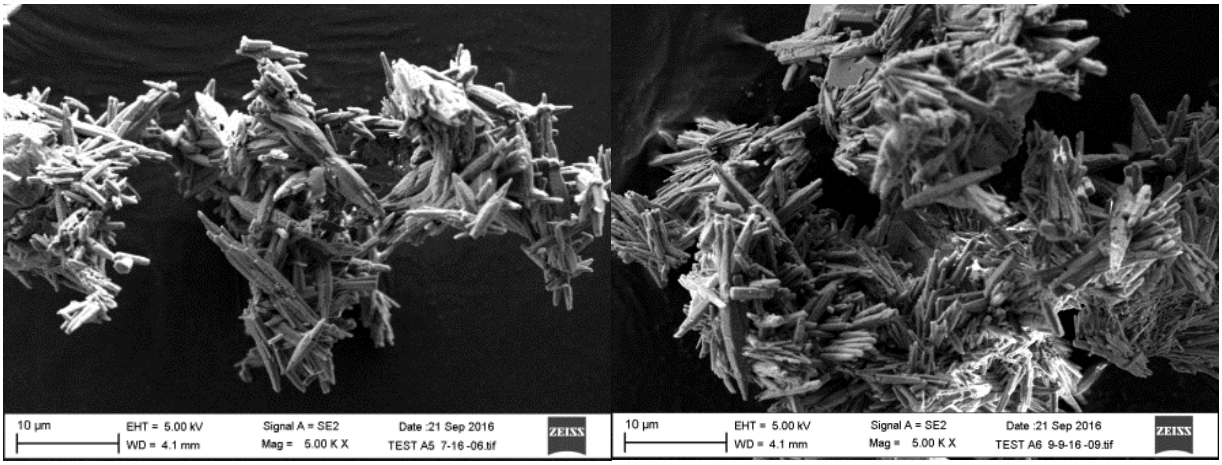

Figure 8.15: Aragonite samples from tests 14 and 15.

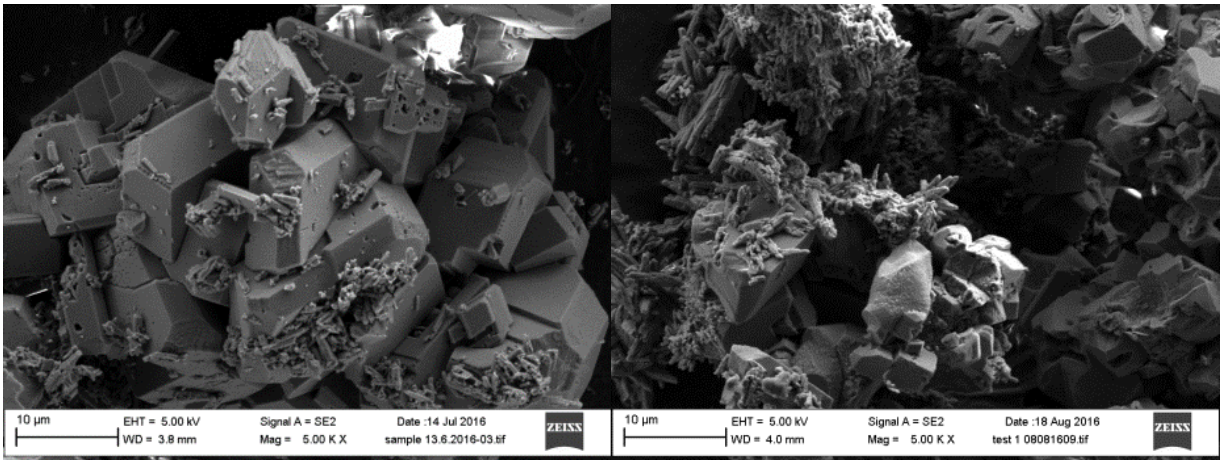

Figure 8.16: Mixture of aragonite and rhombohedral calcite from tests 3 and 10

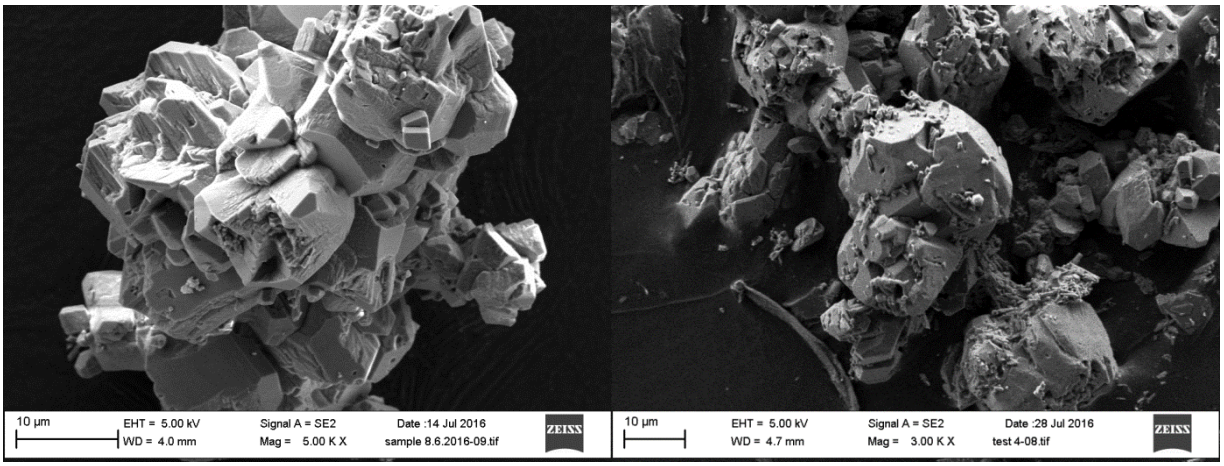

Figure 8.17: Agglomeration and unclear shape tests 2 and 7

The progression of pH and temperature throughout all of the experiments are shown in Figure 8.18 and Figure 8.19. It can be seen that the pH decreases over the experiment time and the temperature increases over the experiment time. This is due to the exothermic nature of the reactions taking place.

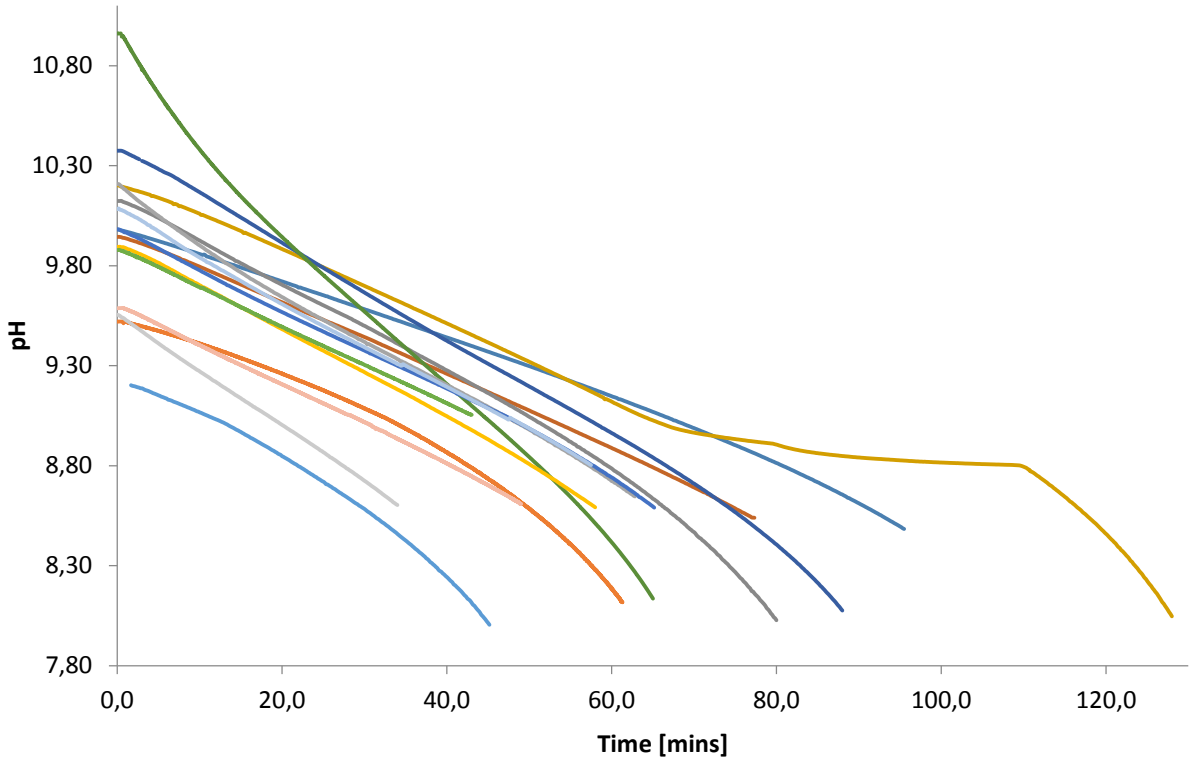

Figure 8.18: pH progression over experimental time.

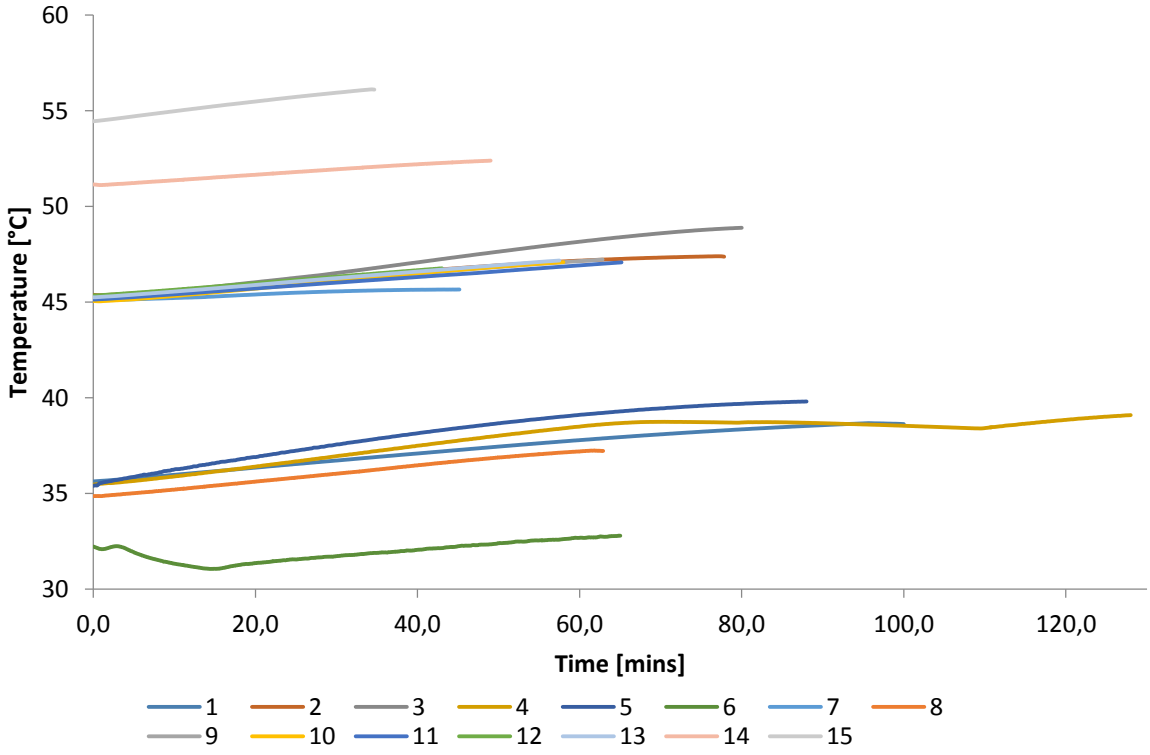

Figure 8.19: Temperature progression over the experimental time.

In Figure 8.20, a comparison is made between the pH progression of the four experiments showing the highest proportions of calcite (2, 3, 7, 8) and the four experiments showing the highest proportions of aragonite (11, 12, 15, 15). Comparing these we see that the aragonite rich experiments generally were shorter, ended at a higher pH and have a more linear pH drop over time. The calcite rich experiments are longer, have a lower end pH (exception test 2) and show a more curved pH progression, with a steeper drop near the end of the experiment. It is hard to draw conclusions what affects the steeper pH drops of some experiments over others, there does not seem to be a clear relationship between this and any of the parameters (temperature, initial calcium concentration, supersaturation, initial pH).

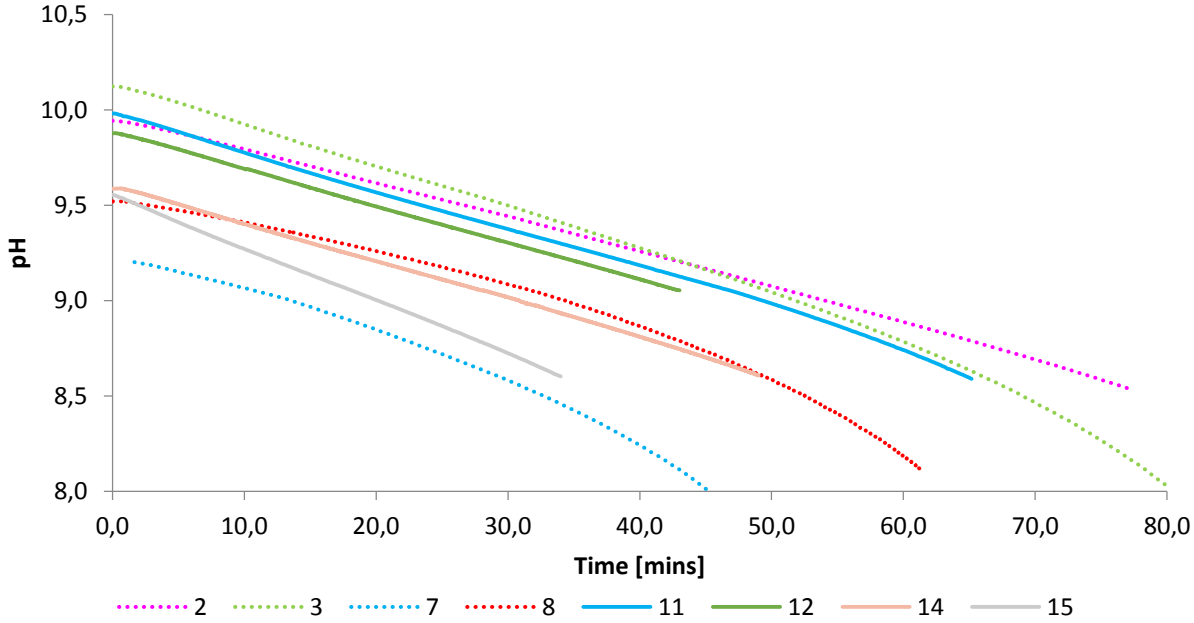

Figure 8.20: pH progression of the four calcite highest tests (dotted lines) and the four aragonite highest tests (solid lines)

In Figure 8.21, the progression of temperature over time of all experiments performed at 45°C are shown. Those rich in aragonite are shown as solid lines and those rich in calcite as dotted lines. Here also, the temperature increase in aragonite rich tests shows a more linear increase, whereas those rich in calcite the temperature increase tapering off at the end. The maximum temperature increase lay at almost 4 degrees Celsius.

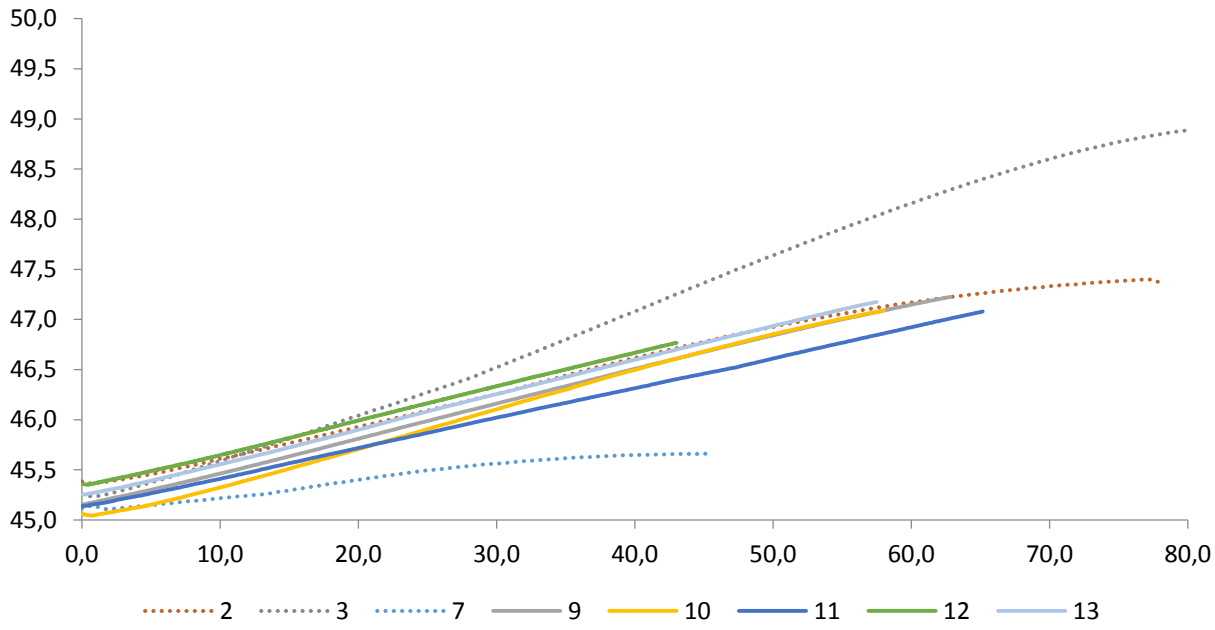

Figure 8.21: Temperature progression over test time comparison at 45°C (dotted lines- calcite rich, solid lines- aragonite rich)

8.5 Particle Size Distribution

PSD analyses were made on a selection of the experiments. The results of these six analyses (Table 8.7) show d_{50} of between 12,47 and 40,58 µm. When comparing with Table 2.1, these sizes are too large on an order of 1-2 magnitudes for commercial use. For the first four samples analysed, the samples were taken from after filtering. The final two samples were taken directly from the reactor before filtration as it was theorised that some small particles were passing through the filters and not being included in the PSD analysis. These samples do show much smaller PSDs, however it may also be possible that this was due to the morphology (mostly aragonite as compared to calcite) or other conditions. The first four tests produced calcite. The literature review indicated that higher supersaturations lead to smaller PSDs, however also to higher agglomeration. When considering this for the four calcite results, tests 3 and 5 do indeed have the higher d_{50} and have a higher supersaturation and were performed at a lower temperature. This however does not hold for the two aragonite rich tests (12 and 13), that may have been effected by the sampling. More tests should be performed in order to draw conclusions based on this. Although test 5 shows a small d_{50}, it shows the largest d_{90} indicating a wider PSD, possibly due to agglomeration.

Table 8.7: PSD analysis. Samples 3, 5, 7 and 8 were taken after filtration of the solution. Samples 12 and 13 were taken directly from the reactor.

Test	d_{10} [µm]	d_{50} [µm]	d_{90} [µm]
3	6,139	40,58	76,49
5	5,366	24,3	80,29
7	3,432	32,76	59,22
8	5,089	24,26	48,07
12	1,062	12,47	28,33
13	1,322	15,63	28,03

Tests 12 and 13 show a clear bimodial distribution of particle sizes, with a smaller node at a lower particle size, as is also found in literature [73]. Tests 3, 5, 7 and 8 show three or four nodes. These results are shown in Figure 8.22.

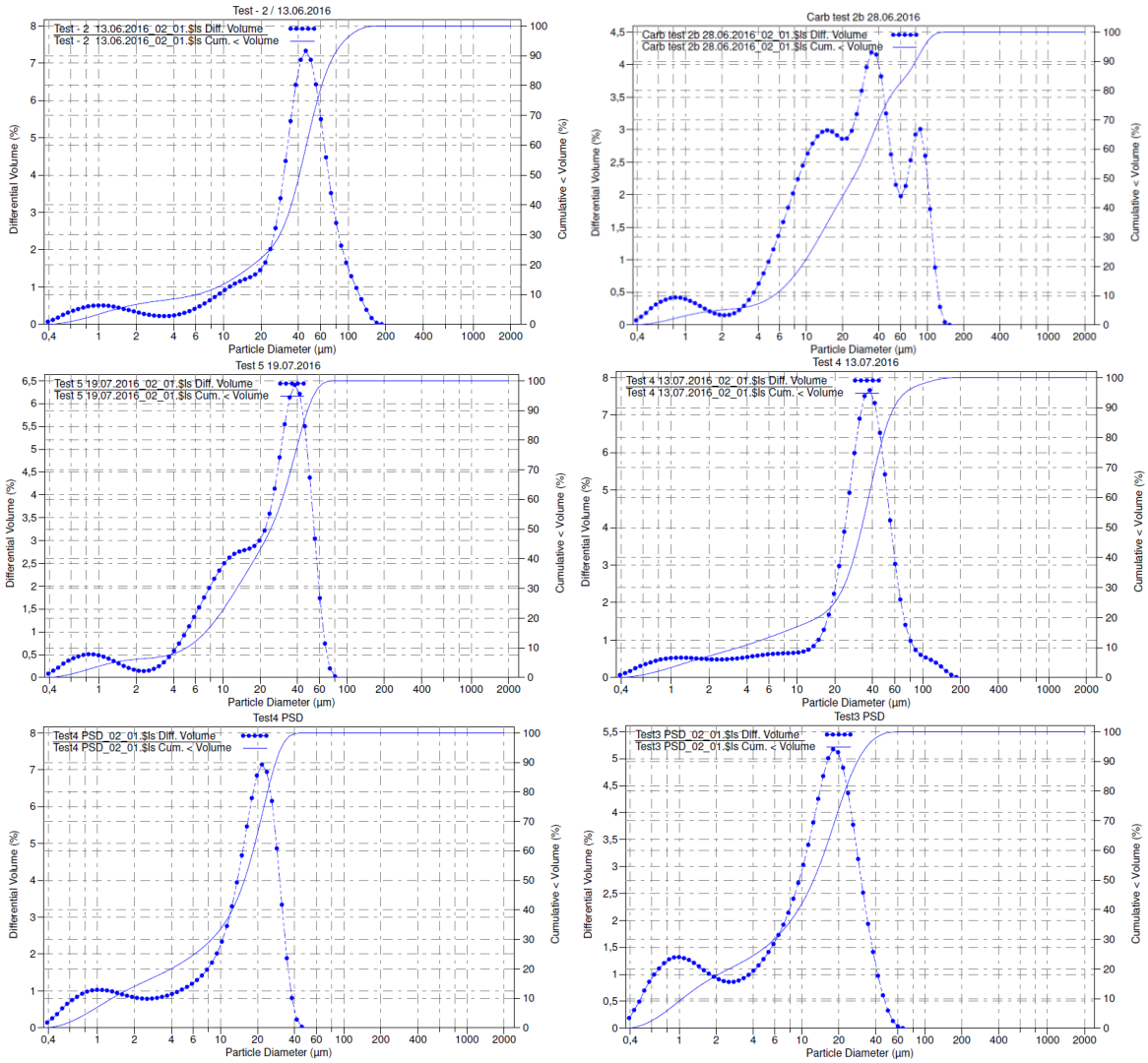

Figure 8.22: Distribution of particle diameter for (top left to bottom right) tests 3, 5, 7, 8, 12 and 13.

9 Conclusions

The objective of this work has been to study the carbonation process through modelling and experimentation to understand the conditions necessary to consistently produce PCC of the desired morphology and size. Overall, insight has been gained into the conditions necessary to produce certain PCC morphologies consistently; however, the size of the PCC still remains an issue to be solved before the X2PCC process can be commercially viable. The following paragraphs present a summary of the findings of this work and conclusions on this.

The properties of the Ca-NH_4Cl-H_2O solution have been measured at varying temperatures. The specific heat capacity is slightly lower than that of pure water whereas the density and dynamic viscosity are slightly higher than that of pure water. The individual diffusivity coefficients have additionally been calculated based on the temperature.

The activity coefficients of the main ions in the system have been calculated using the Pitzer model at varying temperatures and varying calcium concentrations. Additionally, the mean activity coefficients have been calculated with the Bromley model at room temperature and varying calcium concentrations. It is found that the Pitzer and Bromley models agree in the case of $CaCO_3$ however give differing results for NH_4Cl as the ionic strength of the system increases. The activity coefficients of calcium and carbonate ions decrease slightly with temperature (in the considered range of 15-60 °C) and decrease with increasing calcium concentration in the system. The solubility product, K_{sp}, for the 1M NH_4Cl system has been estimated for aragonite and calcite, based on experimental data for the solubility of $CaCO_3$ from literature and applying the activity coefficients from the Pitzer model. The solubility of calcium carbonate in this system was found to be roughly 10 times higher than in water and was found to increase with increasing temperature as opposed to water where it decreases. This does not take into account the presence of calcium ions and is based on a limited amount of experimental data. The solubility product has a very large effect on the magnitude of the supersaturation ratio, and can lead to large errors. The solubility of CO_2 in a 1M NH_4Cl solution was found to be very close to that of CO_2 in pure water. Based on the activity coefficients, K_{sp} and CO_2 solubility, a model to calculate the supersaturation ratio was calculated. The supersaturation ratio increases with calcium concentration and decreases with temperature. Applying this model with experimental data showed that the supersaturation remained reasonably constant in most experiments, tapering off at the end in some, and in a few cases dropping more strongly.

The X2PCC process can produce high purity PCC in line with the requirements from industry. In four of fifteen experiments, other compounds appeared as minor components; however, it is possible that this may be as a result of errors in the analysis. Needle like aragonite was formed in significant amounts at temperatures above 45 °C. The conditions that favour aragonite are low initial supersaturations, high end pHs (above 8,6) and shorter experimental times. Calcite in the rhombohedral form occurred at all temperatures investigated, the conditions that favour calcite are low end pHs and longer experimental times. There are also indications that a high initial calcium concentration favours calcite. As calcite was formed during longer experiments and aragonite during shorter experiments, it may indicate that Ostwald's rule of stages occurs,

where less stable polymorphs (aragonite and vaterite) transform into the more stable forms (calcite) over time. Further experiments would be needed to test this. No scalenohedral calcite was formed, perhaps due to the fact that high enough supersaturations could not be achieved due to the limitations in the concentration of calcium and carbonate ions. Only very small traces of vaterite were formed in three experiments at the lowest temperature (35°C) and very high supersaturations. During carbonation experiments, the pH drops and the temperature increases, due to the exothermic nature of the reactions.

When considering the extraction process, increasing and decreasing the SLR does not lead to significant increases in the calcium concentration. Increasing the temperature from room temperature to 40 °C during extraction also does not lead to an increase in the calcium concentration. The current extraction process with 1M NH_4Cl is limited in its ability to achieve high calcium concentrations that may be desirable for producing certain morphologies and decreasing the PSD. When calculating the calcium extraction efficiency, the initial calcium concentration of the solution before extraction (i.e. residual calcium in the recycled solution from the previous carbonation process) should be taken into account as this otherwise leads to much higher efficiencies even reaching over 100%. The calcium extraction efficiencies achieved when this was corrected for lay between 25 and 47% (excluding anomalies). The same calcium extraction efficiencies when the initial calcium concentration was not considered lay between 31 and 121%. The calcium extraction efficiency is highest at low SLRs, however, the actual calcium concentration achieved may be lower than at high SLRs despite the lower efficiencies, as there is less calcium available in the slag. The calcium concentration throughout the one hour extraction process remains reasonably constant, indicating that shorter extraction times might be equally as effective. However, this may be due to irregularities in the sample taking as the solution in the reactor during extraction is not homogenous.

The PCC produced has too large a size (d_{50} 12-40μm), by an order of magnitude of 2. Aragonite rich samples showed a smaller d_{50} and PSD over calcite, however, this may have been due to changes in the sample taking (directly from the reactor as opposed to after filtration). There is some indication that higher supersaturation (as indicated by literature) and lower temperatures lead to a smaller PSD, however more tests would need to be made to draw definitive conclusions on this. The aragonite samples showed a bimodal size distribution whereas the calcite samples showed three or four nodes in their distribution.

10 Recommendations

This work builds on the work done by many others on the X2PCC project. In the course of this study, some items could not be investigated due to time constraints and other items of interest became apparent. The following presents ideas and recommendations for future work on the X2PCC project based on learnings from conducting this work.

- The particle size distribution is too large. Population balance modelling and further experimentation should be made into reducing this. Improved sample taking should be investigated. It should be tested if there is a difference in the PSD analysis when a sample is taken from the reactor or after filtration. This could be tested by running experiments and taking samples for PSD analysis both from the reactor and after filtration and comparing the results. More extensive experiments should be made analysing the PSD to see if the theory holds that higher supersaturations and lower temperatures lead to smaller PSDs as well as the effect of morphology on PSD. If it is not possible to achieve appropriate particle sizes, post production processing should be investigated to reduce the size of the PCC. It should be investigated that this option is feasible on a cost and energy consumption aspect.

- Tests should be made investigating the effect of CO_2 flow rate and concentration on the carbonation process. In this work it was assumed that the solution was saturated with CO_2, however, it is possible that the CO_2 needed for equilibrium solubility is not reached yet and a greater flow rate is required for this. If this is the case, higher flow rates would result in increasing the initial supersaturation and possibly create conditions needed for producing scalenohedral calcite or a smaller PSD. It may also affect the agglomeration of the PCC produced. Lower CO_2 flow rates may be favourable for aragonite.

- More accurate measurements or calculations of K_{sp} should be made if possible as this has a very great effect on the accuracy supersaturation model.

- CFD modelling and precipitation diagrams could be used to better understand and model the system. A wider range of experimental data would be required in order to produce the precipitation diagrams.

- PCC samples should be taken throughout the carbonation process and the morphology analysed to determine whether Ostwald's rule of stages holds, and understand the progression of morphology over the precipitation process. The experiment should be performed at conditions where both calcite and aragonite have been produced (e.g. 45°C) and performed over a long time and until a low end pH (e.g. pH 8) to ensure any unstable polymorphs have transformed to calcite, with PCC sample taken regularly from the beginning to the end of the process.

- Further tests should be made varying the end pH to see if pure aragonite can be achieved.

- Tests should be performed at higher temperatures (above 55 °C) to see whether pure aragonite can be formed, as these higher temperatures are recommended in literature. Alternative heating methods (than tap water) may need to be employed.

- In order to achieve high calcium concentrations from the extraction process that may needed for certain morphologies and to decrease the PSD, alternative methods should be investigated. Running the extraction experiment twice with fresh slag each time could be investigated to see if this can maximise the calcium extraction by using all the available reactive NH_4Cl in the solution. Experiments could also be made at higher NH_4Cl concentrations, to see the effects on the calcium concentration and the produced PCC. This may result in the need to wash the product, however, it could be interesting from the standpoint of an increased supersaturation and resulting morphologies, increased yield and a smaller PSD.

References

[1] J. Hansen *et al.*, 'Assessing "Dangerous Climate Change": Required Reduction of Carbon Emissions to Protect Young People, Future Generations and Nature', *PLoS ONE*, vol. 8, no. 12, p. e81648, Dec. 2013.

[2] 'EUR-Lex - 52015DC0614 - EN - EUR-Lex'. [Online]. Available: http://eur-lex.europa.eu/legal-content/EN/TXT/?uri=CELEX:52015DC0614. [Accessed: 06-Aug-2016].

[3] S. Eloneva, *Reduction of CO2 emissions by mineral carbonation : steelmaking slags as rawmaterial with a pure calcium carbonate end product*. Aalto-yliopiston teknillinen korkeakoulu, 2010.

[4] S. Eloneva, S. Teir, J. Salminen, C.-J. Fogelholm, and R. Zevenhoven, 'Fixation of CO2 by carbonating calcium derived from blast furnace slag', *Energy*, vol. 33, no. 9, pp. 1461–1467, Sep. 2008.

[5] P. A. Ciullo, Ed., *Industrial minerals and their uses: a handbook and formulary*. Westwood, N.J: Noyes Publications, 1996.

[6] 'Calcium Carbonate | IMA Europe'. [Online]. Available: http://www.ima-europe.eu/about-industrial-minerals/industrial-minerals-ima-europe/calcium-carbonate. [Accessed: 13-Apr-2016].

[7] J. Paltakari, *Pigment Coating and Surface Sizing of Paper*. Helsinki: Paperi ja Puu Oy, 2009.

[8] 'Precipitated Calcium Carbonate (PCC)'. [Online]. Available: http://www.mineralstech.com/Pages/SMI/Precipitated-Calcium-Carbonate-(PCC).aspx. [Accessed: 22-Mar-2016].

[9] H.-P. Mattila and R. Zevenhoven, 'Production of Precipitated Calcium Carbonate from Steel Converter Slag and Other Calcium-Containing Industrial Wastes and Residues', in *Advances in Inorganic Chemistry*, vol. 66, Elsevier, 2014, pp. 347–384.

[10] S. Teir, S. Eloneva, and R. Zevenhoven, 'Production of precipitated calcium carbonate from calcium silicates and carbon dioxide', *Energy Convers. Manag.*, vol. 46, no. 18–19, pp. 2954–2979, Nov. 2005.

[11] 'Recommendation from the Scientific Committee on Occupational Exposure Limits for Calcium oxide (CaO) and calcium hydroxide (Ca(OH)2)', Feb-2008. [Online]. Available: http://ec.europa.eu/social/BlobServlet?docId=3866&langId=en.

[12] J. A. Kosin and C. R. Andrews, 'Process for producing calcium carbonate and products thereof', US4888160 A, 19-Dec-1989.

[13] W. Zappa, 'Pilot-scale Experimental Work on the Production of Precipitated Calcium Carbonate (PCC) from Steel Slag for CO2 Fixation', Master thesis, Aalto University, Espoo, 2014.

[14] J. W. Mullin, 'Crystallization (4th Edition) - Knovel'. [Online]. Available: https://app.knovel.com/web/toc.v/cid:kpCE00002P/viewerType:toc/root_slug:crystallization-4th-edition/url_slug:kt00BWTBPT. [Accessed: 23-Mar-2016].

[15] L. Xiang, Y. Xiang, Z. G. Wang, and Y. Jin, 'Influence of chemical additives on the formation of super-fine calcium carbonate', *Powder Technol.*, vol. 126, no. 2, pp. 129–133, Jul. 2002.

[16] ‘Nano Pcc’. [Online]. Available: http://www.adamasmineral.com/nano-pcc.html. [Accessed: 27-Apr-2016].
[17] ‘Nano Precipitated Calcium Carbonate (NPCC) for Plastic Industry’. [Online]. Available: http://reinste.com/pdf/Nano%20Precipitated%20Calcium%20Carbonate%20(NPCC)%20for%20Plastic%20Industry.pdf. [Accessed: 16-Aug-2016].
[18] ‘Global Calcium Carbonate Market 2015-2020: Trend, Forecast, and Opportunity Analysis’. [Online]. Available: http://www.researchandmarkets.com/reports/3421586/global-calcium-carbonate-market-2015-2020-trend. [Accessed: 16-Aug-2016].
[19] L. Xiang, Y. Xiang, Y. Wen, and F. Wei, ‘Formation of CaCO3 nanoparticles in the presence of terpineol’, *Mater. Lett.*, vol. 58, no. 6, pp. 959–965, Feb. 2004.
[20] S. Aldea *et al.*, ‘Crystallization of Nano-Calcium Carbonate: The Influence of Process Parameters’, *Chem. Ing. Tech.*, p. n/a-n/a, Jul. 2016.
[21] A. U. Badnore and A. B. Pandit, ‘Synthesis of nanosized calcium carbonate using reverse miniemulsion technique: Comparison between sonochemical and conventional method’, *Chem. Eng. Process. Process Intensif.*, vol. 98, pp. 13–21, Dec. 2015.
[22] H.-P. Mattila, ‘Utilization of steelmaking waste materials for production of calcium carbonate (CaCO3)’, Ph.D, Turku, Finland, 2014.
[23] Roskill, ‘Ground & Precipitated Calcium Carbonate: Global Industry, Markets & Outlook, 2nd Edition Brochure’. 2016.
[24] European Commission (EC), ‘Integrated Pollution Prevention and Control- Reference Document on Best Available Techniques for the Manufacture of Large Volume Inorganic Chemicals - Solids and Others industry’. Aug-2007.
[25] P. Stratton, ‘An overview of the North American calcium carbonate market’, Oct-2012. [Online]. Available: http://eippcb.jrc.ec.europa.eu/reference/BREF/lvic-s_bref_0907.pdf. [Accessed: 28-Jul-2016].
[26] O. N. Martínez Miras, ‘Pilot-scale Experimental Work on Sustainable Process Method of Production of Precipitated Calcium Carbonate from Steel Slag and Carbon Dioxide’, Master thesis, Aalto University, Espoo, 2016.
[27] S. El-Sherbiny, S. M. El-Sheikh, and A. Barhoum, ‘Preparation and modification of nano calcium carbonate filler from waste marble dust and commercial limestone for papermaking wet end application’, *Powder Technol.*, vol. 279, pp. 290–300, Jul. 2015.
[28] A. Said, H.-P. Mattila, M. Järvinen, and R. Zevenhoven, ‘Production of precipitated calcium carbonate (PCC) from steelmaking slag for fixation of CO2’, *Appl. Energy*, vol. 112, pp. 765–771, Dec. 2013.
[29] ‘Position Paper on the Status of Ferrous Slag’. [Online]. Available: http://www.euroslag.com/fileadmin/_media/images/Status_of_slag/Position_Paper_April_2012.pdf. [Accessed: 20-Aug-2016].
[30] H.-P. Mattila, I. Grigaliūnaitė, and R. Zevenhoven, ‘Chemical kinetics modeling and process parameter sensitivity for precipitated calcium carbonate production from steelmaking slags’, *Chem. Eng. J.*, vol. 192, pp. 77–89, Jun. 2012.
[31] A. Myerson, *Handbook of Industrial Crystallization*. Burlington, US: Butterworth-Heinemann, 2002.
[32] W. Beckmann, *Crystallization : Basic Concepts and Industrial Applications (1)*. Somerset, DE: Wiley-VCH, 2013.

[33] M. Ukrainczyk, J. Kontrec, V. Babić-Ivančić, L. Brečević, and D. Kralj, 'Experimental design approach to calcium carbonate precipitation in a semicontinuous process', *Powder Technol.*, vol. 171, no. 3, pp. 192–199, Feb. 2007.
[34] J. F. Z. Jr, D. M. Clark, M. Rafal, and N. C. Scrivner, *Handbook of Aqueous Electrolyte Thermodynamics: Theory & Application*. John Wiley & Sons, 2010.
[35] O. US EPA, 'Ionic strength introduction | CADDIS: Sources, Stressors & Responses | US EPA'. [Online]. Available: https://www3.epa.gov/caddis/ssr_ion_int.html. [Accessed: 04-Jul-2016].
[36] T. Solomon, 'The Definition and Unit of Ionic Strength', *J. Chem. Educ.*, vol. 78, no. 12, p. 1691, Dec. 2001.
[37] R. Sander, 'Compilation of Henry's law constants (version 4.0) for water as solvent', *Atmospheric Chem. Phys.*, vol. 15, no. 8, pp. 4399–4981, Apr. 2015.
[38] A. Yasunishi and F. Yoshida, 'Solubility of carbon dioxide in aqueous electrolyte solutions', *J. Chem. Eng. Data*, vol. 24, no. 1, pp. 11–14, Jan. 1979.
[39] 'ChemEngineering - Henry's Law'. [Online]. Available: https://chemengineering.wikispaces.com/Henry%27s+Law. [Accessed: 15-Aug-2016].
[40] A. D. Randolph and M. A. Larson, *Theory of particulate processes: analysis and techniques of continuous crystallization*, 2nd ed. San Diego: Academic Press, 1988.
[41] P. Ponzo, 'Mass transfer in three-phase reactive crystallization', Master thesis, Aalto University, 2015.
[42] J. Franke and A. Mersmann, 'The influence of the operational conditions on the precipitation process', *Chem. Eng. Sci.*, vol. 50, no. 11, pp. 1737–1753, Jun. 1995.
[43] M. Ukrainczyk, J. Kontrec, V. Babić-Ivančić, L. Brečević, and D. Kralj, 'Precipitated calcium carbonate prepared by batch and semicontinuous processes', *Kem. U Ind. Chem. Chem. Eng.*, vol. 56, no. 7–8, pp. 385–390, 2007.
[44] R. B. Fischer, 'Nucleation in Precipitation Reactions from Homogeneous Solution', *Anal. Chem.*, vol. 32, no. 9, pp. 1127–1130, Aug. 1960.
[45] S. Wachi and A. G. Jones, 'Mass transfer with chemical reaction and precipitation', *Chem. Eng. Sci.*, vol. 46, no. 4, pp. 1027–1033, 1991.
[46] I. V. Markov, *Crystal growth for beginners: fundamentals of nucleation, crystal growth, and epitaxy*, 2. ed, Reprinted. Hackensack, NJ: World Scientific, 2008.
[47] M. Schnebelen, K. Mozet, A. Jakob, D. Sy, E. Plasari, and H. Muhr, 'Agglomeration Mechanisms and Kinetics during the Carbonation of a Suspension of Lime in a Pilot Batch Reactor', *Cryst. Struct. Theory Appl.*, no. 4, pp. 35–46.
[48] Y. S. Han, G. Hadiko, M. Fuji, and M. Takahashi, 'Factors affecting the phase and morphology of CaCO3 prepared by a bubbling method', *J. Eur. Ceram. Soc.*, vol. 26, no. 4–5, pp. 843–847, Jan. 2006.
[49] Z. Hu and Y. Deng, 'Supersaturation control in aragonite synthesis using sparingly soluble calcium sulfate as reactants', *J. Colloid Interface Sci.*, vol. 266, no. 2, pp. 359–365, Oct. 2003.
[50] E. Altay, T. Shahwan, and M. Tanoğlu, 'Morphosynthesis of CaCO3 at different reaction temperatures and the effects of PDDA, CTAB, and EDTA on the particle morphology and polymorph stability', *Powder Technol.*, vol. 178, no. 3, pp. 194–202, Sep. 2007.

[51] M. Matsumoto, T. Fukunaga, and K. Onoe, 'Polymorph control of calcium carbonate by reactive crystallization using microbubble technique', *Chem. Eng. Res. Des.*, vol. 88, no. 12, pp. 1624–1630, Dec. 2010.
[52] R. Gupta, 'Synthesis of Precipitated Calcium Carbonate Nanoparticles Using Modified Emulsion Membranes', Georgia Institute of Technology, 2004.
[53] J. Carmona, 'The mechanism of precipitation of chain-like calcite', *J. Cryst. Growth*, vol. 262, no. 1–4, pp. 479–489, Feb. 2004.
[54] G. Li, Z. Li, and H. Ma, 'Preparation of aragonite by carbonization in CaCl2–NH4Cl solution without any additives', *Monatshefte Für Chem. - Chem. Mon.*, vol. 145, no. 1, pp. 187–194, Jan. 2014.
[55] Q. Liu, Q. Wang, and L. Xiang, 'Influence of poly acrylic acid on the dispersion of calcite nano-particles', *Appl. Surf. Sci.*, vol. 254, no. 21, pp. 7104–7108, Aug. 2008.
[56] M. Kitamura, H. Konno, A. Yasui, and H. Masuoka, 'Controlling factors and mechanism of reactive crystallization of calcium carbonate polymorphs from calcium hydroxide suspensions', *J. Cryst. Growth*, vol. 236, no. 1–3, pp. 323–332, Mar. 2002.
[57] M. Lei, P. G. Li, Z. B. Sun, and W. H. Tang, 'Effects of organic additives on the morphology of calcium carbonate particles in the presence of CTAB', *Mater. Lett.*, vol. 60, no. 9–10, pp. 1261–1264, May 2006.
[58] S. Kobe, G. Dražić, A. C. Cefalas, E. Sarantopoulou, and J. Stražišar, 'Nucleation and crystallization of CaCO3 in applied magnetic fields', *Cryst. Eng.*, vol. 5, no. 3–4, pp. 243–253, Sep. 2002.
[59] M. Kitamura, 'Crystallization and Transformation Mechanism of Calcium Carbonate Polymorphs and the Effect of Magnesium Ion', *J. Colloid Interface Sci.*, vol. 236, no. 2, pp. 318–327, Apr. 2001.
[60] J. Kawano, N. Shimobayashi, A. Miyake, and M. Kitamura, 'Precipitation diagram of calcium carbonate polymorphs: its construction and significance', *J. Phys. Condens. Matter*, vol. 21, no. 42, p. 425102, Oct. 2009.
[61] R. Isopescu, C. Mateescu, M. Mihai, and G. Dabija, 'The effects of organic additives on induction time and characteristics of precipitated calcium carbonate', *Chem. Eng. Res. Des.*, vol. 88, no. 11, pp. 1450–1454, Nov. 2010.
[62] A. Rizzuti and C. Leonelli, 'Crystallization of aragonite particles from solution under microwave irradiation', *Powder Technol.*, vol. 186, no. 3, pp. 255–262, Sep. 2008.
[63] S. Knez and C. Pohar, 'The magnetic field influence on the polymorph composition of CaCO3 precipitated from carbonized aqueous solutions', *J. Colloid Interface Sci.*, vol. 281, no. 2, pp. 377–388, Jan. 2005.
[64] A. C. Cefalas *et al.*, 'Nanocrystallization of CaCO3 at solid/liquid interfaces in magnetic field: A quantum approach', *Appl. Surf. Sci.*, vol. 254, no. 21, pp. 6715–6724, Aug. 2008.
[65] F. Alimi, M. Tlili, M. Ben Amor, C. Gabrielli, and G. Maurin, 'Influence of magnetic field on calcium carbonate precipitation', *Desalination*, vol. 206, no. 1–3, pp. 163–168, Feb. 2007.
[66] M. Matsumoto, T. Fukunaga, and K. Onoe, 'Polymorph control of calcium carbonate by reactive crystallization using microbubble technique', *Chem. Eng. Res. Des.*, vol. 88, no. 12, pp. 1624–1630, Dec. 2010.
[67] J. García Carmona, J. Gómez Morales, and R. Rodríguez Clemente, 'Rhombohedral–scalenohedral calcite transition produced by adjusting the solution electrical conductivity

in the system Ca(OH)2–CO2–H2O', *J. Colloid Interface Sci.*, vol. 261, no. 2, pp. 434–440, May 2003.
[68] Ö. Cizer, C. Rodriguez-Navarro, E. Ruiz-Agudo, J. Elsen, D. Van Gemert, and K. Van Balen, 'Phase and morphology evolution of calcium carbonate precipitated by carbonation of hydrated lime', *J. Mater. Sci.*, vol. 47, no. 16, pp. 6151–6165, Aug. 2012.
[69] Y. Sun, M.-S. Yao, J.-P. Zhang, and G. Yang, 'Indirect CO2 mineral sequestration by steelmaking slag with NH4Cl as leaching solution', *Chem. Eng. J.*, vol. 173, no. 2, pp. 437–445, Sep. 2011.
[70] G. H. Fairchild and V. J. Kroc, 'Clustered precipitated calcium carbonate particles', 5,695,733.
[71] I. S. Bleakley and T. R. Jones, 'Slaking, carbonating and neutralizing using regant', 5232678A.
[72] H. Wei and J. Garside, 'Application of CFD Modelling to Precipitation Systems', *Chem. Eng. Res. Des.*, vol. 75, no. 2, pp. 219–227, Feb. 1997.
[73] J. Hostomsky and A. G. Jones, 'Calcium carbonate crystallization, agglomeration and form during continuous precipitation from solution', *J. Phys. Appl. Phys.*, vol. 24, no. 2, pp. 165–170, Feb. 1991.
[74] S. H. Sonawane *et al.*, 'An innovative method for effective micro-mixing of CO2 gas during synthesis of nano-calcite crystal using sonochemical carbonization', *Chem. Eng. J.*, vol. 143, no. 1–3, pp. 308–313, Sep. 2008.
[75] M. Schnebelen, M. Ricaud, A. Jakob, D. Sy, E. Plasari, and H. Muhr, 'Determination of Crystallization Kinetics and Size Distribution Parameters of Agglomerated Calcium Carbonate Nanoparticles during the Carbonation of a Suspension of Lime', *Cryst. Struct. Theory Appl.*, vol. 04, no. 02, p. 16, May 2015.
[76] 'IUPAC-NIST Solubilities Database'. [Online]. Available: http://srdata.nist.gov/solubility/sol_detail.aspx?goBack=Y&sysID=62_73. [Accessed: 14-Aug-2016].
[77] 'IUPAC-NIST Solubilities Database'. [Online]. Available: http://srdata.nist.gov/solubility/sol_detail.aspx?goBack=Y&sysID=62_89. [Accessed: 17-Aug-2016].
[78] 'Bunsen'. [Online]. Available: http://srdata.nist.gov/solubility/IUPAC/SDS-27-28/SDS-27-28-intro_12.pdf. [Accessed: 17-Aug-2016].
[79] S. Lalleman, M. Bertrand, E. Plasari, C. Sorel, and P. Moisy, 'Determination of the Bromley contributions to estimate the activity coefficient of neodymium electrolytes', *Chem. Eng. Sci.*, vol. 77, pp. 189–195, Jul. 2012.
[80] K. S. Pitzer, 'Thermodynamics of electrolytes. I. Theoretical basis and general equations', *J. Phys. Chem.*, vol. 77, no. 2, pp. 268–277, Jan. 1973.
[81] S. Rigopoulos and A. Jones, 'Modeling of Semibatch Agglomerative Gas−Liquid Precipitation of $CaCO_3$ in a Bubble Column Reactor', *Ind. Eng. Chem. Res.*, vol. 42, no. 25, pp. 6567–6575, Dec. 2003.
[82] A. P. Collier and M. J. Hounslow, 'Growth and aggregation rates for calcite and calcium oxalate monohydrate', *AIChE J.*, vol. 45, no. 11, pp. 2298–2305, Nov. 1999.
[83] R. Beck, M. Seiersten, and J.-P. Andreassen, 'The constant composition method for crystallization of calcium carbonate at constant supersaturation', *J. Cryst. Growth*, vol. 380, pp. 187–196, Oct. 2013.

[84] Z. Duan and D. Li, ‘Coupled phase and aqueous species equilibrium of the H2O–CO2–NaCl–CaCO3 system from 0 to 250°C, 1 to 1000bar with NaCl concentrations up to saturation of halite’, *Geochim. Cosmochim. Acta*, vol. 72, no. 20, pp. 5128–5145, Oct. 2008.
[85] Y. Sun, M.-S. Yao, J.-P. Zhang, and G. Yang, ‘Indirect CO2 mineral sequestration by steelmaking slag with NH4Cl as leaching solution’, *Chem. Eng. J.*, vol. 173, no. 2, pp. 437–445, Sep. 2011.
[86] F. Deyhimi and B. Ghalami-Choobar, ‘Potentiometric determination of activity coefficients for NH4Cl in the ternary NH4Cl/LiCl/H2O mixed electrolyte system’, *J. Electroanal. Chem.*, vol. 584, no. 2, pp. 141–146, Oct. 2005.
[87] J. Cheng, C. Yang, and Z.-S. Mao, ‘CFD-PBE simulation of premixed continuous precipitation incorporating nucleation, growth and aggregation in a stirred tank with multi-class method’, *Chem. Eng. Sci.*, vol. 68, no. 1, pp. 469–480, Jan. 2012.
[88] G. Liu, *Greenhouse gases: capturing, utilization and reduction*. 2012.
[89] J. Li and Z. Duan, ‘A thermodynamic model for the prediction of phase equilibria and speciation in the H2O–CO2–NaCl–CaCO3–CaSO4 system from 0 to 250°C, 1 to 1000 bar with NaCl concentrations up to halite saturation’, *Geochim. Cosmochim. Acta*, vol. 75, no. 15, pp. 4351–4376, Aug. 2011.
[90] S. L. Marshall, P. M. May, and G. T. Hefter, ‘Least-Squares Analysis of Osmotic Coefficient Data at 25 .degree.C According to Pitzer’s Equation. 1. 1:1 Electrolytes’, *J. Chem. Eng. Data*, vol. 40, no. 5, pp. 1041–1052, Sep. 1995.
[91] A. J. G. de Mendonça, M. . M. Vaz, M. Isabel, and A. Ferra, ‘Determination of Pitzer Parameters for Sodium Benzoate at 298.15K’, *Port. Electrochimica Acta*, vol. 19, pp. 73–82, 2001.
[92] L. N. Plummer, D. L. Parkhurst, G. W. Fleming, and S. A. Dunkle, ‘A Computer Program Incorporating Pitzer’s Equations for Calculation of Geochemical Reactions in Brines’, *ResearchGate*, vol. 884153, no. 4153, Jan. 1988.
[93] D. J. Bradley and K. S. Pitzer, ‘Thermodynamics of electrolytes. 12. Dielectric properties of water and Debye-Hueckel parameters to 350.degree.C and 1 kbar’, *J. Phys. Chem.*, vol. 83, no. 12, pp. 1599–1603, Jun. 1979.
[94] H. Zhou, L. Huangfu, Y. Bao, X. Bai, R. Ma, and Z. Sha, ‘Solubility of ammonium chloride in a MgCl2–NH4Cl–NH3–H2O system at 298K: Experiments, modeling and prediction’, *Fluid Phase Equilibria*, vol. 383, pp. 174–181, Dec. 2014.
[95] L. A. Bromley, ‘Thermodynamic properties of strong electrolytes in aqueous solutions’, *AIChE J.*, vol. 19, no. 2, pp. 313–320, Mar. 1973.
[96] B. J. Merkel and B. Planer-Friedrich, *Groundwater Geochemistry: A Practical Guide to Modeling of Natural and Contaminated Aquatic Systems*. Springer Science & Business Media, 2008.
[97] H. Zhao, J. Chen, C. Liu, W. Shen, C. Cai, and Y. Ren, ‘Solubility of Calcium Carbonate in Ammonium Chloride Aqueous Solution at T = (298.15, 323.15, and 348.15) K’, *J. Chem. Eng. Data*, vol. 60, no. 11, pp. 3201–3208, Nov. 2015.
[98] A. Seidell, *Solubilities of inorganic and organic compounds; a compilation of quantitative solubility data from the periodical literature*. New York, Van Nostrand, 1919.
[99] B. Coto, C. Martos, J. L. Peña, R. Rodríguez, and G. Pastor, ‘Effects in the solubility of CaCO3: Experimental study and model description’, *Fluid Phase Equilibria*, vol. 324, pp. 1–7, Jun. 2012.

[100] L. N. Plummer and E. Busenberg, 'The solubilities of calcite, aragonite and vaterite in CO2-H2O solutions between 0 and 90°C, and an evaluation of the aqueous model for the system CaCO3-CO2-H2O', *Geochim. Cosmochim. Acta*, vol. 46, no. 6, pp. 1011–1040, Jun. 1982.
[101] K. Hyllestad, 'Scaling of Calcium Carbonate on a Heated Surface in a Flow Through System with Mono Ethylene Glycol.', Norwegian University of Science and Technology, Trondheim, 2013.
[102] D. B. Patience, 'Crystal Engineering through Particle Size and Shape Monitoring, Modeling, and Control', University of Wisconsin-Madison, 2002.
[103] A. Jones, S. Rigopoulos, and R. Zauner, 'Crystallization and precipitation engineering', *Comput. Chem. Eng.*, vol. 29, no. 6, pp. 1159–1166, May 2005.
[104] D. Ramkrishna, *Population balances: theory and applications to particulate systems in engineering*. San Diego, CA: Academic Press, 2000.
[105] J. A. Dirksen and T. A. Ring, 'Fundamentals of crystallization: Kinetic effects on particle size distributions and morphology', *Chem. Eng. Sci.*, vol. 46, no. 10, pp. 2389–2427, 1991.
[106] M. H. Al-Rashed and A. G. Jones, 'CFD modelling of gas–liquid reactive precipitation', *Chem. Eng. Sci.*, vol. 54, no. 21, pp. 4779–4784, Nov. 1999.
[107] R. Zauner and A. G. Jones, 'Mixing Effects on Product Particle Characteristics from Semi-Batch Crystal Precipitation', *Chem. Eng. Res. Des.*, vol. 78, no. 6, pp. 894–902, Sep. 2000.
[108] J. A. Wójcik and A. G. Jones, 'Experimental Investigation into Dynamics and Stability of Continuous MSMPR Agglomerative Precipitation of CaCO3 Crystals', *Chem. Eng. Res. Des.*, vol. 75, no. 2, pp. 113–118, Feb. 1997.
[109] P.-C. Chen, C. Y. Tai, and K. C. Lee, 'Morphology and growth rate of calcium carbonate crystals in a gas-liquid-solid reactive crystallizer', *Chem. Eng. Sci.*, vol. 52, no. 21–22, pp. 4171–4177, Nov. 1997.
[110] J.-P. Andreassen, R. Beck, and M. Nergaard, 'Biomimetic type morphologies of calcium carbonate grown in absence of additives', *Faraday Discuss.*, vol. 159, p. 247, 2012.
[111] Z. Q. Yu, J. W. Chew, P. S. Chow, and R. B. H. Tan, 'Recent Advances in Crystallization control: An Industrial Perspective', *Chem. Eng. Res. Des.*, vol. 85, no. 7, pp. 893–905, 2007.
[112] L. Wang and R. O. Fox, 'Application of in situ adaptive tabulation to CFD simulation of nano-particle formation by reactive precipitation', *Chem. Eng. Sci.*, vol. 58, no. 19, pp. 4387–4401, Oct. 2003.
[113] W. Zappa, 'Pilot-scale Experimental Work on the Production of Precipitated Calcium Carbonate (PCC) from Steel Slag for CO2 Fixation', Master thesis, Aalto University, Espoo, 2014.
[114] M. Vučak, J. Perić, A. Žmikić, and M. N. Pons, 'A study of carbon dioxide absorption into aqueous monoethanolamine solution containing calcium nitrate in the gas–liquid reactive precipitation of calcium carbonate', *Chem. Eng. J.*, vol. 87, no. 2, pp. 171–179, Jun. 2002.
[115] H.-P. Mattila and R. Zevenhoven, 'Design of a Continuous Process Setup for Precipitated Calcium Carbonate Production from Steel Converter Slag', *ChemSusChem*, vol. 7, no. 3, pp. 903–913, Mar. 2014.